2020

Role of ciliary proteins ADP Ribosylation Factor Like GTPase 13B (ARL13B) and Bardet-Biedl Syndrome-8 (BBS8) in photoreceptor outer segment morphogenesis, maintenance, and viability

Tanya L. Dilan
West Virginia University, tldilan@mix.wvu.edu

Role of ciliary proteins ADP Ribosylation Factor Like GTPase 13B (ARL13B) and Bardet-Biedl Syndrome-8 (BBS8) in photoreceptor outer segment morphogenesis, maintenance, and viability

Tanya Lee Dilan Perez

Dissertation submitted to the School of Medicine
at West Virginia University
in partial fulfillment of the requirements
for the degree of

Doctor of Philosophy
in
Biochemistry and Molecular Biology

Visvanathan Ramamurthy Ph.D., Committee Chairperson

Max Sokolov, Ph.D.

Peter Stoilov, Ph.D.

Michael D. Schaller, Ph.D.

David M. Smith, Ph.D.

Gordon P. Meares, Ph. D.

Department of Biochemistry and Molecular Biology

Morgantown, West Virginia

2019

Keywords: *ARL13B*, photoreceptors, BBSome, intraflagellar transport, cilia, retinitis pigmentosa, small GTPases

ABSTRACT

Role of ciliary proteins ADP Ribosylation Factor Like GTPase 13B (ARL13B) and Bardet-Biedl Syndrome-8 (BBS8) in photoreceptor outer segment morphogenesis, maintenance and viability

Tanya Lee Dilan Perez

Photoreceptor neurons are modified primary cilia with an extended ciliary compartment known as the outer segment (OS). The mechanisms behind the elaboration of photoreceptor cilia, OS morphogenesis, and maintenance remain poorly understood. In this work, we focused on dissecting the role of two ciliary proteins, the small GTPase ADP-ribosylation factor-like GTPase 13B (ARL13B) and Bardet-Biedl Syndrome-8 (BBS8) in the context of photoreceptor biology. Both BBS8 and ARL13B are linked to defects in ciliogenesis (cilia development) and Retinitis Pigmentosa (vision loss). ARL13B is implicated in regulating ciliary length, and recent research has demonstrated that ARL13B is the guanine nucleotide exchange factor (GEF) or activator of ARL3, a known regulator in the transport of phosphodiesterase and other lipid-modified proteins. BBS8 is part of the Bardet-Biedl Syndrome complex (BBSome); the BBSome is a stable multiprotein complex linked to retinitis pigmentosa, yet its role in photoreceptor neurons remains poorly understood. It is thought that the BBSome is essential for ciliogenesis and anterograde protein trafficking. However, recent studies have questioned these findings in photoreceptor cilia. Recent findings connect the BBSome with the connecting cilia (transition zone) diffusion barrier, in this region, it is thought that the BBSome acts as a gatekeeper and aids in maintaining the protein composition of photoreceptor outer segments.

To investigate the role of ARL13B and BBS8 in the development and maintenance of ciliated photoreceptor neurons *in vivo*, we generated pan-retina knockout models of both proteins, with ablation of the protein taking place at embryonic day 9.5. Additionally, to study the role of these proteins in fully mature rod photoreceptors, we utilized a rod photoreceptor-specific tamoxifen-inducible murine model (*PDE6g-Cre^{ERT2})*. This murine model allowed us to ablate our proteins in fully formed rod photoreceptors and study the effects on photoreceptor maintenance. Our studies showed that both ARL13B and BBS8 are needed for photoreceptor viability during postnatal retinal development; ARL13B mutants, however, displayed additional defects in retinal proliferation compared to BBS8. In BBS8 mutants, outer segments and their characteristic membranous discs were able to develop, but they

became highly dysmorphic over time. In contrast, outer segments in ARL13B-null retina failed to form, where the OS did form, they resembled highly vesiculated rudiments. The length of the microtubule axoneme was affected in both models of cilia disease. However, BBS8-null axonemes had increased tubulin acetylation. Although tubulin hyperacetylation was not present in ARL13B-null retina, we found intraflagellar transport protein-88 (IFT88), to be highly mislocalized. IFT88 is an IFT-B complex protein crucial for the transport of tubulin dimers to the growing axoneme.

As mentioned previously, ARL13B has been shown to be the activator of ARL3 *in vitro*; our findings indicate the miss-accumulation of ARL3-associated cargoes (i.e., Phosphodiesterase 6 or PDE6) in ARL13B-null retina. As with other BBS models, deleting BBS8 resulted in the accumulation of inner segment proteins to the photoreceptor outer segment (i.e., Syntaxin 3). Interestingly we also observe mislocalization, albeit at reduced levels, of Syntaxin 3 in ARL13B-null photoreceptors. BBS8 deletion resulted in dynamic changes to other BBSome partner subunits. One subunit we found to be highly increased in the absence of BBS8 was BBS4, the most similar to BBS8 in terms of structure (i.e., tetratricopeptide repeat domain protein). Lastly, tamoxifen-inducible BBS8-null mutants took an average of three months to lose visual function. In contrast, ARL13B mutants took only three weeks to develop reduced photoresponse.

In conclusion, in this study, we sought to perform a careful analysis of the different phenotypic profiles present in both BBS8 and ARL13B mutant models. We were able to show apparent deviations in photoreceptor cellular processes ranging from early retinogenesis, photoreceptor outer segment development, maintenance, and protein transport. Current studies are now focused on determining what specific protein domains of both ARL13B and BBS8 correlate to different photoreceptor processes and how these domains are affected in diseased states.

DEDICATION

This work is dedicated to the strong, fierce ladies that shaped me into the person I am today. Mayra, Sonia and Tita, thank you for your unconditional love, and emotional support. Las quiero mucho.

ACKNOWLEDGMENTS

First and foremost, I would like to thank my advisor, Dr. Visvanathan Ramamurthy, for the endless support you have provided me during my time in graduate school. I learned so much about science and academia with you as my mentor. Thank you for taking the time to help me become a better public speaker and for bringing so much enthusiasm to a project idea. You taught me to not be afraid of vocalizing my ideas, know when to pick my scientific battles, and to always be curious. I could not have asked for a better advisor.

Next, I would like to thank my labmates, who are some of the sweetest people I have met in graduate school. Thamarai, thank you for always being such a positive person, I will miss the home-cooked Indian food in the lab and the henna tattoos! Jesse, thank you for all the Chipotle lunches and the brainstorming conversations we had on our projects. Abi, Daniella, Rawa, Uri, and Faezeh, I am so lucky to have had worked alongside a group of smart and passionate female scientists, thank you for the fun lab meetings (with wine and chocolates!). Ezequiel, being able to speak Spanish with you about science and life, I felt like I was at home. Thank you, and I wish you the best as a new father.

I want to thank my dissertation committee for inspiring and training me to become a better scientist. The lively (sometimes intense) debates were scary at first, but now looking back, they are some of my favorite grad school moments. I would like to thank Dr. Schaller and Dr. Sokolov for always finding the time to help me brainstorm when I was stuck with an experiment and for providing non-science related advice when I felt overwhelmed. I would also like to thank Dr. Stoilov for challenging me to think critically and to look at a problem from as many angles as I can.

To the great friends I have made here in West Virginia. Dylan, thank you for looking out for me and for introducing me to all of the beautiful areas of this wild and wonderful state. Rachel, I am so glad I met someone like you in graduate school, whose adventurous spirit resonates so much with mine. Thank you for making this last semester so much fun, and I wish you success and many more adventures! Lastly, Keyana, I am so grateful for your wise advice, moral support, and for the shared laughs and cries, we had together. I genuinely wish you all of the success and happiness in the world.

Finally, I would like to thank my wonderful parents, Mayra I. Perez and Eric Rochette, your love and support kept me going throughout the entire doctoral process. Thank you for always believing in me and inspiring me to reach for the stars. Los amo mucho y gracias, este doctorado es para ustedes! Lastly, Mateo, I miss you dearly, thank you for bringing so much joy and laughter during my final years of graduate school.

TABLE OF CONTENTS

ABSTRACT ii
DEDICATION iv
ACKNOWLEDGMENTS v
TABLE OF CONTENTS vii
Chapter 1 - Introduction 1
The Mammalian Retina 1
The outer segment is a modified primary cilium 2
Ciliary structures found in photoreceptor neurons 3
Photoreceptor outer segment morphogenesis 6
Intraflagellar transport and photoreceptor microtubule elongation 6
Mechanism of photoreceptor OS disc morphogenesis 8
Ciliopathies in the context of photoreceptor development and function 10
Bardet-Biedl Syndrome and the BBSome complex 11
The BBSome in the context of murine photoreceptors and Bardet-Biedl syndrome protein-8 12
The small GTPase ARL13B and its diverse ciliary roles 13
ARL13B-GEF activation of ARL3 in the context of photoreceptors 14
ARL13B and Joubert Syndrome patient mutations 15
ARL13B deletion in zebrafish leads to a mild retinal phenotype 16
Conclusions 16
References 18
Chapter 2 - Bardet-Biedl Syndrome -8 (BBS8) protein is crucial for the development of outer segments in photoreceptor neurons 24
Abstract 25
Introduction 26
Results 28
Discussion 42
Materials and Methods 48
References 55
Supplemental Information 58

Chapter 3 - ARL13B, a Joubert Syndrome-associated protein, is critical for retinogenesis and elaboration of photoreceptor outer segments..... 68

Abstract..... 70

Introduction..... 71

Results..... 73

Discussion..... 92

Materials and Methods..... 98

References..... 104

Chapter 4 - Discussion and Future Perspectives..... 108

Phenotypic similarities and differences between ARL13B and BBS8 mutants..... 109

Retinogenesis..... 109

Outer segment morphogenesis..... 112

Development of ciliary structures: the microtubule axoneme, tubulin post-translational modifications, and the Intraflagellar transport protein complex..... 113

Microtubule axoneme and tubulin post-translational modifications..... 114

Intraflagellar transport complex..... 116

Protein transport to the photoreceptor OS: Rhodopsin, Syntaxin 3 and Phosphodiesterase-6 (PDE6)..... 118

Protein transport: Rhodopsin..... 118

Protein transport: Syntaxin 3..... 119

Protein transport: Phosphodiesterase 6 (PDE6)..... 121

Photoreceptor Maintenance..... 123

Piecing it together: Hypothetical models for ARL13B and BBS8 in photoreceptor neurons..... 124

The BBSome, a complex involved in the photoreceptor ciliary gate or ciliary exit? Both?124

The dynamic and complex role of ARL13B in photoreceptor biology..... 127

Present studies..... 129

Concluding remarks..... 132

References..... 133

1

Introduction

1.1 The Mammalian Retina

The first step in the visual system consists of focusing and transmitting light onto the neural retina, a thin layer of tissue (~0.3mm thick) lining the posterior eyewall. The retina acts as a light receiver, amplifying, extracting, and compressing light stimuli into electrochemical signals, which are subsequently passed on to the midbrain and thalamus through the optical nerve. (Figure 1.1) (*4-6*).

The retina is a highly laminated structure with three layers and five types of neurons. The 'light-sensing'

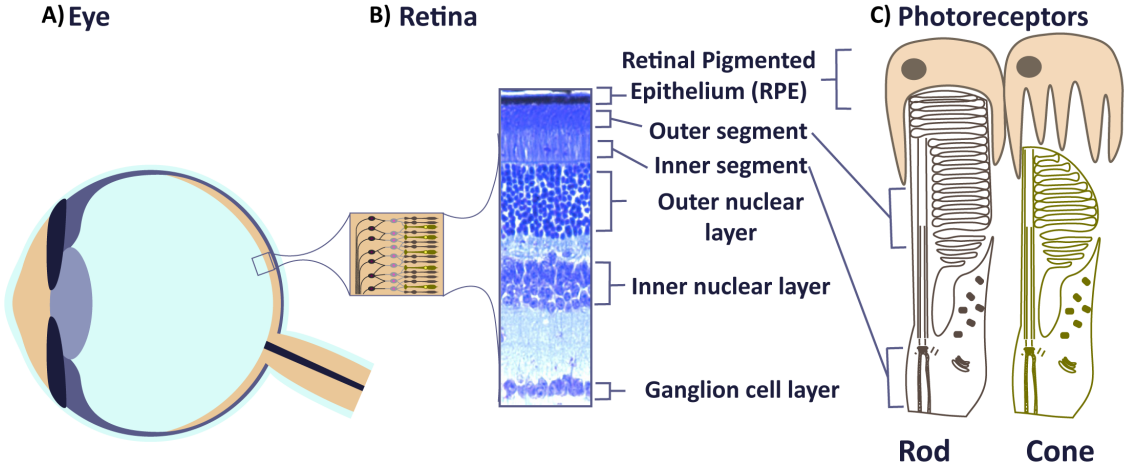

Figure 1.1: The visual system. A) Cross-section of the eye, the black square is enlarged in B) to depict the retina. Cross-section of a murine retina stained with toluidine blue depicting the distinct retinal layers. C) Rod and cone photoreceptors in contact with the retinal pigment epithelium representing the outer nuclear layer

cells, termed photoreceptors, are found in the outermost part of the retina, in contact with the Retinal

Pigment Epithelium (RPE) (*6*). The photoreceptor cell bodies make up the so-called "outer nuclear layer" of the retina (Figure 1.1B). The next layer is called the inner nuclear layer, which contains the cell bodies of the retinal interneurons (i.e., horizontal cells, bipolar cells, and amacrine cells). The last and innermost layer—the ganglion cell layer—houses the retinal neurons whose axon terminals are part of the optic nerve, the conduit from the retina to the higher-order central nervous system (Figure 1.1B) (*5*).

Photoreceptors are divided into two categories, rods and cones, based on their structure and function. Rods mediate vision in dim light conditions and are the predominant cell-type within the retina(*5*). Cones mediate vision under bright light conditions and are also responsible for color vision. Both rods and cones have distinct compartments: 1.) the outer segment, which is comprised of stacked membranous discs packed with proteins necessary to sense light photons (a process termed the "phototransduction cascade"), 2.) the inner segment, which houses the metabolic (mitochondria) and protein synthesis (endoplasmic reticulum, Golgi complex) machinery needed to fulfill the energetic requirements and the synthesis and folding of new proteins in the neuron (*4-6*), and 3.) the synapse, where vesicles are tethered to provide tonic release of glutamate to neighboring retinal interneurons (*7, 8*).

1.2 The outer segment is a modified primary cilium

The photon-sensing compartment of photoreceptor neurons, also known as the outer segment (OS), is comprised of membranous-stacked discs that get entirely renewed every ten days through phagocytosis by the retinal pigment epithelium (RPE) (*9*). This compartment is connected to the inner segment and the rest of the cell body via a narrow bridge-like structure termed the connecting cilia (CC)/transition zone. Together, the outer segment and connecting cilia make up the modified primary cilia compartment of the photoreceptor. Cilia are microtubule-based organelle protrusions that are formed

from centriolar anchors, also known as basal bodies (*10*). There are two types of cilia: motile cilia and primary (or non-motile) cilia. Primary or sensory cilia are usually present as a single structure in most mammalian cells, where they extend from the apical plasma membrane and have evolved to act as signaling 'antennae' to sense extracellular molecules and mechanical force (*11*). Motile cilia are mainly found in specialized cells in the vertebrate system (i.e., sperm, lateral ventricle, respiratory ducts, female reproductive system) (*12*).

1.2.1 Ciliary structures found in photoreceptor neurons

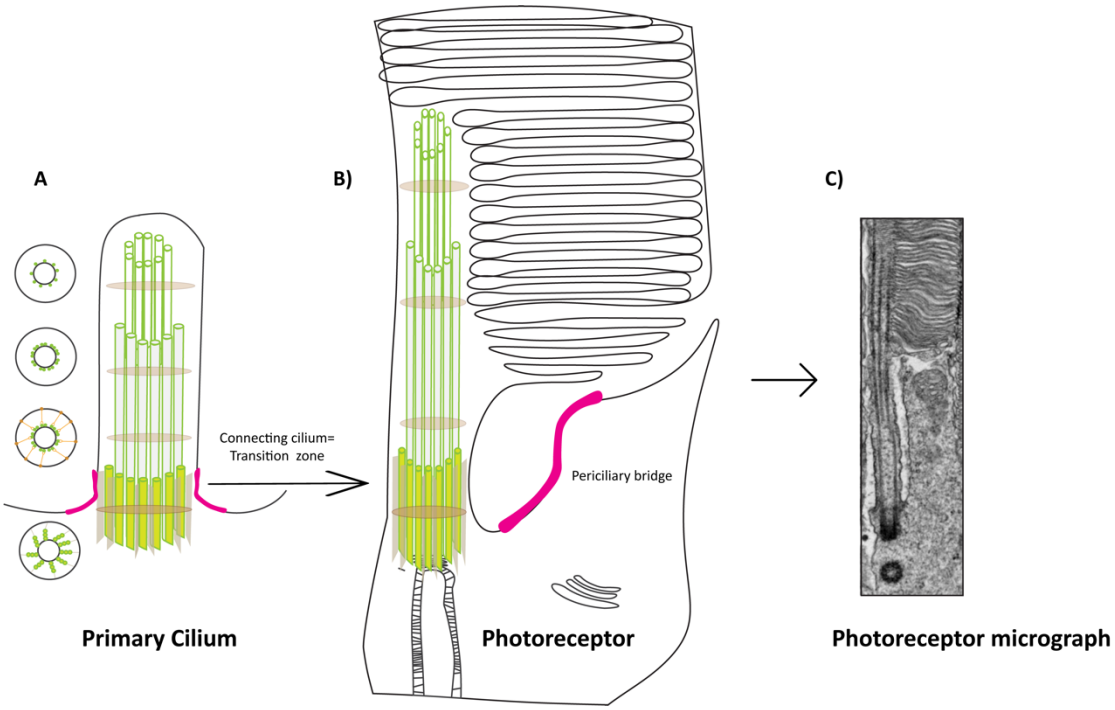

Figure Legend next page

Figure 1.2.1 Ciliary structures are conserved between modified photoreceptor cilia and conventional primary cilia. A) Schematic diagram comparing primary cilium (A) with photoreceptor cilia (outer segment) (B); Cilium in (A) is subdivided into tangential sections showing the different sub-ciliary compartments (bottom to top): basal body, transition zone, axoneme doublets, and axoneme singlets. C)Electron micrograph of a murine photoreceptor depicting the ciliary basal body, connecting cilium (transition zone), axoneme, and the modified ciliary outer segment discs. Diagrams adapted and modified from Pearring et al., 2013.

Photoreceptor outer segments share major structural compartments with traditional primary cilia, i.e., the axoneme and basal body (*6*). These compartments are highlighted in Figure 1.2.1a-b. The ciliary axoneme is a bundle of nine circumferentially arranged doublet microtubules (consisting of a full A-tubule that scaffolds a partial B-tubule, Figure 1.2.1b), which extends upward from an anchor point, also known as the mother centriole/basal body (Figure 1.2.1a) (*11, 13*). The photoreceptor axoneme is arranged in a "9+0" configuration (Figure 1.2.1b). This is distinct from motile cilia, which forms a "9 + 1" configuration with an extra inner doublet (*14*). Between the basal body and ciliary axoneme, there is a transition zone (connecting cilia) where triplet MTs become doublets (Figure 1.2.1b) (*6*). In contrast to the axoneme of a traditional primary cilium—which is characterized by microtubule doublets—the photoreceptor outer segment axoneme contains regions of doublet and singlet microtubules (Figure1.2.1b) (*15-17*). The relative length of the axoneme differs between rod and cone

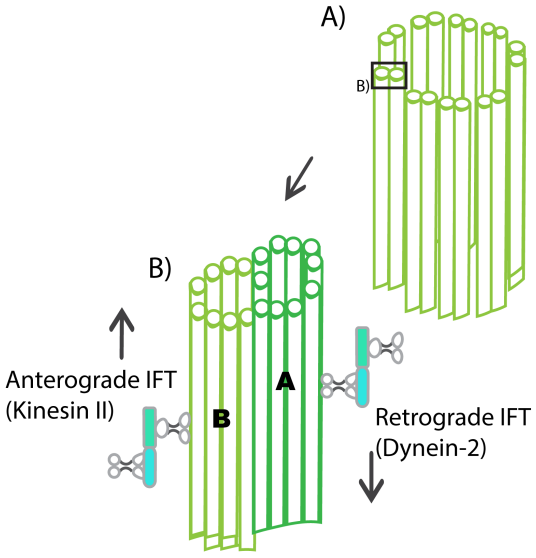

Figure 1.2.2 Arrangement of Axonemal microtubules. A) Arrangement of axonemal microtubules into nine microtubule doublets. B) Enlarged square from a) depicting a doublet consisting of a complete A- tubule and a partially complete B-tubule. The anterograde IFT motor Kinesin II binds to the B-tubule while the retrograde IFT motor Dynein 2 binds to the A-tubule.

photoreceptors; Rod axonemes extend through most of the outer segment (in most species), whereas cone axonemes extend through the entire length of their outer segments (*18-21*). Starting from the base of the connecting cilia, both photoreceptor cilia and traditional primary cilia have vane-like structures connecting the microtubules at the intersection of the mother centriole and the axoneme termed transition fibers (*22*). The molecular composition of the transition fibers remains an open area of research. Additionally, the transition zones of both photoreceptors and primary cilia house structures connecting the microtubules and plasma membrane called "Y-links" (*23*). Y-links anchor the microtubules to the adjacent plasma membrane. The region of the plasma membrane were the Y-links make contact is also known as the ciliary necklace (*23*).

The photoreceptor transition zone separates the ciliary compartment from the cell body (inner segment). It serves as a diffusion barrier that regulates the entry and exit of proteins into and out of the cilium (*24-26*). Elegant studies using a chemically inducible diffusion trap within cilia (C-IDTc) and *in vitro* reconstitution of soluble trafficking across the ciliary gate of IMCD3 cells detected no ciliary entry for proteins above 45kDa in size (*25*). In photoreceptors, Calvert and colleagues calculated the rate of diffusion of soluble proteins by generating tandem fusion GPF moieties of different lengths and expressing them in Xenopus retinae, showing an inverse relationship between size and OS accumulation (*27*). Interestingly, this barrier effect is lessened with hypotonic swelling of the cell (and, by extension, the outer segment), suggesting an alternate form of protein diffusion regulation which relies on steric volume exclusion from the crowded OS disc space rather than the previously mentioned molecular sieve model (*27*). In addition to the ciliary barrier mechanism, the composition and localization of transition zone resident proteins is a growing area of research. Genetic interaction studies have revealed the presence of three main modules (NPHPs, MKS, CEP290) as well as other protein components (i.e., the

BBSome, which will be the topic of chapter 2) within the transition zone. Ciliary proteins such as SPATA7, retinitis pigmentosa GTPase regulator (RPGR) and RPGRIP1, which are not necessary for primary cilia function, are critical for photoreceptor connecting cilia function (*28-31*). In addition, the photoreceptor connecting cilia (~1.5μm in mice) is almost three times the length of the transition zone in other cell types (~200-500nm) (*31*). Additionally, the highly elaborated photoreceptor outer segment at the distal end of the connecting cilia requires unique (photoreceptor-specific) proteins and complex membranous architecture, suggesting that the photoreceptor connecting cilia may have specialized functions in order to aid in the morphogenesis and maintenance of the OS.

1.3 Photoreceptor outer segment morphogenesis

The initial steps of outer segment morphogenesis are similar to those of traditional primary cilia (*6*). Similar to primary cilia, photoreceptor OS development commences with the docking of the mother centriole to a ciliary vesicle (*6*). Upon attachment to the ciliary vesicle, axonemal extension begins at the mother centriole, which causes the ciliary vesicle to invaginate and form the ciliary sheath. The fusion of the ciliary vesicle to the plasma membrane leads to the outer segment becoming externalized from the inner segment, and the outer sheath of the ciliary vesicle becomes the periciliary membrane (*6, 32*). Importantly, while these developmental steps are shared between photoreceptor and primary cilia, the final stages of OS morphogenesis—specifically outer segment disc formation and OS extension—remain unclear.

1.3.1 Intraflagellar transport and photoreceptor microtubule elongation

The assembly of the photoreceptor axoneme (and traditional ciliary axoneme) requires the translocation of vast amounts of tubulin heterodimers to the growing cilia. Since these tubulin subunits are added to the distal plus-end of the growing axoneme, the delivery of tubulin subunits into the cilia and their transport to the ciliary tip are crucial for cilia/photoreceptor OS assembly (*33*). The intraflagellar transport (IFT) protein complex is a bidirectional movement process where large protein complexes termed IFT trains are transported from the base of the cilia to the ciliary tip and vice-versa (Figure 1.2.2). Kinesin-II family motor proteins are responsible for anterograde transport of cargo from the base of the cilia to the ciliary tip, whereas dynein-2 motor proteins facilitate retrograde transport from the ciliary tip back to the base of the cilia along on the axoneme (*34, 35*). First identified in the flagella of *Chlamydomonas*, IFT's are composed of at least 20 different proteins and dissociate into two sub-complexes; IFT-A and IFT-B, as well as an accessory module consisting of Bardet-Biedl Syndrome (BBS) proteins which will be discussed in detail later in this chapter (Figure 1.2.1) (*36-39*). Mutational studies of IFT-A proteins in *Chlamydomonas* showed the accumulation of IFT-B proteins close to the ciliary tip (bulged membrane phenotype), which suggested that IFT-A aids in the retrograde transport of IFT-B proteins to the ciliary base (Figure 1.2.1)(*38*). Similarly, mutational studies of IFT-B proteins show defective or abolished ciliogenesis leading to the conclusion that the IFT-B complex is likely associated with anterograde transport (Figure 1.2.1) (*35, 40*). Previous reports suggest that the IFT machinery plays an essential role in axonemal extension/regulation by aiding in the transport of tubulin into cilia (*41-44*). In addition, mutations in IFT components result in the decreased ciliary entry of other cargo proteins crucial for maintaining ciliary length regulation, one of them being MAP4 (microtubule-associated protein, a negative regulator of ciliogenesis, which results in increased cilia length and subsequent renal defects when defective) (*45*). In zebrafish photoreceptors, mutants of IFT-B components (i.e., IFT88, IFT172) resulted in absent photoreceptor OS (*46, 47*). In murine models, the

deletion of IFT components results in embryonic lethality. Hypomorphic mutations of IFT88 in mice, however, produced shorter and disorganized outer segments, as well as the mislocalization of OS-resident proteins to the IS and ONL compartments (*48*). Interestingly, IFT88 (IFT-B member) defects in murine photoreceptors resulted in the accumulation of extracellular vesicles; a phenotype also observed in our studies (see Chapter 3).

1.3.2 Mechanism of photoreceptor OS disc morphogenesis

Photoreceptor outer segments (POS) are elaborated flattened membranous discs, analogous to thylakoid membranes in chloroplasts. OS's contain hundreds of structural and phototransduction cascade proteins. Rod photoreceptor outer segments (POS) start developing in the murine retina at postnatal day 8 (P8) and are entirely mature by P21 (*49*). They are continuously renewed (~10% total disc content per day) through phagocytosis mediated by the Retinal pigment epithelium (RPE) (*9*). The most widely supported model of OS morphogenesis during photoreceptor development is the Steinberg et al. membrane evagination model (*50*). This model proposes that the growth of the ciliary plasma membrane creates an evagination that grows away from the ciliary axoneme. Specifically, rod discs are derived from the plasma membrane at the distal tip of the connecting cilium. In this region, the membrane folds inward, forming a disc that is still continuous with the plasma membrane. At this point, the lumen is continuous with the extracellular space at the base of the connecting cilium (Figure 1.3.1a-b). As new discs

are formed, the older discs 'pinch' off and become free-floating (Figure 1.3.1b-c). It is thought that OS discs are still linked to the plasma membrane and the photoreceptor axoneme via accessory proteins; however, the mechanism and the identity of the proteins that drive OS disc evagination is still not fully understood. Structural photoreceptor-specific proteins such as Peripherin-2/rds and Rom1, which localize to the photoreceptor disc rims, have been proposed to be involved in this membrane fission process ('pinching' off), but again the specific steps remain unclear (*51, 52*). In addition to structural proteins, members of the phototransduction cascade are also thought to be important in maintaining the structure of the OS discs. For example, it is presumed that Rhodopsin, the G-coupled protein receptor (GPCR) essential for sensing light photons during the phototransduction cascade, also serves a structural/maintenance role in photoreceptor discs, in addition to its primary role as a photon receptor (*53*). This notion arises due to the protein being the most abundant photoreceptor disc protein, and from

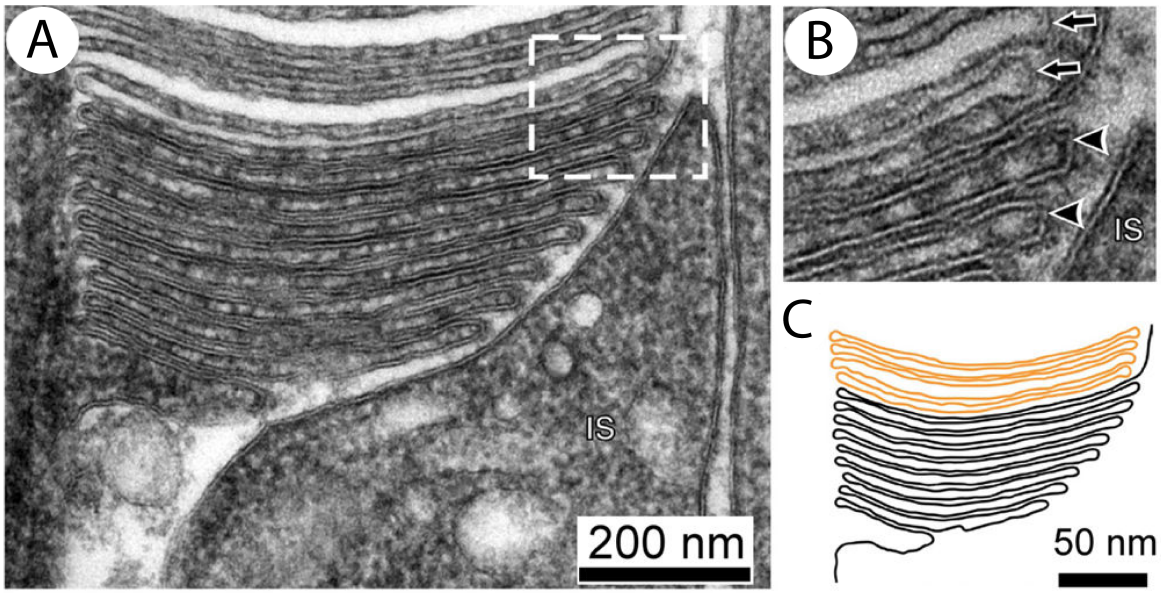

Figure 1.3.1 Electron micrograph demonstrating open discs; The boxed region in A) is enlarged in B) and illustrates as a tracing in C). Arrowheads show new discs; arrows show mature discs. (figure adapted from Goldberg et al., 2016,(*3*).

previous work showing that overexpression of Rhodopsin leads to disc enlargement, and that rhodopsin availability limits disc assembly and outer segment girth in normal rods (*53, 54*).

1.4 Ciliopathies in the context of photoreceptor development and function

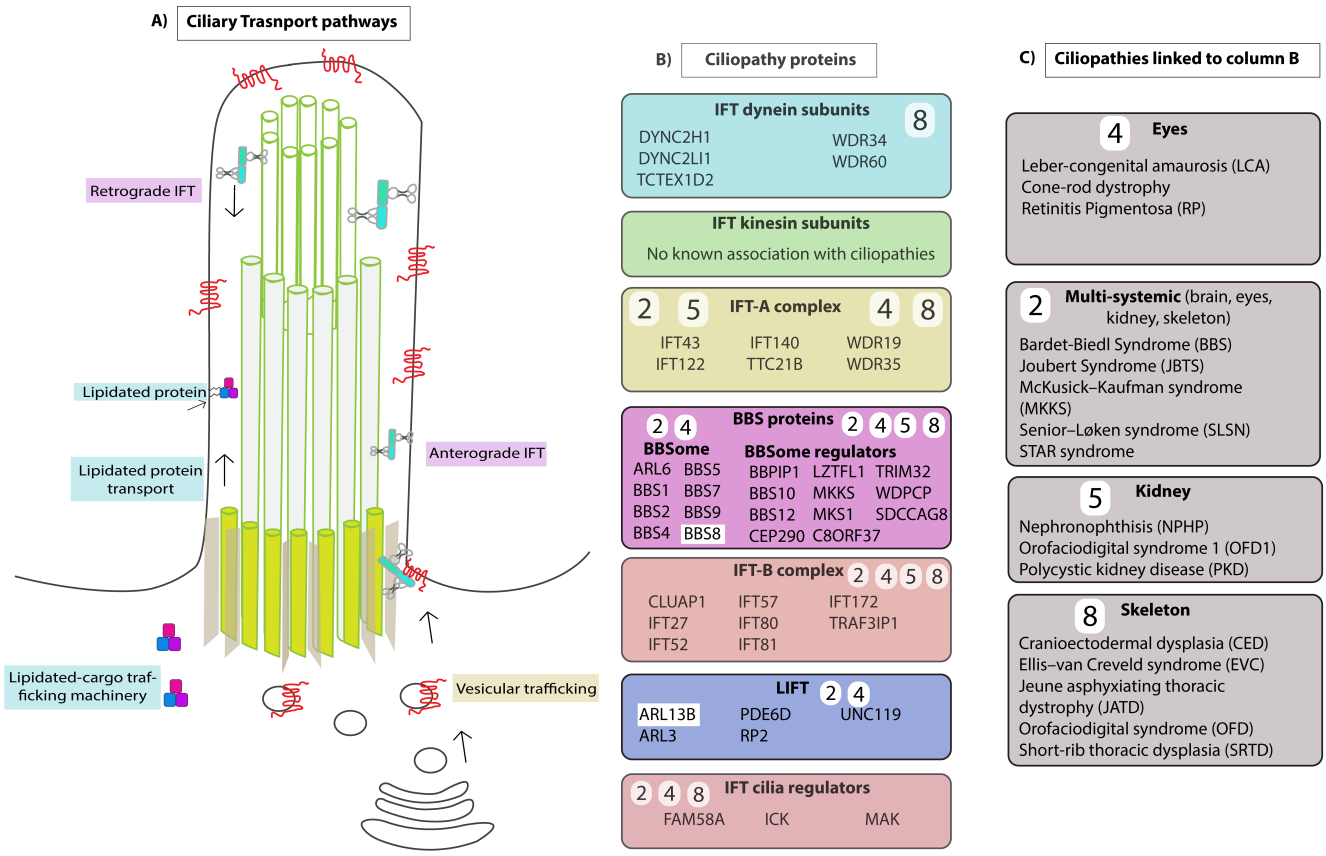

Figure 1.4.1. Associations between ciliary proteins, transport pathways, and ciliopathies. A) Main ciliary pathways: Intraflagellar protein transport complex (IFT) and lipidated-protein intraflagellar trafficking (LIFT); Ciliary proteins are transported from the Golgi and/or cytosol to the base of the cilium and subsequently to the cilium proper. B) Ciliary proteins that comprise both the IFT and LIFT transport pathways, the numbers indicate the ciliopathies (column C) that correspond to defects in these proteins. C) Ciliopathies linked to defects in ciliary trafficking proteins and the tissue affected. Schematic adapted and modified from Reiter et al., 2017.

Human diseases that affect cilia are known as 'ciliopathies' and are characterized by symptoms including cognitive impairment, renal abnormalities, polydactyly, obesity, infertility, and vision loss (Figure 1.4.1c) (*55*). Ciliopathies are divided into two main categories: motile ciliopathies and sensory ciliopathies (*55*). We will focus on sensory ciliopathies for the remainder of the chapter. As the name implies, sensory ciliopathies arise from dysfunction of sensory/ signaling events within (mostly) primary or non-motile cilia. Sensory ciliopathies can arise from 1) defective cilia formation, 2) aberrant ciliary

maintenance, 3) dysregulation of ciliary transduction pathway components, and/or 4) defective ciliary transport or improper entry/exit of ciliary cargoes needed for proper function (*55*). As mentioned previously, the molecular details governing photoreceptor outer segment disc morphogenesis and maintenance remain poorly understood. The **long-term goal** of this study was to provide new insights into photoreceptor outer segment development and maintenance. *We focused on two ciliopathy proteins that are linked to Retinitis pigmentosa (vision loss), are highly enriched in photoreceptor OS's, and have no known function in the phototransduction pathway:* Bardet-Biedl Syndrome (BBS)-8 and ADP-ribosylation factor-like GTPase 13B (ARL13B). The following sub-chapters and chapters summarize what is known about these ciliary proteins thus far, as well as the key findings of our studies in the context of photoreceptor OS development, maintenance, and function.

1.4.1 Bardet-Biedl Syndrome and the BBSome complex

Bardet-Biedl syndrome (BBS) an autosomal homozygous recessive disorder characterized by a host of traditional ciliopathy symptoms (renal cysts, infertility, excess digits, obesity, visual and hearing impairment), and is one of the most common ciliopathies observed in patients (*56*). To date, 21 genes have been associated with BBS, and a subset of these gene products forms a stable octameric complex termed the BBSome (*56, 57*). In addition to the BBS proteins which constitute the core complex (BBS8, BBS9, BBS1, BBS2, BBS7, BBS18/BBIP10, BBS4, and BBS5), the assembly of the BBSome relies on the activity of a BBS–chaperonin complex comprised of BBS6, BBS10 and BBS12 in conjunction with the CCT/TRiC (TriC: T-complex protein-1 ring complex) family chaperonins (*58-60*). Lastly, membrane recruitment of the BBSome complex is aided by the small GTPase BBS3/ARL6, which binds to BBS1 in its nucleotide-active form(*57, 61*). It was initially thought that the BBSome's primary role was to serve as a coat complex and aid in the transport of proteins to the cilia—specifically GPCR's—as

evidenced by the lack of somatostatin receptor 3 (SSTR3) and melanin-concentrating hormone receptor 1 (MCHR1) in neuronal cilia of *Bbs* mutant mice (*62, 63*) . Recent studies, however, point to a role in aiding protein exit from the cilium via retrograde transport (*64, 65*). Nager and colleagues demonstrated that SSTR3, in cells treated with somatostatin (SST), failed to exit in BBS3 knockout IMCD3 cells (*65*). Instead, the receptor accumulated in the ciliary tip and subsequently released as an 'ecto-vesicle' by fission of the ciliary tip through an actin-dependent pathway. This accumulation of SSTR3 and subsequent removal via ecto-vesicles was also observed in BBS1 and BBS2 knockout cell lines (*65*). Therefore, we may observe an absence of SSTR3 in neuronal cilia because the cilia are undergoing this fission event in order to clear the accumulated GPCR's in BBS mutants. Additionally, and in agreement with its role in trafficking, the BBSome has been shown to travel at velocities similar to IFT in the cilia of murine olfactory sensory neurons, and defects in IFT particles leads to aberrant BBS subunit localization (*66, 67*). It is thought that the BBSome acts as an adapter for IFT trains; however, there is no clear evidence of direct interaction between BBS subunits and the IFT complex (*68*).

1.4.2 The BBSome in the context of murine photoreceptors and Bardet-Biedl syndrome protein 8

Functional genetic studies using mouse models all point towards a similar trend amongst BBS subunits in that embryonic removal of BBS subunits leads to slow progressive loss of photoreceptors (*69-71*). For example, BBS2$^{-/-}$ mice displayed a loss of photoreceptors at around P42 (*69*). Similarly, BBS4$^{-/-}$ and BBS7$^{-/-}$ retina experiences photoreceptor loss starting at six weeks and six months, respectively (*70, 71*). At present, two known mutations in BBS8 cause non-syndromic Retinitis Pigmentosa (vision loss), IVS1–2A > G, and c.1347G > C (p.Gln449His) (*72, 73*). Bardet-Biedl Syndrome protein 8 (BBS8), also known as TTC8, is a tetratricopeptide repeat protein and a component of the BBSome complex. The previously mentioned IVS1-2A>G mutation leads to the missplicing of BBS8 exon 2A, which results in

a frameshift in the BBS8 reading frame (Riazuddin et al., 2010a; Murphy et al., 2015b). It subsequently eliminates the protein, specifically in photoreceptor neurons (*72, 74*). This photoreceptor-specific phenotype is due to Exon 2A being skipped in other cell types, explaining why other cell types are not affected by the mutation (*74*). These findings prompted us to perform a more in-depth study of the unique role of ciliary BBS8 in vision (Chapter 2).

1.4.3 The small GTPase ARL13B and its diverse ciliary roles

Small GTPases are molecular "switches" that cycle between GTP bound "on" and GDP bound "off" states (*75, 76*). The ciliary protein ADP-ribosylation factor-like GTPase 13B (ARL13B) is an atypical small GTPase within the ARF/ARL family of small GTPases. ARL13B is larger compared to other ARF/ARL family members, with an extra ~20 kDa C-terminal domain containing a coiled-coil domain and a proline-rich domain (PRD) (*77, 78*). Furthermore, ARL13B contains two cysteine residues in the N-terminal region that are reported to be palmitoylated (*77, 79*). This lipid modification aids in function, stability, membrane association, and ciliary localization of the protein (*79*). ARL13B is highly enriched within primary cilia and ablating the protein leads to shorter cilia. However, most interestingly, overexpression of the protein leads to an increase in cilia length, suggesting a potential role as a ciliary length regulator (*78, 80*). Moreover, ARL13B is the guanine nucleotide exchange factor (GEF) or activator of ARL3, another small GTPase linked to Retinitis pigmentosa (*81*). Activation of ARL3 is essential for the transport of prenylated protein cargoes to the POS (*2, 82, 83*).

ARL13B was first linked to cilia development (ciliogenesis) in a zebrafish model carrying a mutant gene (*scorpion*^{hi459}), which exhibited polycystic kidneys and defective cilia formation in the pronephric duct (*84*). Additionally, mutations in ARL13B have been linked to Joubert Syndrome (JS), an autosomal

recessive ciliopathy characterized by congenital cerebellar ataxia, hypotonia, abnormal eye movements, cognitive impairment and the hallmark "Molar tooth" sign (elongation of the superior cerebellar peduncles) (*85*). Germline deletion of *Arl13b* in mice (known as *hennin* mutants) resulted in embryonic lethality with *hennin* mutant embryos displaying anophthalmia (lack of eye formation) (*78*). Extensive work has been done in understanding ARL13B's regulatory role in Sonic Hedgehog (Shh) signaling, with mice lacking ARL13B showing disruptions in Shh signaling and defective neuronal tube patterning (*78, 86-88*). At present time, ARL13B-dependent regulation of Shh signaling in the retina remains elusive.

1.4.4 ARL13B-GEF activation of ARL3 in the context of photoreceptors

ARL13B was first identified as an ARL3 interactor in a yeast-2-hybrid (Y2H) screen, and ARL13B-GEF activity towards ARL3 was confirmed by measuring fluorescent GDP-analogue dissociation rates, which were significantly accelerated in the presence of ARL13B in a concentration-dependent manner (Figure 1.4.2) (*81*). ARL3-null retina is shown to have a similar, albeit slower retinal phenotype compared to ARL13B-null retina (*82, 89*). The ARL13B GEF role towards ARL3 has not been carefully studied in an animal model, and it is a vital avenue for future research towards understanding ARL13B's

a)

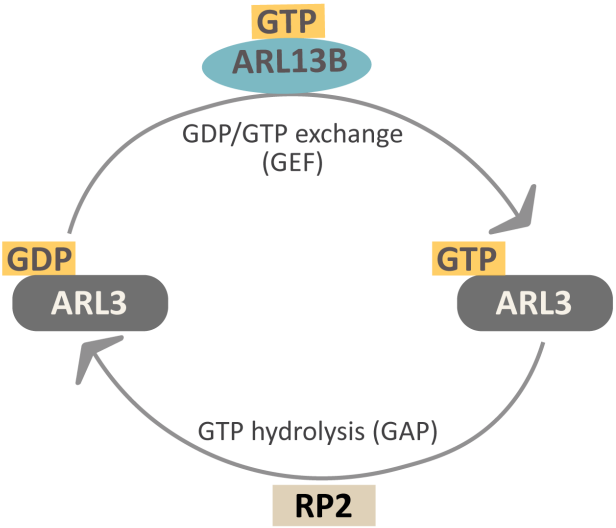

Figure 1.4.2 GTPase cycle of ARL13b and ARL3

A) ARL3 activation by GDP/GTP exchange stimulated by the guanine nucleotide exchange factor (GEF) ARL13B in its GTP active form. Inactivation of ARL3 by GTP hydrolysis stimulated by its GTPase activating protein (GAP) Retinitis pigmentosa-2 (RP2). Mutations in *ARL3* and *RP2* are linked to Retinitis pigmentosa (*1, 2*)

regulatory roles in photoreceptors.

1.4.5 ARL13B and Joubert Syndrome patient mutations

A JS homozygous patient mutation occurring in the highly conserved GTP-binding domain of ARL13B (c.G236A, p.R79Q) was shown to interfere with GTPase binding activity (Figure 1.4.13) (*85, 90*). A more recent study, however, demonstrated that the GTP binding activity of the p.R79Q mutation is not

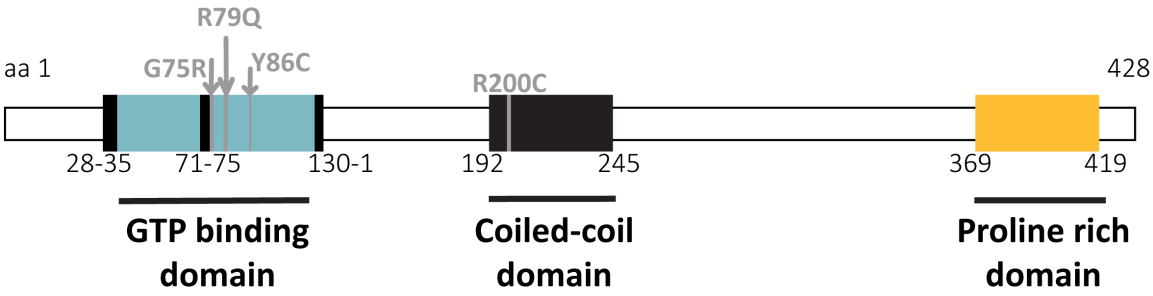

Figure 1.4.3 Schematic diagram of ARL13B gene structure. ARL13B functional domains and patient mutations linked to JS (p.G75R, p.R79Q, p.Y86C, and p.R200C), modified from Rafiullah et al., 2017.

affected, but that the ARL3 GEF activity was impaired (*90*). These confounding differences could be potentially attributed to the different protein expression systems used in each study; Cantagrel and colleagues used a bacterial system for protein expression, and the Khan study utilized mammalian expression of ARL13B for their biochemical assays. Interestingly, the p.R79Q patient showed evidence of mild retinopathy with no changes in visual response as judged by electroretinograms. In addition, the other two siblings carrying the mutations did not present any signs of retinopathy (*85*). It is worth noting the other two siblings with p.79Q mutations and no visual phenotype also carried an additional cilia-related mutation (*85*). There is evidence of phenotypic amelioration in mouse models carrying two cilia-related mutations as opposed to one mutation (*91*). Visual impairment in the context of ARL13B was

first reported in a JS patient carrying a homozygous missense variant in *ARL13B/JBTS8 (*c.257A>G, p.Tyr86Cys). This patient exhibited classic JS symptoms, including retinal impairment (*92*). The variability in visual phenotype may reflect a unique requirement for ARL13B in visual function. To this end, we anticipate that future work will focus on determining the differences between patient mutations that lead to a visual phenotype and those that do not (see Chapter 4). Understanding these differences at a molecular level will contribute significantly to further understanding ARL13B's function and that of its functional domains in the context of photoreceptor viability and function.

1.4.6 ARL13B deletion in zebrafish leads to a mild retinal phenotype

The role of ARL13B in photoreceptor function and vision remained elusive until a recent study assessed the retina in the *scorpion^{hi459}* zebrafish model (*93*). Loss of ARL13B in the retina revealed that the small GTPase is not crucial for zebrafish retinal development (*93*). Ultrastructural analysis of *scorpion^{hi459}* zebrafish retinas revealed no evidence of photoreceptor outer segment disorganization or ciliary defects (*93*). These results varied greatly with our murine model studies (Chapter 3). Rhodopsin was localized correctly to the OS of the *scorpion^{hi459}* photoreceptors. However, in this zebrafish model, OS's were shorter, and photoreceptors underwent progressive degeneration (*93*). Interestingly, ablating ARL13B in murine photoreceptors (Chapter 3), leads to a very severe phenotype compared to zebrafish studies.

1.5 Conclusions

Cilia, once thought to be vestigial organelles, have now been associated with several syndromic blinding diseases. Retinitis pigmentosa or early vision loss is a common symptom of ciliary diseases or 'ciliopathies'; despite its prevalence as a ciliopathy symptom, the connections between ciliary defects and vision loss are just now being carefully elucidated. In the visual system, photon-sensing beings in

the retina, specifically within photoreceptor neurons. Photoreceptor contains a highly modified primary cilia compartment termed the outer segment. This compartment houses all the necessary protein machinery for visual phototransduction to commence. The outer segment undergoes constant renewal, and it's a site for massive protein trafficking. Despite abundant studies focusing on the molecular mechanism behind the phototransduction cascade pathway, how the outer segment compartment is elaborated, and how its maintained remains poorly understood. In this work, we sought to determine the role of two ciliary proteins, Bardet-Biedl Syndrome-8 (BBS8) and ADP ribosylation factor-like 13B (ARL13B), in photoreceptor outer segment morphogenesis, maintenance, and viability. Mutations in BBS8 and ARL13B are both linked to Retinitis Pigmentosa (vision loss) and the ciliopathy diseases Bardet-Biedl Syndrome and Joubert Syndrome, respectively. In addition, previous reports have shown both proteins are crucial for ciliary development and signaling; however, their role in photoreceptor cilia remains poorly understood. The following chapters delineate our results and future perspectives for both BBS8 and ARL13B in the context of photoreceptor cilia.

References:

Baccus SA (2007) Timing and Computation in Inner Retinal Circuitry. Annual Review of Physiology 69:271-290.

Berbari NF, Lewis JS, Bishop GA, Askwith CC, Mykytyn K (2008) Bardet–Biedl syndrome proteins are required for the localization of G protein-coupled receptors to primary cilia. Proceedings of the National Academy of Sciences 105:4242.

Besharse JC, Forestner DM, Defoe DM (1985) Membrane assembly in retinal photoreceptors. III. Distinct membrane domains of the connecting cilium of developing rods. The Journal of neuroscience : the official journal of the Society for Neuroscience 5:1035-1048.

Bhogaraju S, Cajanek L, Fort C, Blisnick T, Weber K, Taschner M, Mizuno N, Lamla S, Bastin P, Nigg EA, Lorentzen E (2013) Molecular basis of tubulin transport within the cilium by IFT74 and IFT81. Science (New York, NY) 341:1009-1012.

Bizet AA et al. (2015) Mutations in TRAF3IP1/IFT54 reveal a new role for IFT proteins in microtubule stabilization. Nat Commun 6:8666.

Boesze-Battaglia K, Dispoto J, Kahoe MA (2002) Association of a photoreceptor-specific tetraspanin protein, ROM-1, with triton X-100-resistant membrane rafts from rod outer segment disc membranes. The Journal of biological chemistry 277:41843-41849.

Breslow DK, Koslover EF, Seydel F, Spakowitz AJ, Nachury MV (2013) An in vitro assay for entry into cilia reveals unique properties of the soluble diffusion barrier. The Journal of cell biology 203:129-147.

Broekhuis JR, Verhey KJ, Jansen G (2014) Regulation of cilium length and intraflagellar transport by the RCK-kinases ICK and MOK in renal epithelial cells. PloS one 9:e108470-e108470.

Cantagrel V et al. (2008) Mutations in the cilia gene ARL13B lead to the classical form of Joubert syndrome. American journal of human genetics 83:170-179.

Caspary T, Larkins CE, Anderson KV (2007) The graded response to Sonic Hedgehog depends on cilia architecture. Dev Cell 12:767-778.

Cevik S, Hori Y, Kaplan OI, Kida K, Toivenon T, Foley-Fisher C, Cottell D, Katada T, Kontani K, Blacque OE (2010) Joubert syndrome Arl13b functions at ciliary membranes and stabilizes protein transport in Caenorhabditis elegans. J Cell Biol 188:953-969.

Cherfils J, Zeghouf M (2013) Regulation of small GTPases by GEFs, GAPs, and GDIs. Physiol Rev 93:269-309.

Cohen AI (1960) The ultrastructure of the rods of the mouse retina. Am J Anat 107:23-48.

Craft JM, Harris JA, Hyman S, Kner P, Lechtreck KF (2015) Tubulin transport by IFT is upregulated during ciliary growth by a cilium-autonomous mechanism. The journal of cell biology 208:223-237.

Dharmat R, Eblimit A, Robichaux MA, Zhang Z, Nguyen T-MT, Jung SY, He F, Jain A, Li Y, Qin J, Overbeek P, Roepman R, Mardon G, Wensel TG, Chen R (2018) SPATA7 maintains a novel photoreceptor-specific zone in the distal connecting cilium. The journal of cell biology 217:2851.

Ding J-D, Salinas RY, Arshavsky VY (2015) Discs of mammalian rod photoreceptors form through the membrane evagination mechanism. The journal of cell biology 211:495-502.

Duldulao NA, Lee S, Sun Z (2009) Cilia localization is essential for in vivo functions of the Joubert syndrome protein Arl13b/Scorpion. Development 136:4033-4042.

Eblimit A et al. (2015) Spata7 is a retinal ciliopathy gene critical for correct RPGRIP1 localization and protein trafficking in the retina. Human molecular genetics 24:1584-1601.

Eckmiller MS (1996) Renewal of the ciliary axoneme in cone outer segments of the retina of Xenopus laevis. Cell and Tissue Research 285:165-169.
Gilliam JC, Chang JT, Sandoval IM, Zhang Y, Li T, Pittler SJ, Chiu W, Wensel TG (2012) Three-dimensional architecture of the rod sensory cilium and its disruption in retinal neurodegeneration. Cell 151:1029-1041.
Goldberg AFX, Moritz OL, Williams DS (2016) Molecular basis for photoreceptor outer segment architecture. Prog Retin Eye Res 55:52-81.
Gotthardt K, Lokaj M, Koerner C, Falk N, Giessl A, Wittinghofer A (2015) A G-protein activation cascade from Arl13B to Arl3 and implications for ciliary targeting of lipidated proteins. Elife 4.
Goyal S, Jäger M, Robinson PN, Vanita V (2016) Confirmation of TTC8 as a disease gene for nonsyndromic autosomal recessive retinitis pigmentosa (RP51). Clinical Genetics 89:454-460.
Green JA, Schmid CL, Bley E, Monsma PC, Brown A, Bohn LM, Mykytyn K (2016) Recruitment of β-Arrestin into Neuronal Cilia Modulates Somatostatin Receptor Subtype 3 Ciliary Localization. Molecular and Cellular Biology 36:223.
Gross JM, Perkins BD, Amsterdam A, Egaña A, Darland T, Matsui JI, Sciascia S, Hopkins N, Dowling JE (2005) Identification of zebrafish insertional mutants with defects in visual system development and function. Genetics 170:245-261.
Hanke-Gogokhia C, Wu Z, Gerstner CD, Frederick JM, Zhang H, Baehr W (2016) Arf-like Protein 3 (ARL3) Regulates Protein Trafficking and Ciliogenesis in Mouse Photoreceptors. J Biol Chem 291:7142-7155.
Hanke-Gogokhia C, Wu Z, Sharif A, Yazigi H, Frederick JM, Baehr W (2017) The guanine nucleotide exchange factor Arf-like protein 13b is essential for assembly of the mouse photoreceptor transition zone and outer segment. J Biol Chem 292:21442-21456.
Hao L, Thein M, Brust-Mascher I, Civelekoglu-Scholey G, Lu Y, Acar S, Prevo B, Shaham S, Scholey JM (2011) Intraflagellar transport delivers tubulin isotypes to sensory cilium middle and distal segments. Nat Cell Biol 13:790-798.
Hong DH, Pawlyk BS, Shang J, Sandberg MA, Berson EL, Li T (2000) A retinitis pigmentosa GTPase regulator (RPGR)-deficient mouse model for X-linked retinitis pigmentosa (RP3). Proceedings of the National Academy of Sciences of the United States of America 97:3649-3654.
Horner VL, Caspary T (2011) Disrupted dorsal neural tube BMP signaling in the cilia mutant Arl13b hnn stems from abnormal Shh signaling. Developmental biology 355:43-54.
Huang S, Hirota Y, Sawamoto K (2009) Various facets of vertebrate cilia: motility, signaling, and role in adult neurogenesis. Proc Jpn Acad Ser B Phys Biol Sci 85:324-336.
Ishikawa H, Marshall WF (2011) Ciliogenesis: building the cell's antenna. Nature Reviews Molecular Cell Biology 12:222-234.
Ivanova AA, Caspary T, Seyfried NT, Duong DM, West AB, Liu Z, Kahn RA (2017) Biochemical characterization of purified mammalian ARL13B protein indicates that it is an atypical GTPase and ARL3 guanine nucleotide exchange factor (GEF). J Biol Chem 292:11091-11108.
Jayasundera T, Branham KEH, Othman M, Rhoades WR, Karoukis AJ, Khanna H, Swaroop A, Heckenlively JR (2010) RP2 phenotype and pathogenetic correlations in X-linked retinitis pigmentosa. Archives of ophthalmology (Chicago, Ill : 1960) 128:915-923.
Jin H, White SR, Shida T, Schulz S, Aguiar M, Gygi SP, Bazan JF, Nachury MV (2010) The conserved Bardet-Biedl syndrome proteins assemble a coat that traffics membrane proteins to cilia. Cell 141:1208-1219.
Johnson KA, Rosenbaum JL (1992) Polarity of flagellar assembly in Chlamydomonas. The Journal of Cell Biology 119:1605.

Kaplan MW, Iwata RT, Sears RC (1987) Lengths of immunolabeled ciliary microtubules in frog photoreceptor outer segments. Experimental eye research 44:623-632.
Kee HL, Dishinger JF, Blasius TL, Liu C-J, Margolis B, Verhey KJ (2012) A size-exclusion permeability barrier and nucleoporins characterize a ciliary pore complex that regulates transport into cilia. Nat Cell Biol 14:431-437.
Keeling J, Tsiokas L, Maskey D (2016) Cellular Mechanisms of Ciliary Length Control. Cells 5:6.
Kozminski KG, Johnson KA, Forscher P, Rosenbaum JL (1993) A motility in the eukaryotic flagellum unrelated to flagellar beating. Proceedings of the National Academy of Sciences of the United States of America 90:5519-5523.
Larkins CE, Aviles GD, East MP, Kahn RA, Caspary T (2011) Arl13b regulates ciliogenesis and the dynamic localization of Shh signaling proteins. Mol Biol Cell 22:4694-4703.
Lechtreck KF (2015) IFT-Cargo Interactions and Protein Transport in Cilia. Trends Biochem Sci 40:765-778.
Lin Y-C, Niewiadomski P, Lin B, Nakamura H, Phua SC, Jiao J, Levchenko A, Inoue T, Rohatgi R, Inoue T (2013) Chemically inducible diffusion trap at cilia reveals molecular sieve-like barrier. Nature chemical biology 9:437-443.
Luby-Phelps K, Fogerty J, Baker SA, Pazour GJ, Besharse JC (2008) Spatial distribution of intraflagellar transport proteins in vertebrate photoreceptors. Vision research 48:413-423.
Makino CL, Wen X-H, Michaud NA, Covington HI, DiBenedetto E, Hamm HE, Lem J, Caruso G (2012) Rhodopsin Expression Level Affects Rod Outer Segment Morphology and Photoresponse Kinetics. PloS one 7:e37832.
Malicki JJ, Johnson CA (2017) The Cilium: Cellular Antenna and Central Processing Unit. Trends Cell Biol 27:126-140.
Manara E, Paolacci S, D'Esposito F, Abeshi A, Ziccardi L, Falsini B, Colombo L, Iarossi G, Pilotta A, Boccone L, Guerri G, Monica M, Marta B, Maltese PE, Buzzonetti L, Rossetti L, Bertelli M (2019) Mutation profile of BBS genes in patients with Bardet-Biedl syndrome: an Italian study. Ital J Pediatr 45:72-72.
Mariani LE, Bijlsma MF, Ivanova AI, Suciu SK, Kahn RA, Caspary T (2016) Arl13b regulates Shh signaling from both inside and outside the cilium. Molecular biology of the cell 27:3780-3790.
Marshall WF, Rosenbaum JL (2001) Intraflagellar transport balances continuous turnover of outer doublet microtubules. The Journal of Cell Biology 155:405.
Mirvis M, Stearns T, James Nelson W (2018) Cilium structure, assembly, and disassembly regulated by the cytoskeleton. Biochemical Journal 475:2329-2353.
Mishra AK, Lambright DG (2016) Invited review: Small GTPases and their GAPs. Biopolymers 105:431-448.
Morgans CW (2000) Presynaptic proteins of ribbon synapses in the retina. Microscopy Research and Technique 50:141-150.
Mourão A, Nager AR, Nachury MV, Lorentzen E (2014) Structural basis for membrane targeting of the BBSome by ARL6. Nat Struct Mol Biol 21:1035-1041.
Murphy D, Singh R, Kolandaivelu S, Ramamurthy V, Stoilov P (2015) Alternative Splicing Shapes the Phenotype of a Mutation in BBS8 To Cause Nonsyndromic Retinitis Pigmentosa. Molecular and cellular biology 35:1860-1870.
Mykytyn K, Mullins RF, Andrews M, Chiang AP, Swiderski RE, Yang B, Braun T, Casavant T, Stone EM, Sheffield VC (2004) Bardet–Biedl syndrome type 4 (BBS4)-null mice implicate Bbs4 in flagella formation but not global cilia assembly. Proceedings of the National Academy of Sciences of the United States of America 101:8664.

Nachury MV, Loktev AV, Zhang Q, Westlake CJ, Peranen J, Merdes A, Slusarski DC, Scheller RH, Bazan JF, Sheffield VC, Jackson PK (2007) A core complex of BBS proteins cooperates with the GTPase Rab8 to promote ciliary membrane biogenesis. Cell 129:1201-1213.
Nager AR, Goldstein JS, Herranz-Pérez V, Portran D, Ye F, Garcia-Verdugo JM, Nachury MV (2017) An Actin Network Dispatches Ciliary GPCRs into Extracellular Vesicles to Modulate Signaling. Cell 168:252-263.e214.
Najafi M, Calvert PD (2012) Transport and localization of signaling proteins in ciliated cells. Vision research 75:11-18.
Nishimura DY, Fath M, Mullins RF, Searby C, Andrews M, Davis R, Andorf JL, Mykytyn K, Swiderski RE, Yang B, Carmi R, Stone EM, Sheffield VC (2004) Bbs2-null mice have neurosensory deficits, a defect in social dominance, and retinopathy associated with mislocalization of rhodopsin. Proceedings of the National Academy of Sciences of the United States of America 101:16588.
Owa M, Uchihashi T, Yanagisawa H-a, Yamano T, Iguchi H, Fukuzawa H, Wakabayashi K-i, Ando T, Kikkawa M (2019) Inner lumen proteins stabilize doublet microtubules in cilia and flagella. Nat Commun 10:1143.
Pazour GJ, Baker SA, Deane JA, Cole DG, Dickert BL, Rosenbaum JL, Witman GB, Besharse JC (2002) The intraflagellar transport protein, IFT88, is essential for vertebrate photoreceptor assembly and maintenance. The Journal of Cell Biology 157:103-114.
Pearring JN, Salinas RY, Baker SA, Arshavsky VY (2013) Protein sorting, targeting and trafficking in photoreceptor cells. Prog Retin Eye Res 36:24-51.
Pedersen LB, Rosenbaum JL (2008) Chapter Two Intraflagellar Transport (IFT): Role in Ciliary Assembly, Resorption and Signalling. In: Current Topics in Developmental Biology, pp 23-61: Academic Press.
Rachel RA, Li T, Swaroop A (2012) Photoreceptor sensory cilia and ciliopathies: focus on CEP290, RPGR and their interacting proteins. Cilia 1:22.
Rachel RA, Yamamoto EA, Dewanjee MK, May-Simera HL, Sergeev YV, Hackett AN, Pohida K, Munasinghe J, Gotoh N, Wickstead B, Fariss RN, Dong L, Li T, Swaroop A (2015) CEP290 alleles in mice disrupt tissue-specific cilia biogenesis and recapitulate features of syndromic ciliopathies. Human molecular genetics 24:3775-3791.
Reiter JF, Leroux MR (2017) Genes and molecular pathways underpinning ciliopathies. Nat Rev Mol Cell Biol 18:533-547.
Riazuddin SA, Iqbal M, Wang Y, Masuda T, Chen Y, Bowne S, Sullivan LS, Waseem NH, Bhattacharya S, Daiger SP, Zhang K, Khan SN, Riazuddin S, Hejtmancik JF, Sieving PA, Zack DJ, Katsanis N (2010) A splice-site mutation in a retina-specific exon of BBS8 causes nonsyndromic retinitis pigmentosa. American journal of human genetics 86:805-812.
Roepman R, Wolfrum U (2007) Protein networks and complexes in photoreceptor cilia. Subcell Biochem 43:209-235.
Roof D, Adamian M, Jacobs D, Hayes A (1991) Cytoskeletal specializations at the rod photoreceptor distal tip. Journal of Comparative Neurology 305:289-303.
Roy K, Jerman S, Jozsef L, McNamara T, Onyekaba G, Sun Z, Marin EP (2017) Palmitoylation of the ciliary GTPase ARL13b is necessary for its stability and its role in cilia formation. J Biol Chem 292:17703-17717.
Sale WS, Besharse JC, Piperno G (1988) Distribution of acetylated alpha-tubulin in retina and in vitro-assembled microtubules. Cell Motil Cytoskeleton 9:243-253.

Schmitz F (2009) The Making of Synaptic Ribbons: How They Are Built and What They Do. The Neuroscientist 15:611-624.
Sedmak T, Wolfrum U (2010) Intraflagellar transport molecules in ciliary and nonciliary cells of the retina. J Cell Biol 189:171-186.
Seo S, Zhang Q, Bugge K, Breslow DK, Searby CC, Nachury MV, Sheffield VC (2011) A Novel Protein LZTFL1 Regulates Ciliary Trafficking of the BBSome and Smoothened. PLOS Genetics 7:e1002358.
Sinha S, Belcastro M, Datta P, Seo S, Sokolov M (2014) Essential role of the chaperonin CCT in rod outer segment biogenesis. Investigative ophthalmology & visual science 55:3775-3785.
Sloboda RD (2005) Intraflagellar transport and the flagellar tip complex. Journal of Cellular Biochemistry 94:266-272.
Song P, Dudinsky L, Fogerty J, Gaivin R, Perkins BD (2016) Arl13b Interacts With Vangl2 to Regulate Cilia and Photoreceptor Outer Segment Length in Zebrafish. Investigative ophthalmology & visual science 57:4517-4526.
Steinberg RH, Fisher SK, Anderson DH (1980) Disc morphogenesis in vertebrate photoreceptors. Journal of Comparative Neurology 190:501-518.
Strom SP, Clark MJ, Martinez A, Garcia S, Abelazeem AA, Matynia A, Parikh S, Sullivan LS, Bowne SJ, Daiger SP, Gorin MB (2016) De Novo Occurrence of a Variant in ARL3 and Apparent Autosomal Dominant Transmission of Retinitis Pigmentosa. PloS one 11:e0150944.
Sun Z, Amsterdam A, Pazour GJ, Cole DG, Miller MS, Hopkins N (2004) A genetic screen in zebrafish identifies cilia genes as a principal cause of cystic kidney. Development 131:4085-4093.
Sung C-H, Chuang J-Z (2010) The cell biology of vision. The Journal of cell biology 190:953-963.
Taschner M, Bhogaraju S, Lorentzen E (2012) Architecture and function of IFT complex proteins in ciliogenesis. Differentiation 83:S12-S22.
Thomas S, Cantagrel V, Mariani L, Serre V, Lee JE, Elkhartoufi N, de Lonlay P, Desguerre I, Munnich A, Boddaert N, Lyonnet S, Vekemans M, Lisgo SN, Caspary T, Gleeson J, Attie-Bitach T (2015) Identification of a novel ARL13B variant in a Joubert syndrome-affected patient with retinal impairment and obesity. Eur J Hum Genet 23:621-627.
Tsujikawa M, Malicki J (2004) Intraflagellar transport genes are essential for differentiation and survival of vertebrate sensory neurons. Neuron 42:703-716.
Wei Q, Zhang Y, Li Y, Zhang Q, Ling K, Hu J (2012) The BBSome controls IFT assembly and turnaround in cilia. Nat Cell Biol 14:950-957.
Wen X-H, Shen L, Brush RS, Michaud N, Al-Ubaidi MR, Gurevich VV, Hamm HE, Lem J, Dibenedetto E, Anderson RE, Makino CL (2009) Overexpression of rhodopsin alters the structure and photoresponse of rod photoreceptors. Biophys J 96:939-950.
Wensel TG, Zhang Z, Anastassov IA, Gilliam JC, He F, Schmid MF, Robichaux MA (2016) Structural and molecular bases of rod photoreceptor morphogenesis and disease. Prog Retin Eye Res 55:32-51.
Williams CL, McIntyre JC, Norris SR, Jenkins PM, Zhang L, Pei Q, Verhey K, Martens JR (2014) Direct evidence for BBSome-associated intraflagellar transport reveals distinct properties of native mammalian cilia. Nat Commun 5:5813-5813.
Wingfield JL, Lechtreck K-F, Lorentzen E (2018) Trafficking of ciliary membrane proteins by the intraflagellar transport/BBSome machinery. Essays Biochem 62:753-763.
Wright ZC, Singh RK, Alpino R, Goldberg AF, Sokolov M, Ramamurthy V (2016) ARL3 regulates trafficking of prenylated phototransduction proteins to the rod outer segment. Human molecular genetics 25:2031-2044.

Ye F, Nager AR, Nachury MV (2018) BBSome trains remove activated GPCRs from cilia by enabling passage through the transition zone. The Journal of Cell Biology 217:1847.
Young RW (1967) The renewal of photoreceptor cell outer segments. The Journal of cell biology 33:61-72.
Zhang Q, Nishimura D, Vogel T, Shao J, Swiderski R, Yin T, Searby C, Carter CS, Kim G, Bugge K, Stone EM, Sheffield VC (2013) BBS7 is required for BBSome formation and its absence in mice results in Bardet-Biedl syndrome phenotypes and selective abnormalities in membrane protein trafficking. Journal of cell science 126:2372-2380.

2

Title: Bardet-Biedl Syndrome -8 (BBS8) protein is crucial for the development of outer segments in photoreceptor neurons

Abbreviated title: BBS8 and photoreceptor development

Authors: Tanya L. Dilan[1,2^], Ratnesh K. Singh[1,2^], Thamaraiselvi Saravanan[1], Abigail Moye[1,2], Andrew F.X. Goldberg[4], Peter Stoilov[2*] and Visvanathan Ramamurthy[1,2,3*]

Affilitions:,[1]Departments of Ophthalmology[1] and Biochemistry[2], and Blanchette Rockefeller Neurosciences Institute[3], West Virginia University, Morgantown, WA 26506, USA and [4]Eye Research Institute, Oakland University, Rochester, MI 48309, USA

Published: *Human Molecular Genetics* 2018 15;27(2):283-294. doi: 10.1093/hmg/ddx399.

Corresponding author (s): Visvanathan Ramamurthy, Departments of Ophthalmology and Biochemistry; Eye Institute, One Medical Center Drive, West Virginia University, Morgantown, WV 26506-9193, USA. Email: ramamurthyv@wvumedicine.org (or)
Peter Stoilov, Department of Biochemistry, West Virginia University, Morgantown, WV 26506, USA**.** Email: pstoilov@hsc.wvu.edu; Tel: 304 598 6940; Fax: 304 598 6928.

^ These authors contributed equally to this work

Keywords: Blindness, Bardet Biedl syndrome; photoreceptors; protein trafficking; outer segment; connecting cilium

ABSTRACT

Bardet-Biedl syndrome (BBS) is an autosomal recessive ciliopathy characterized by developmental abnormalities and vision loss. To date, mutations in 21 genes have been linked to BBS. The products of eight of these BBS genes form a stable octameric complex termed the BBSome. Mutations in BBS8, a component of the BBSome, cause early vision loss, but the role of BBS8 in supporting vision is not known. To understand the mechanisms by which BBS8 supports rod and cone photoreceptor function, we generated animal models lacking BBS8. The loss of BBS8 protein led to concomitant decrease in the levels of BBSome subunits, BBS2 and BBS5 and increase in the levels of the BBS1 and BBS4 subunits. BBS8 ablation was associated with severe reduction of rod and cone photoreceptor function and progressive degeneration of each photoreceptor subtype. We observed disorganized and shortened photoreceptor outer segments (OS) at post-natal day 10 as the OS elaborates. Interestingly, loss of BBS8 led to changes in the distribution of photoreceptor axonemal proteins and hyper-acetylation of ciliary microtubules. In contrast to properly localized phototransduction machinery, we observed OS accumulation of syntaxin3, a protein normally found in the cytoplasm and the synaptic termini. In conclusion, our studies demonstrate the requirement for BBS8 in early development and elaboration of ciliated photoreceptor OS, explaining the need for BBS8 in normal vision. The findings from our study also imply that early targeting of both rods and cones in BBS8 patients is crucial for successful restoration of vision.

INTRODUCTION

Bardet-Biedl syndrome (BBS) is a pleiotropic ciliopathy often accompained by vision loss (*94-99*). A subset of gene products linked to BBS (BBS1, BBS2, BBS4, BBS5, BBS7, BBS8, BBS9, BBIP1 or BBS18) interact to form an octameric complex termed the BBSome (*58, 100*). In neurons, the BBSome promotes the trafficking of GPCRs to ciliary membranes (*58, 101*). The proposed trafficking of GPCRs by the BBSome is supported by animal models that show mis-localization of Stomatin-like protein 3 (SLP3) in olfactory sensory neurons in the absence of BBS8 and melanin-concentrating hormone receptor 1 (MCHR1) in neurons lacking BBS2 and BBS4 (*102, 103*).

The function of the BBSome in photoreceptor neurons is poorly understood despite multiple mutations in BBS subunits associated with blinding diseases. In highly polarized photoreceptor cells, the major GPCR rhodopsin is present in the outer segment (OS). The outer segment is an elaborated stack of ciliary membranes that house proteins involved in the phototransduction cascade. The outer segment is attached to the photoreceptor cytoplasm (inner segment) by the connecting cilium, a narrow conduit through which proteins synthesized in the cytoplasm move to the OS (*104, 105*). The entire photoreceptor OS is renewed every 10 days as new discs are formed at the base of the OS, while apical disc membranes are phagocytized by the retinal pigment epithelium (RPE) (*106*). The constant renewal of the OS requires a robust and tightly regulated protein trafficking system and is crucial for the proper function of photoreceptors. By analogy to its role in trafficking GPCRs in neurons, it was thought that rhodopsin, a GPCR, is also transported to the outer segment by a mechanism involving the BBSome. However, the evidence for the involvement of BBSome in trafficking rhodopsin is weak (*105*). Recent work has suggested an alternative role for the BBSome in photoreceptors, where it acts

either as a ciliary gatekeeper or in retrograde protein movement to keep cytoplasmic proteins out of the photoreceptor OS (*107*).

Bardet-Biedl Syndrome protein 8 (BBS8), also known as TTC8, a tetratricopeptide repeat (TPR) protein and a component of the octameric BBSome complex (*58, 94, 100*). Bardet-Biedl Syndrome patients with mutations in BBS8 were first reported in families of Saudi Arabian and Pakistani lineage. These patients displayed obesity, excess digits, developmental delay and onset of retinitis pigmentosa as early as one year of age (*94*). Interestingly, two mutations in BBS8, IVS1-2A>G and c.1347G>C (p.Gln449His) cause non-syndromic Retinitis pigmentosa (RP) (*108, 109*). The phenotype of IVS1-2A>G mutation is confined to photoreceptor cells through cell type specific alternative splicing, which causes BBS8 protein ablation specifically in photoreceptors (*110*). The mechanism of the non-syndromic RP phenotype of c.1347G>C (p.Gln449His) has not been investigated, but possible scenarios include a splicing mechanism similar to the IVS1-2A>G mutation, or a unique role for BBS8 in photoreceptors (*108*). In this study, we sought to gain insight into the role of BBS8 in photoreceptor neurons. Our studies show an early and crucial role for BBS8 in elaboration of the photoreceptor outer segments, their function and subsequent survival. Interestingly, loss of BBS8 led to changes in the composition of cognate BBS partner subunits that form the octameric BBSome complex, and altered distribution of ciliary markers demonstrating a critical role for BBS8 in development of photoreceptor cilium.

RESULTS

Generation of complete and retina specific BBS8 knockout animals

To study the role of BBS8 in photoreceptor cells, we recovered a BBS8 global knockout (BBS8-*null*) mouse model from sperm obtained from UC Davis KOMP repository. This line contains a stop cassette that knocks in a β-galactosidase reporter after exon 2 and terminates the *Bbs8* gene transcription (Fig. 1A). While we obtained sufficient number of complete knockout animals for our experiments, the number of knockout pups from heterozygous crosses was always below Mendelian ratios. Additionally, the knockout males were infertile and females were obese (data not shown). To avoid these confounding issues, we generated a retina specific BBS8 knockout (Ret-*Bbs8*) using a Cre recombinase under *Six3*

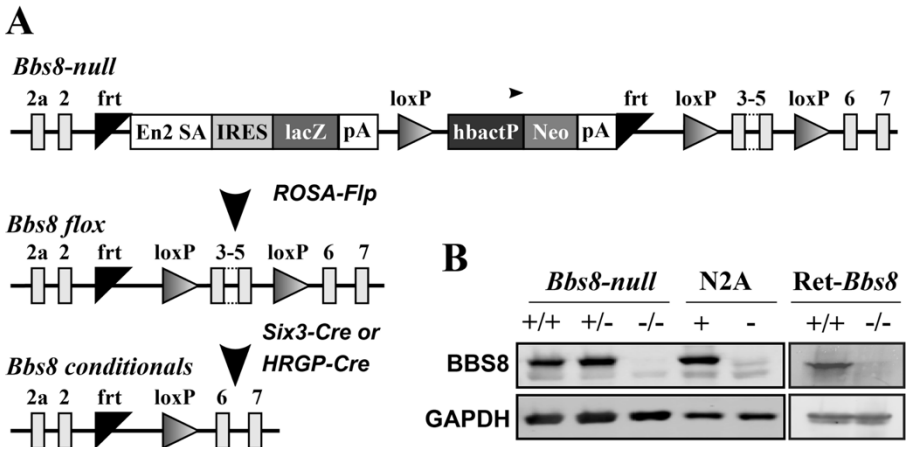

Figure 1. Validation of animal models used in this study.(A) Schematic of the KOMP *Bbs8* null allele and the generation of floxed and conditional *Bbs8* alleles. In the KOMP knock-in, exons 3,4 and 5 of the *Bbs8* gene are floxed. In addition, a lacZ reporter and Neomycin resistance cassettes are knocked-in between exons 2 and 3. The reporter cassettes contain poly-adenylation sites that terminate the transcription of the *Bbs8* gene. Flp recombination deletes the two cassettes, restores BBS8 protein expression and creates a floxed *Bbs8* allele. Subsequent Cre expression from cell or tissue specific promoter excises exons 3,4 and 5 and creates a conditional knockout allele. (B) Western blot validation of the animal models and the specificity of the BBS8 antibody. Equal amount of retinal extracts (100 µg) from postnatal day 10 (P10) BBS8 null (-/-) and littermate controls (+/+, wild-type and +/-, heterozygous animals) were loaded on SDS-PAGE followed by immunoblotting with an antibody against the C-termini of BBS8 (Left Panel). On the right, retinal extracts from P15 Ret-*Bbs8* animals (+/+, *Six3-Cre*: *Bbs8 fl/fl*), +/-, (*Six3-Cre*: *Bbs8 fl/+* were loaded. Glyceraldehyde 3-phosphate dehydrogenase (GAPDH) serves as a loading control. Extracts from cultured N2A cells transfected with plasmid over-expressing *Bbs8* (+) or vector control (-) were used to test the specificity of the BBS8 antibody used.

promoter (Fig. 1A). Retinal extracts of BBS8-*null* and the pan-retina specific BBS8 knockout (Ret-*Bbs8*) animals showed no detectable BBS8 protein (Fig. 1B). To demonstrate the specificity of the antibody, we overexpressed BBS8 in Neuro 2a (N2A) cells (N2A +, in Fig. 1) and cell extracts were probed for BBS8 by immunoblotting. In comparison to mock-transfected N2A cells, a robust immunoreactivity corresponding to BBS8 was found in *Bbs8* transfected cells, verifying the specificity of the antibody employed in this study (Fig. 1B).

Early reduction in rod photoresponse in the absence of BBS8

To assess the photoreceptor function in the absence of BBS8, we measured scotopic (dark-adapted) and photopic (light-adapted) responses by electroretinography (ERG) in *Ret-Bbs8*$^{-/-}$ animals (Fig. 2). The two primary measures of electroretinography are the amplitudes of the 'a' and 'b' waves, which reflect photoreceptor activity and inner neuron activity, respectively (*111*). At P16, an age when retinal development is largely complete, but photoreceptor outer segments (OSs) in wild-type retinas have not yet achieved their full length, scotopic and photopic ERG responses were significantly reduced (Fig.

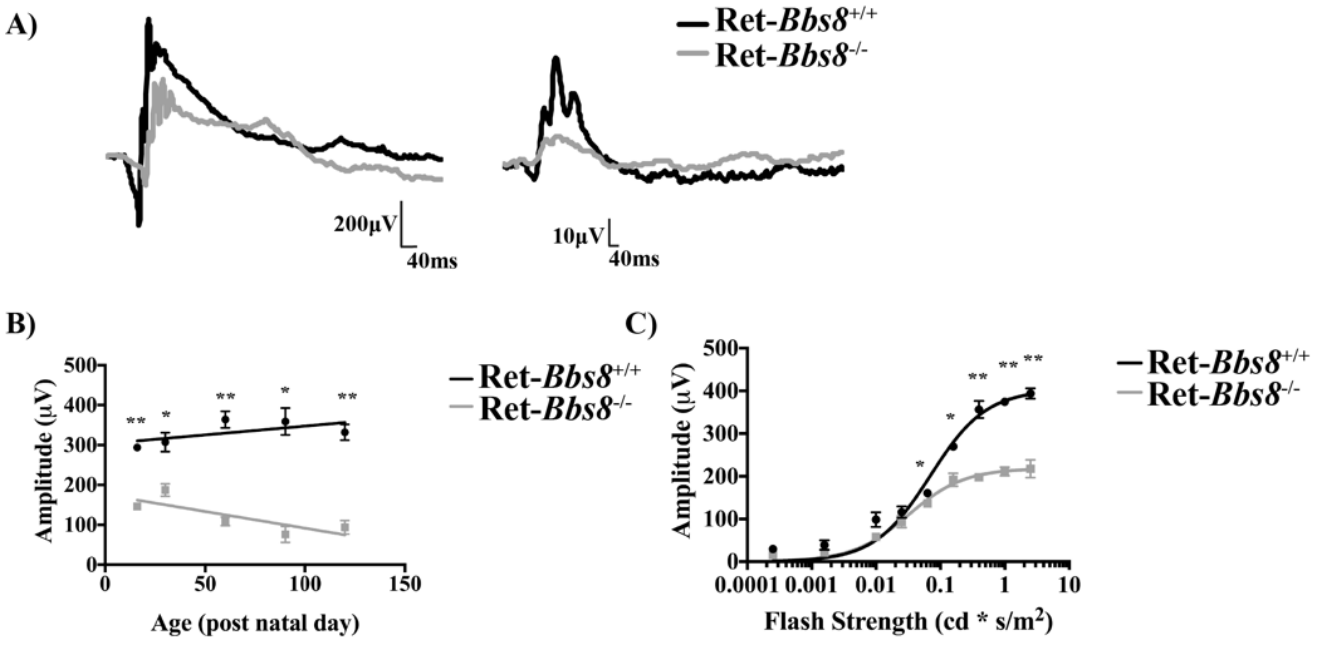

Figure legend on next page

Figure 2. Reduced photoresponse as measured by electroretinography (A) Scotopic ERG response from Ret-*Bbs8* $^{+/+}$ (Black) and Ret-*Bbs8* $^{-/-}$ (Grey) animals measured at P16 (left panel). Representative trace of a scotopic ERG response measured at -0.8 $cd.s^{-1}m^2$. Photopic ERG response measured under light-adapted conditions at 0.69 log $cd.s^{-1}m^2$ at P16 (right panel). (B) Decline in rod photoreceptor response measured by "a" wave response plotted against the age of the animal at which ERG was recorded. Data are represented as mean ± SEM (*n*=6, unpaired two-tailed *t*-test; * P < 0.05, **P < .0009). (C) Stimulus intensity curve of scotopic "a"-wave at P16 of Ret-*Bbs8* $^{-/-}$ and littermate controls (*n*=6). The data were fitted with a hyperbolic function with a half-saturating intensity of 0.07 ± 0.01 cd.s m^{-2} (Littermate control, n=6) and 0.03 ± 0.01 cd.s m^{-2} (Ret-*Bbs8*$^{-/-}$, n=6), and maximum amplitudes of 403 ± 20 μV (Littermate control, n=6) and 219 ± 6 μV (Ret-*Bbs8*$^{-/-}$, n=6). Data are represented as mean ± SEM (*n*=6, unpaired two-tailed *t*-test; * P ≤0.01, **P ≤.0009).

2A). Scotopic "a"-wave amplitude was reduced by half in Ret-*Bbs8*$^{-/-}$ animals (218 ± 5 μV) compared to wild-type littermate controls (403 ± 20 μV, n=6, Student's *t*-test, P=0.0002) (Fig. 2A and 2C). The scotopic response progressively declined as animals aged (Fig. 2B). In the absence of BBS8, the scotopic light response saturated at lower light intensities ($I_{½}$ = 0.07 ± 0.01 cd.s m^{-2} in Ret-*Bbs8*$^{+/+}$ vs. 0.03 ± 0.01 cd.s m^{-2} in Ret-*Bbs8*$^{-/-}$) (Fig. 2C). Altogether, our electrophysiology studies show an early reduction of photoresponse and suggest that BBS8 plays a role in the development and function of photoreceptors.

Loss of BBS8 leads to progressive photoreceptor cell death

To determine if the progressive decrease in photoresponse with age was a result of photoreceptor cell death, we stained retinal sections of Ret-*Bbs8*$^{-/-}$ and wild type littermates with propidium iodide at various ages (Fig 3). At P10, retinal lamination appeared normal with no changes in the number of photoreceptor nuclei in comparison to littermate controls, suggesting normal retinal development in the absence of BBS8 (Fig. 3A and 3B; 13-14 nuclear layers, n=3). At P17, in addition to brightly stained PI nuclei indicative of cell death (arrows), thinning of the photoreceptor outer nuclear layer (ONL) was observed in Ret-*Bbs8*$^{-/-}$ mice compared to wild type controls (Fig. 3A). By four months of age, retina lacking BBS8 lost the majority of their photoreceptor nuclei (Fig. 3A and 3B; 12-14 nuclei in littermate vs. 3-4 nuclei, n=3, *P* = 0.0001). Quantification of photoreceptor nuclei at various regions in the retina

showed uniform thinning in the retina lacking *Bbs8* (Fig. 3B). Our results show that the BBS8 is not needed for the early commitment of photoreceptor cells, but is required for the survival of photoreceptors in the mature retina.

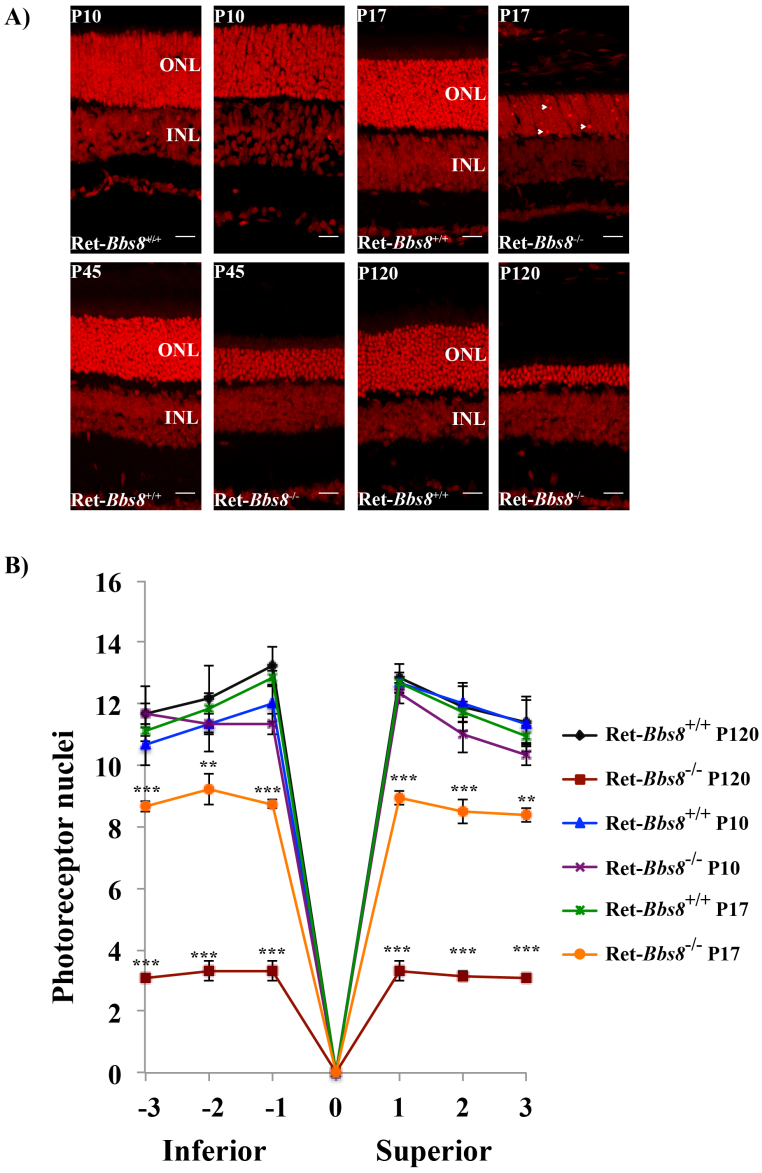

Figure 3. Progressive loss of photoreceptors in the retina lacking BBS8. (A) Retinal sections from animals stained with propidium iodide (PI) at indicated age. At P17, brightly stained nuclei indicative of chromatin condensation and cell death are observed (Arrows). PI staining from littermate controls is shown at the left for each age examined. (B) Quantification of the ONL thickness (number of cell nuclei) at different locations within the retina from the inferior to superior regions between Ret-*Bbs8*$^{+/+}$ and Ret-*Bbs8*$^{-/-}$ animals at P10 and P120; Data are represented as mean ± SEM (n=3, unpaired two-tailed t-test; **P ≤0.01, ***P ≤.001).: Outer nuclear layer, INL: Inner nuclear layer.

Loss of BBS8 leads to altered levels of BBS partner subunits

BBS8 is part of a core octameric BBSome complex (*58, 100*) (Supplementary Material, Fig. S1). Therefore, we were interested in examining if the loss of BBS8 alters the levels of other BBSome

subunit proteins (Fig. 4). We measured the protein levels of the seven BBS proteins that make up the core BBSome complex in BBS8-null and wild type littermate animals at P10 and P18 (Fig. 4A and B). BBS5 and BBS2 were reduced by 67% ($P < 0.0001$) and 20% ($P < 0.05$) respectively in the absence of BBS8 at P10 (Fig. 4A and 4C). In contrast, BBS1 expression increased by 75% in BBS8 null animals compared to wild type controls at P10 (Fig. 4A and 4C; $P < 0.0001$). In addition, BBS4, a TPR repeat protein similar to BBS8, increased by 86% in BBS8 deficient animals compared to littermate controls (Fig. 4A and 4C; $P < 0.0001$)(*94, 112, 113*). We observed no significant changes in BBS7 and BBS9

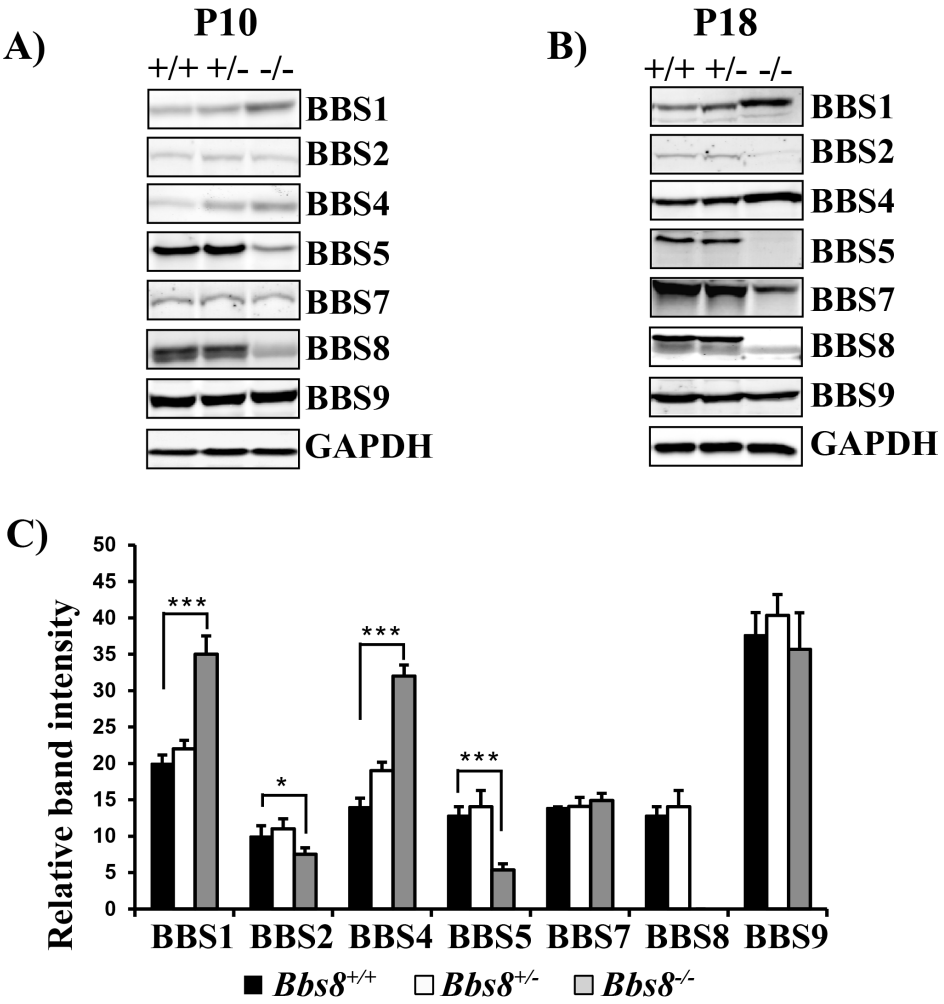

Figure 4. Alteration of BBSome proteins in the absence of BBS8. (A) Immunoblot showing levels of indicated BBS proteins in retinal extracts from *Bbs8* null animals (-/-) prior to photoreceptor degeneration at P10. Littermate controls, both heterozygous and wild-type are shown for comparison. GAPDH serves as a loading control. (B) Similar to Panel A, immunoblot showing the levels of indicated BBS proteins in retinal extracts from P18 animals lacking BBS8. (C) Quantitation of BBS proteins shown in panel A (n=3) normalized to GAPDH levels at P10. *$P < 0.05$; *** $P < 0.0001$ as determined by t-test.

levels. Unfortunately, due to the lack of suitable antibodies to detect BBS18 protein in murine tissues, we were unable to ascertain if BBS18 levels are affected in the absence of BBS8. The change in BBS levels in response to the loss of BBS8 was at the post-transcriptional level; we found no significant

alterations in mRNA levels via RT-qPCR (data not shown). Overall, our results show that absence of BBS8 leads to changes in cognate subunits that form the BBSome (Supplementary Material, Fig. S1).

Mislocalization of Syntaxin 3 in photoreceptors lacking BBS8

Based on the role of the BBSome in trafficking GPCRs in neurons, one proposed role for this protein complex in photoreceptors was the anterograde trafficking of rhodopsin, the major GPCR in photoreceptor neurons (*104*). To evaluate the role for BBS8 in protein trafficking to the outer segment, we investigated the localization of rhodopsin in retinal cryosections obtained from retina lacking BBS8 and compared them to their wild-type littermate controls (Fig. 5A and 5B). At P10, prior to signs of photoreceptor degeneration, the majority of rhodopsin was in the OS in Ret-*Bbs8*$^{-/-}$ animals, similar to littermate controls (Fig. 5A). We also performed similar staining at P17, where photoreceptor degeneration is pervasive (Fig. 5B). Here, we observed mislocalization of rhodopsin in the inner segments (Fig. 5B). Additionally, we examined localization and expression of other OS-resident proteins in the absence of BBS8. At P17, the OS structural protein peripherin-2/rds (PRPH2) and the effector enzyme of the phototransduction cascade, phosphodiesterase-6 (PDE6) were localized to the OS (Supplementary Material, Fig. S2A). However, in our immunohistochemistry analysis, we noticed shortened OS in the absence of BBS8. Therefore, we verified the levels of PRPH2 and PDE6 by immunoblotting. Indeed, we observe a 63% decrease of PRPH2 in Ret-*Bbs8*$^{-/-}$ compared to littermate controls (Supplementary Material, Fig. S2B and S2C; $P = 0.0008$). Similarly, we observed a 47% reduction PDE6β in Ret-*Bbs8*$^{-/-}$ at P12 (Supplementary Material, Fig. S2B and S2C; $P = 0.0002$). Alternatively, a recent study showed mislocalization of syntaxin 3 (STX3) and other cytoplasmic proteins in the outer segments of retina lacking BBS17 and in the BBS1 M390R animal model (15). Since syntaxin is normally present in the inner segments and synaptic termini of photoreceptor neurons

(Fig.5, Green), this finding suggests a gatekeeper role for the BBSome that prevents cytoplasmic proteins from entering the outer segment (*107*). Interestingly, we observed robust accumulation of syntaxin 3 in the OS in the absence of BBS8 at both ages tested (P10 and P17) (Fig. 5).

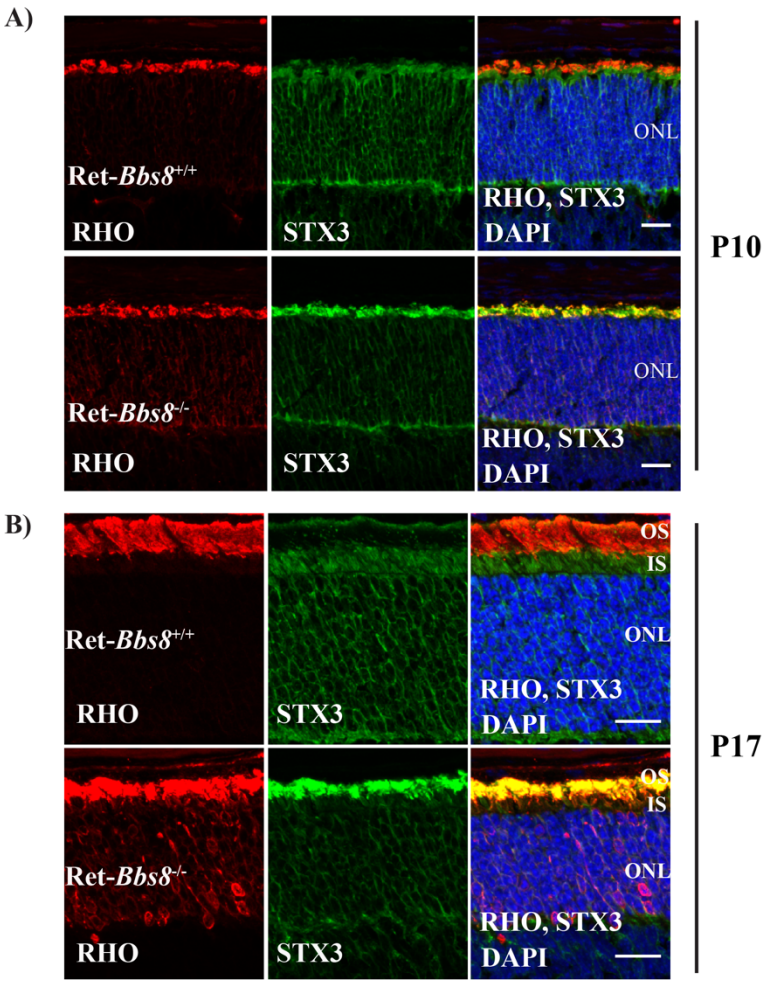

Figure 5. Immunolocalization of rhodopsin and syntaxin 3 in retina lacking BBS8. (A) Retinal cross-sections from Ret-*Bbs8*+/+ littermate control and from Ret-*Bbs8*-/- stained against rhodopsin (Rho-red), syntaxin 3 (STX3-green) and DAPI (blue) at post natal day 10 (P10) and (B) P17 . Scale bar: 20µm. ONL: outer nuclear layer.

Lack of BBS8 causes aberrant rod outer segment ultrastructure

The reduction in photoresponse coupled with a decrease in peripherin-2/rds and OS-resident proteins levels suggests that OS development and/or elaboration may be impaired in the absence of BBS8. Light microscopy of toluidine blue-stained semi-thin sections revealed pyknotic nuclei (Supplementary Material, Fig. S3B, arrow) and shortened inner and outer segments at P18 in *Bbs8*-null animals. We next

examined the photoreceptor ultrastructure both at P10 and at P18 by transmission electron microscopy (TEM). The TEM analysis revealed dysmorphic photoreceptor OS with disoriented discs in animals lacking BBS8 at all ages tested, in comparison to littermate controls (Fig. 6 and Supplementary Material, Fig. S3C-F). Interestingly, we frequently observed extracellular vesicles (EVs) at both P10 and P18 (Fig. 6A and Supplementary Material, Fig. S3G). At P10 the median diameter for EV observed was145 nm (n=142, pooled from 2 animals), in the absence of BBS8 (Fig. 6B). These vesicles were present at the proximal inner segment at P10 and in greater abundance and broader distribution at P18 (Fig. 6B and Supplementary Material, Fig. S3G and S3H). These data demonstrate that BBS8 is critical for the morphogenesis of the outer segment.

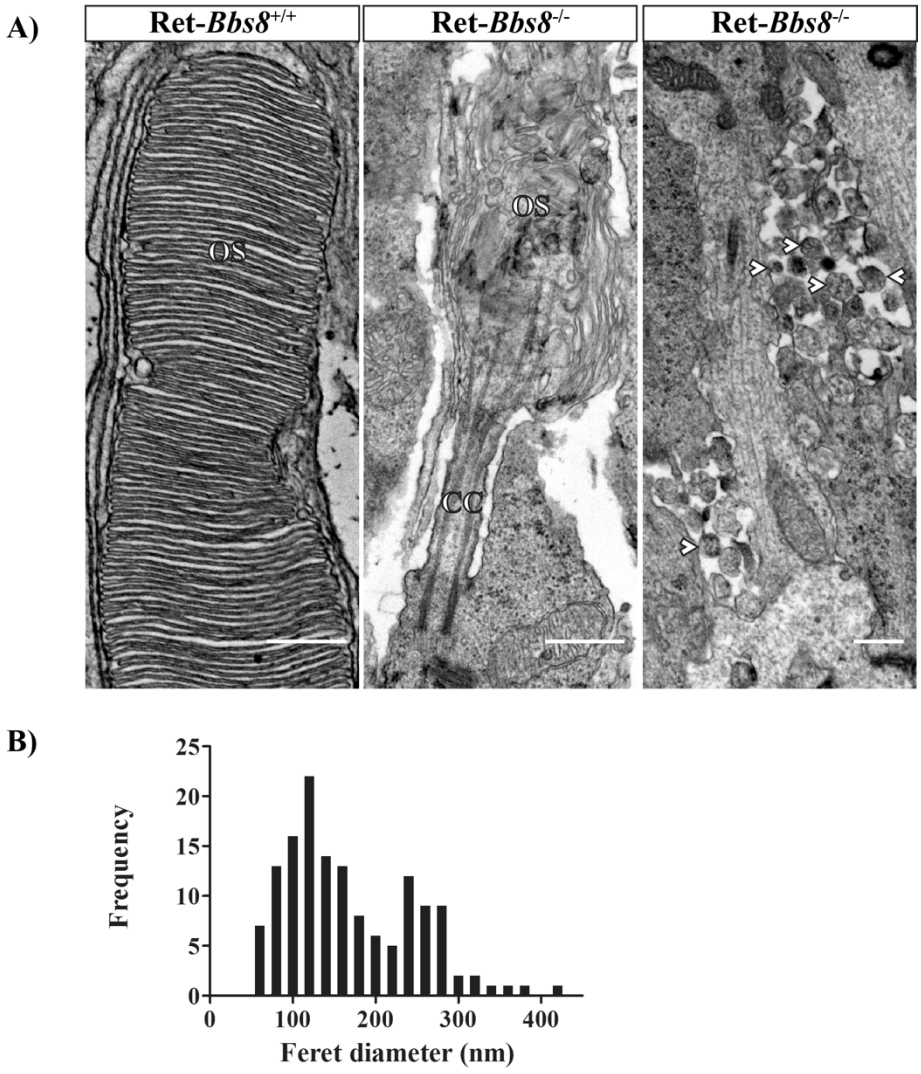

Figure 6: Aberrant photoreceptor ultrastructure in *Bbs8*-null mice.

(A) *Left panel*: TEM images of photoreceptor OSs in P10 retinas of wild-type (left panel; scale bar, 500 nm) and *Bbs8*-null (center panel; scale bar, 500 nm) mice. In contrast to the well-ordered disc stack seen in wild-type controls, knockout animals possessed shortened and dysmorphic OSs, with highly disorganized disc membranes. Retinas from knockout animals also displayed 100-300 nm extracellular vesicles (arrowheads), commonly observed adjacent to the proximal ISs (right panel; scale bar, 500 nm); extracellular vesicles were never observed in the wild-type controls. (B) Distribution of Feret diameter measurements (nm) of extracellular vesicles found in *Bbs8*$^{-/-}$ animals at P10 (N = 142 from two animals).

Ciliary Defects in retina lacking BBS8

BBS proteins are localized to cilia and are associated with ciliogenesis and ciliary protein trafficking in a variety of cell types (*101*). Given this relationship, we decided to examine the structure of the photoreceptor cilia in retina lacking BBS8. The photoreceptor cilia extending from the basal body can be separated into two distinct compartments, connecting cilium (transition zone) and axoneme. The connecting cilium can be labeled with an antibody to X-linked retinitis pigmentosa GTPase regulator (RPGR) (*114, 115*). The axoneme is marked by Retinitis Pigmentosa protein 1 (RP1) and Male germ cell-associated kinase (MAK) (*116-118*). Acetylated tubulin stains the connecting cilium and proximal part of the photoreceptor axoneme (*118, 119*). We used these markers to determine if there are any changes in photoreceptor cilia size and organization in retina lacking *Bbs8* (Fig. 7). In the absence of BBS8 at P10, we observed an increase in acetylated tubulin labeling (Fig. 7A and Supplementary material, Fig. S4C; 1.145μm ± 0.02 in wild type, n=288; 2.301μm ± 0.04 in Ret-*Bbs8*$^{-/-}$, n=278; $P <$ 0.0001). Marginal, but statistically significant increase of RGPR stained zones was also observed along the connecting cilium (Fig. 7B and 7C and Supplementary material, Fig. S4D; 0.9428μm ± 0.01, n=336 in littermate controls, 1.011μm ± 0.01, n= 350 in Ret-*Bbs8*$^{-/-}$; P < 0.0001). In contrast, we observed reduced immnunoreactivity for both axonemal markers RP1 and MAK, suggesting reduced axoneme length. RP1 staining was reduced in Ret-*Bbs8*$^{-/-}$ animals compared to littermate controls (2.32μm ± 0.05 in wild type, n=215; 1.53 ± 0.04 in Ret-*Bbs8*$^{-/-}$, n=190; $P < 0.0001$) (Fig. 7A and 7C and Supplementary material, Fig. S4A). Similarly, MAK staining was reduced in retina lacking BBS8 (1.21μm ± 0.02, n=317 in littermate controls, 0.81μm ± 0.01, n=310 in Ret-*Bbs8*$^{-/-}$; $P < 0.0001$) (Fig. 7B and 7C and Supplementary material Fig. S4B). The total protein levels of RP1 and MAK in the retina were not significantly altered (Supplementary material, Fig. S4E and S4F); however, a trend for increased

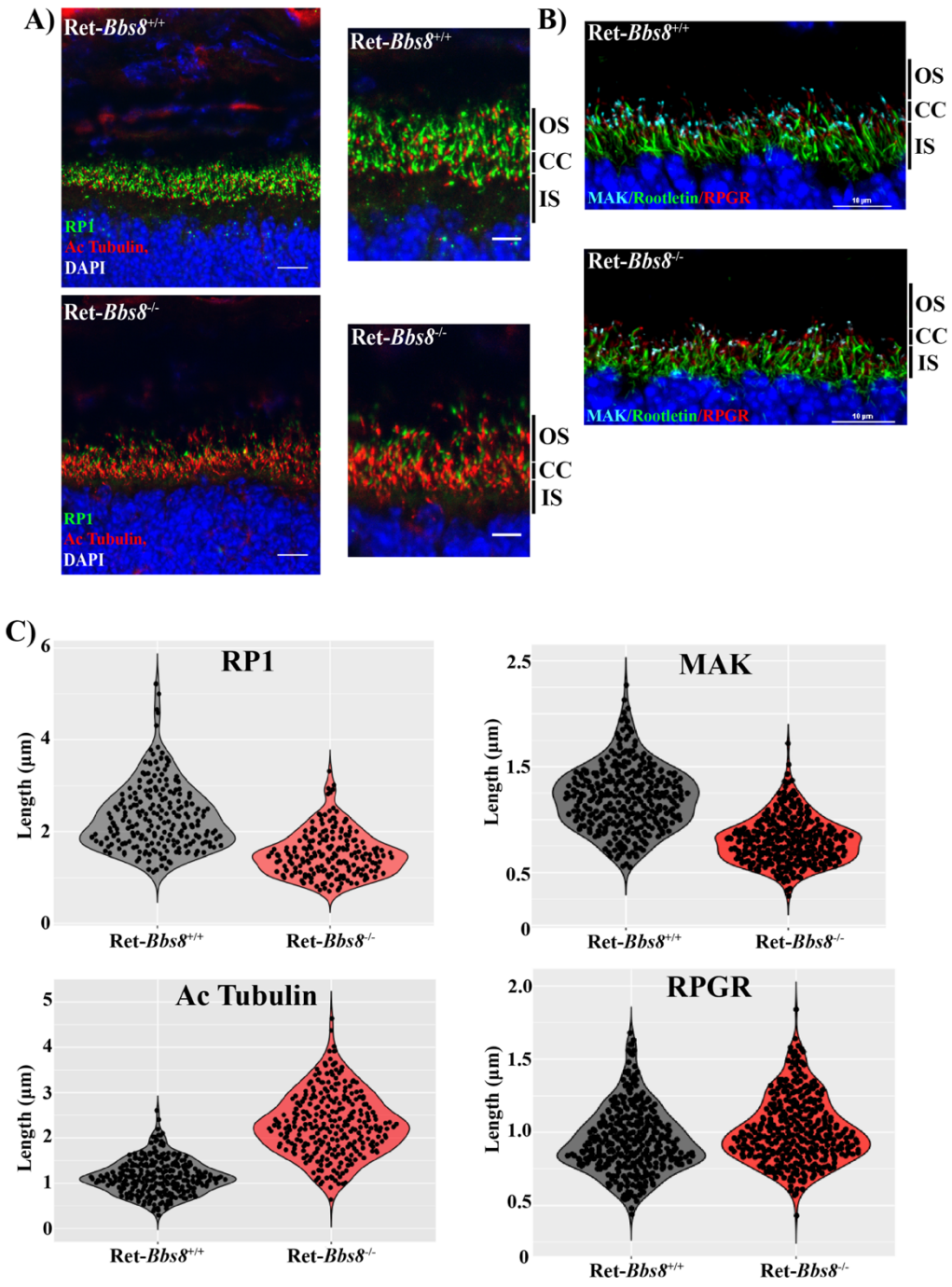

Figure 7: Increased acetylated tubulin stained ciliary zones in the absence of BBS8 at P10. (A) Immunofluorescence images showing RP1 (Retinitis Pigmentosa-1) and acetylated α-tubulin staining the photoreceptor axoneme and connecting cilia in Ret-*Bbs8* $^{+/+}$ and Ret-*Bbs8*$^{-/-}$ animals, respectively. Scale bar: 20 and 10 µm. (B) Retinal cryosections stained against MAK (male germ cell-associated kinase), Rootletin and RPGR (X-linked retinitis pigmentosa GTPase regulator) in Ret-*Bbs8*$^{-/-}$ and littermate controls. Scale bar: 10 µm. (C) Violin plots depicting overall distribution of length measurements for RP1, acetylated α-tubulin, MAK and RPGR stained zones in Ret-*Bbs8*$^{-/-}$ and littermate controls (n=200-300 cilia pooled from 3 animals). All retinal tissues are derived from P10 animals with littermates used as controls.

acetylated tubulin protein levels was observed by immunoblotting (Supplementary material, Fig. S4E

and S4F). Overall, these data show altered distribution of ciliary markers in the absence of BBS8, which likely reflects changes in the organization of the photoreceptor cilia.

BBS8 is crucial for cone photoreceptor viability

We found that the removal of BBS8 in the retina leads to reduction in both rod and cone photoresponses (Fig. 2). This decrease in cone function could be due to a "by-stander" effect (secondary to the loss of rod photoreceptor cells), or it may be due to a direct role of BBS8 in cone photoreceptors. Therefore, to determine if the reduction of cone photoresponse is a cell autonomous effect, we ablated *Bbs8* in developing cone photoreceptors using a mouse line that expresses *Cre* recombinase under the human

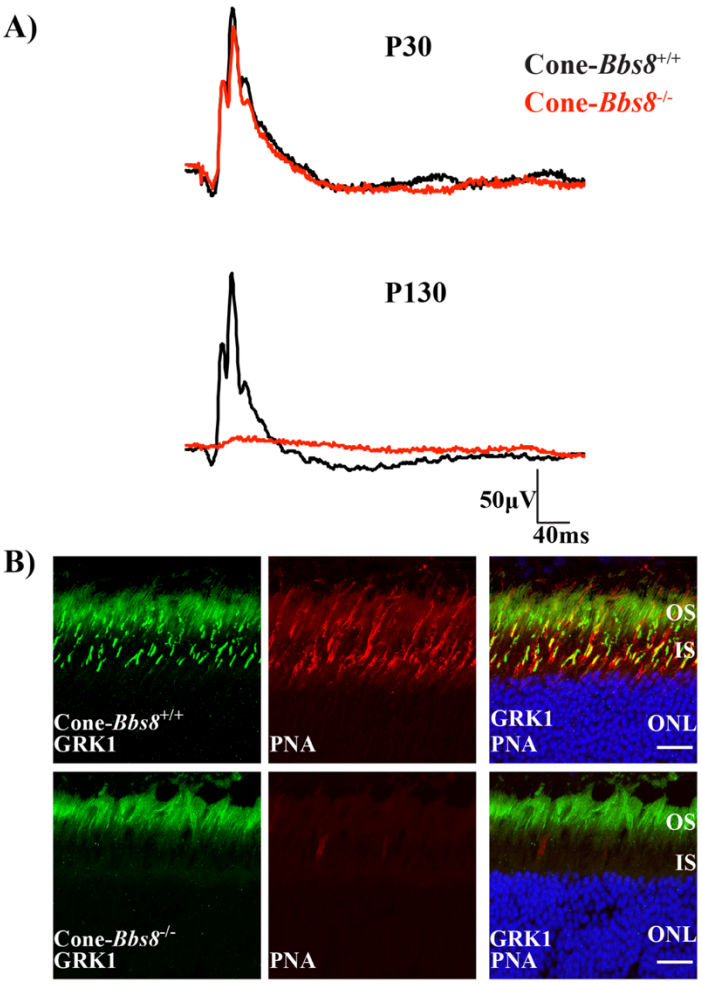

Figure 8: Degeneration of cone photoreceptors missing BBS8. (A) Representative trace of photopic ERG responses measured under light adapted conditions at 0.69 cd.s^{-1}m^2 in Cone-*Bbs8*$^{-/-}$ and littermate controls at P30 and P130. (B) Retinal cryosections stained against G-protein-coupled Receptor Kinase 1 (GRK1; green) and Peanut agglutinin (PNA) in Ret-*Bbs8*$^{-/-}$ and wild type littermate controls at P130. GRK1 stains both rods and cones while PNA marks the extracellular matrix surrounding the cones. Scale bar: 20µm.

red-green pigment promoter (HRGP-cre) (Supplementary Material, Fig. S5) (*120*). We evaluated the specificity of the *Cre* expression in cone photoreceptors by staining retinal cross-sections from cone-*Bbs8*$^{-/-}$ and littermate controls against Cre and the cone marker peanut agglutinin (PNA), which stains the cone outer sheath. As expected, Cre expression was specifically found in PNA+ cells (Supplementary Material, Fig. S5B). In this *Cre* driver line, robust expression of Cre recombinase starts at P10, and recombination as judged by cre reporter expression, is complete by P30 (*120*). Therefore, we performed photopic ERGs to examine cone function at P30 and observed no significant differences in ERG responses between Cone-*Bbs8*$^{-/-}$ and their wild type littermate controls (Fig. 8A). Although the cone ERGs were similar at P30, there is a progressive reduction in cone response with age (Supplementary Material, Fig. S6A), and by 4 months this response was completely ablated (Fig 8A). To investigate if loss of cone response is due to the death of cone photoreceptor cells, we performed immunocytochemistry using various cone markers at P120. GRK1, the kinase expressed in rods and cones (green) in littermate controls was specifically absent in cones from cone-*Bbs8*$^{-/-}$ animals (Fig. 8B). The loss of cones was confirmed by the reduced staining for PNA, cone arrestin, and cone phosphodiesterase 6 (Supplementary Material, Fig. S7). In addition, we observed uniform reduction in cone density by flat-mount in various regions of the retina (data not shown). We also performed scotopic ERGs at this age and saw no significant changes between experimental and wild-type animals, further corroborating the specificity of the cone-*Bbs8* animal model (Supplementary Material, Fig. S6B). Additionally, similar to our Ret-*Bbs8* animal model, we observed mislocalization of syntaxin 3 to cone OS at P30 (Figure 9B). At this stage, the localization of M-opsin was unaltered and was found in the cone OS (Figure 9A). Altogether, our results show that BBS8 presence in cone photoreceptors is essential for their viability (Fig. 8B and Supplementary Material, Fig. S7).

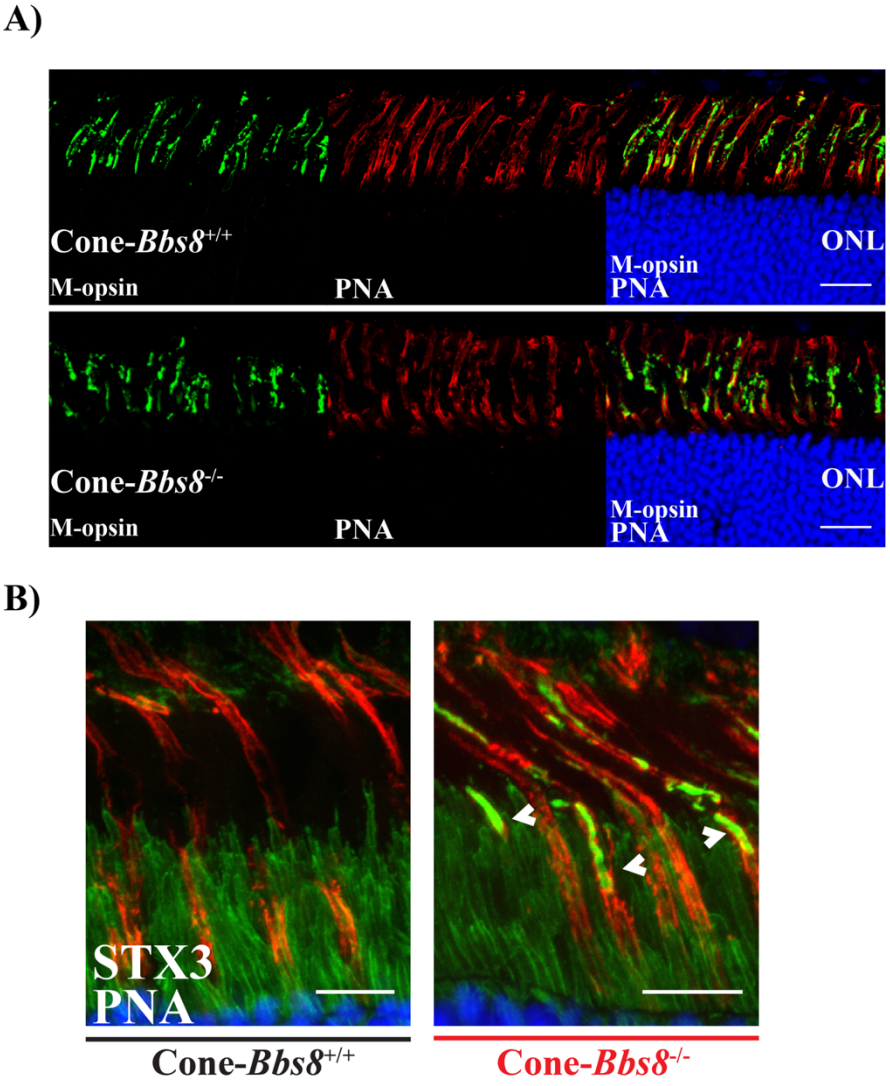

Figure 9: Mislocalization of Syntaxin 3 in cone photoreceptors lacking BBS8. (A) Immunolocalization of M-opsin and peanut agglutinin (PNA) in retinal cross-sections of Cone-*Bbs8*$^{-/-}$ animals compared to littermate controls at P30. Scale bar: 20µm. (B) Retinal cross-sections showing mislocalized synatxin 3 (white arrows; STX3 in green), co-stained with peanut agglutinin (PNA, red), in cones lacking BBS8 (Cone-*Bbs8*$^{-/-}$) compared to wild –type littermate controls at P30. Scale bar: 10µm.

BBS8 is critical for maintaining cone photoreceptor OS structure

We observed defects in rod OS development in our Ret-*Bbs8*$^{-/-}$ animals, and immunocytochemistry hinted at potential defects in cone OS in the Cone-*Bbs8*$^{-/-}$ animals. Therefore, we examined the structure of the cone outer segment by TEM in perfusion-fixed Cone-*Bbs8*$^{-/-}$ animals and wild-type controls at P30. We chose this age because photopic responses were comparable between Cone-*Bbs8*$^{-/-}$ and wild-type controls. Ultrastructural analysis revealed less tightly packed, elongated, and mis-oriented OS disc

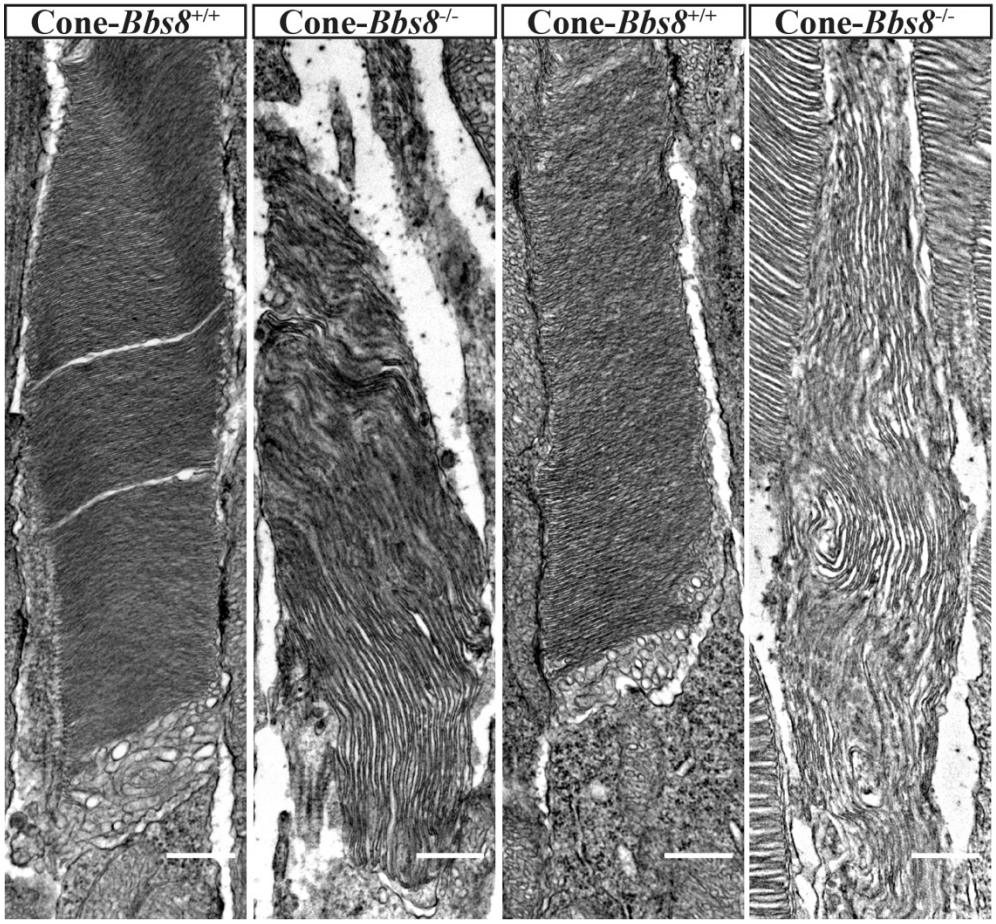

Figure 10: Defective cone OS ultrastructure in Cone-*Bbs8*$^{-/-}$ retinas. (A) Two representative images of cone OS each from wild-type and Cone-*Bbs8*$^{-/-}$ animals are shown. The vast majority of cones in knockout animals possessed abnormal OSs; disc stacks were less dense, of larger diameters, and were misaligned. In contrast, cones in the wild-type control possessed tightly stacked, properly aligned, and normal diameter discs. Scale bars: 500nm.

membranes of Cone-*Bbs8*$^{-/-}$ animals (Fig. 10). In conclusion, despite no significant changes in cone photoresponse at this age, absence of BBS8 leads to aberrant cone OS morphology.

DISCUSSION

Mutations in *BBS8* cause ciliopathies affecting multiple organs and invariably lead to loss of vision in early childhood (*94*). The importance of BBS8 in photoreceptor function is further exemplified by mutations in BBS8 that lead to non-syndromic retinitis pigmentosa, yet the role for BBS8 in photoreceptors is not known (*108-110*). In this study, we sought to investigate the role of BBS8 in the development and function of photoreceptor cells. Our studies using multiple murine models, including a complete knockout, retina and cone- specific removal of BBS8 lead to the following novel findings. We show that BBS8 is required for the development and maintenance of the photoreceptor cilia and outer segments in both rods and cones. Although mutations in BBS proteins are known to affect rod cells, this is the first study to demonstrate that BBSome function is also essential for cone photoreceptor structure, function, and viability. We observed dynamic changes in BBSome subunits that included increased levels of BBS1 and BBS4 in the absence of BBS8. Our studies indicate that altered photoreceptor OS development in the absence of BBS8 is likely due to defective ciliary structure indicated by sizable changes in acetylated tubulin staining zones or as a result of altered ciliary trafficking.

Alterations in cognate BBS subunits

Our study sought to understand the effects of BBS8 on the levels of cognate partner subunits that are part of the core octameric BBSome complex. The core of the BBSome is formed by BBS2/7/9 proteins, followed by the addition of BBS1/5/8, and the final incorporation of BBS4 (*100*). In BBS8 animal models, the expression of the core BBSome proteins are preserved in the retina with a minor reduction in BBS2 levels. BBS4, a tetratricopeptide repeat (TPR) protein similar to BBS8, was highly upregulated

in the absence of BBS8 prior to any significant photoreceptor degeneration (*94, 112, 113*). Interestingly BBS1, a protein that interacts with the small GTPase ARL6 (BBS3), an interaction necessary for the targeting of the BBSome to the membrane, was also up-regulated in the absence of BBS8 (*112*). Lastly, BBS5, a protein that is present in the photoreceptor axoneme and is absent in the connecting cilia was severely down-regulated. BBS5 interacts with arrestin and is hypothesized to alter its light-dependent translocation (*121*). Interestingly, previous reports indicate absence of BBS4 leads to impaired light-dependent translocation of transducin and arrestin in photoreceptor neurons (30). In BBS8 knockouts, we did not find any changes in arrestin or transducin translocation in response to light stimulus (data not shown). This could be due to the increased expression of BBS4 in BBS8 models, leading to proper arrestin and transducin translocation, or that arrestin and transducin can be transported by an alternative mechanism. All changes observed in BBS levels in the absence of BBS8 were post-transcriptional, as message levels were unaltered (data not shown). It is not clear if the observed phenotype is exclusively due to loss of BBS8 or the effect of altered BBSome subunits but further experiments are needed to address the mechanism behind the loss of OS development. One interesting question stemming from these results is if the changes in BBSome subunits after *Bbs8* depletion reflect a dynamic nature of this protein complex, which may exist in different states depending on subunit availability, presence of interacting molecules, or external signals.

Normal rhodopsin trafficking in the absence of BBS8.

Studies from multiple murine models lacking individual BBS subunits suggest a role for the BBSome in rhodopsin trafficking to the outer segments (*122, 123*). This is in agreement with results from primary cilia showing the need for the BBSome in GPCR trafficking (*102*). Alternatively, the BBSome is thought to be involved in retrograde trafficking of cargo from the OS to the IS and/or a role as a ciliary

'gatekeeper', as evidenced by mislocalization of non-OS proteins in the OS in BBS17 (Lztfl1) mutant mice (*107*). In our BBS8 models, we did not observe significant defects in anterograde trafficking of OS-resident cargoes, including rhodopsin. The vast majority of rhodopsin at P10, prior to photoreceptor degeneration, was present in the OS, similar to the littermate controls. However, we observed slight mislocalization at P17, which we believe is likely due to the indirect effect of dysmorphic outer segments in BBS8 knockouts (Supplementary Material, Fig. S2 and S3). Our studies indicate that BBS8 is not needed for rhodopsin trafficking but we cannot rule out the possibility that rhodopsin is able to reach the OS through a partially formed BBSome which may be compensating for the lack of BBS8 in our animal models. Our assays to investigate the formation of the BBSome complex failed because of the early morphological defects observed and the low levels of BBSome subunits in retina at P10. Importantly, animal models lacking BBS8 in rods or cones showed mislocalization of syntaxin in the OS, which agrees with current thinking that the BBSome is either involved in retrograde trafficking of proteins or acts as a ciliary gate in photoreceptors (*107*). However, further studies in photoreceptors are needed to confirm either of these hypotheses.

BBS8 is crucial for OS morphogenesis.

BBS8 animal models generated in this study show the need for BBS8 in the initial elaboration of the photoreceptor outer segments. The changes in photoreceptor ultrastructure correlated with reduced rod response in complete and retina-specific knockouts where BBS8 was conditionally removed in the developing embryonic retina.

Although mutations in BBS are linked to retinitis pigmentosa, which implies a primary impact on rod cells, a recent report documented predominant cone dysfunction in BBS patients (*124*). We investigated the potential importance of BBS8 for murine cones using a conditional knockout model, which ablates BBS8 from cones between P8-10. While we did not detect any abnormalities in cone function at P30 (by ERG), cone outer segments were dysmorphic and showed abnormal ultrastructure, with discs stacked vertically rather than horizontally. Unlike rod photoreceptors, where significant number of functioning cells survived at four months in the absence of BBS8, cone degeneration was far more profound, and function was lost in parallel. The reason for cone degeneration is likely linked to the morphological changes in cone OS. Overall, the findings from our studies show a critical need for BBS8 in cone survival and function.

We also observed an accumulation of electron dense extracellular vesicles (EVs), in the extracellular space adjacent to the photoreceptor inner segments in BBS8 null retina. The accumulation of ectosomes, a class of extra cellular vesicles that are derived from ciliary plasma membranes, were also observed in the absence of BBS and IFT proteins in primary cilium in cultured kidney cells and mouse embryonic fibroblasts (*125*). Intriguingly, mutation of another ciliopathy protein, IFT88, has also been shown to generate EVs of similar appearance and distribution (*126*) . That study documented the presence of rhodopsin in the EVs, and noted that numerous other mouse models defective for OS assembly also accumulate EVs. A more recent investigation identified subretinal EVs in the *retinal degeneration slow* (*rds*) null mouse as ectosomes (*127*). Because that study observed that ectosome shedding was stimulated by peripherin-2/rds loss, and we detected a major reduction (65%) in peripherin-2/rds levels in the absence of BBS8 at P10, it is conceivable that peripherin-2/rds loss in the BBS8 knockout

likewise stimulates EV accumulation. It is also possible that a more general disruption of OS disc membrane morphogenesis contributed to this phenotype.

Hyper-acetylation of ciliary microtubules in the absence of BBS8

Our ultrastructural analyses in BBS8 knockout animals show connecting cilium that are of comparable length to the littermate controls (Supplementary Material, Fig. S3). This is in agreement with RPGR staining, a maker for the connecting cilium (*114, 115*). However, the acetylated tubulin staining on photoreceptor cilia was longer in photoreceptors lacking BBS8 (Fig. 7). In photoreceptors, acetylated tubulin marks connecting cilium and the proximal part of the axoneme (*119*). RP1 exclusively stains the entire axoneme (*116, 117*). In the absence of BBS8, it appears that the increase in acetylated tubulin staining comes at the loss in axonemal staining by RP1 (Supplementary Material, Fig. S4A and S4C). A corresponding reduction in MAK, another axonemal marker confirms this finding (*118*). The observed changes in MAK or RP1 staining of the axoneme could also be due to altered ciliary trafficking. Acetylation of tubulin marks long-lived tubulin molecules and recent studies show the importance of this tubulin post-translational modification in increased mechanical stabilization and protection against breakage (*128, 129*). The observed increase in acetylated tubulin staining could be due to the established interaction between BBS proteins and α-Tubulin N-acetyltransferase-1 (αTAT1), the major α-tubulin acetyl transferase that acetylates tubulin in the cilium or alterations in the BBSome subunit, BBS18, a known regulator of tubulin acetylation (*101, 130*). Interestingly, hyperacetylation of tubulin in the absence of BBS8 was accompanied by an increase in tubulin glutamylation, a C-terminal post-translational modification that marks stable microtubules (Supplementary Material, Fig. S8). Hyperglutamylation is a known cause of photoreceptor neuronal degeneration in *pcd* (*Purkinje cell degeneration*) and in TTLL3 (*Tubulin Tyrosine ligase-like*) mouse models. In these models, increased

glutamylation leads to a compensatory decrease in tubulin glycation (*131-133*). Currently it is unclear how these changes in photoreceptor cilia relate to defects in outer segment formation and photoreceptor cell death. Further studies are underway to investigate the mechanism behind the altered tubulin posttranslational modifications and impaired outer segment formation.

MATERIALS AND METHODS

Animals, Genotyping and Maintenance

BBS8 knockout mouse line (Ttc8 $^{tm1a(KOMP)Wtsi}$) was recovered using sperm obtained from KOMP (https://www.komp.org/geneinfo.php?geneid=85321) (Project id: CSD28015, Knock out first). Along with LoxP sites flanking exon 4 to 6 of the BBS8 gene, the KOMP targeting construct knocks-in a cassette containing a splice acceptor with LacZ reporter, polyadenylation signal and neomycin selection at *Bbs8* locus between exons 3 and 4 that terminates the transcript. The LacZ/neomycin cassette is flanked by FRT sites and can be excised with FLP recombinase to restore the expression of the BBS8 gene. The animals were backcrossed with C57BL/6J (Jackson laboratory) to eliminate the *rd8* allele (*134*). Heterozygous mice were intercrossed, and the progeny were genotyped using genomic DNA prepared from ear punches by PCR. The following primers (5' GGA TCA CAG TCA AGA GTA GAG TC 3' and (5' CAC ACG TGT TTC TCC TTA GAG GC 3') were used to verify the presence of the Neomycin gene. (5' ATC ACG ACG CGC TGT ATC 3' and 5' ACA TCG GGC AAA TAA TAT CG 3') primers were used to assess the presence of the *LacZ* reporter gene.

To produce the conditional knockouts, we first removed the termination cassette (LacZ/neomycin) by crossing BBS8 animals heterozygous for KOMP cassette with transgenic mice expressing FLP recombinase (Jax stock #012930). This cross resulted in a floxed *Bbs8* allele (*Bbs8 +/fl*). The homozygous floxed animals were subsequently crossed with animals expressing Cre recombinase under the retina and forebrain specific *Six3* promoter and bred to produce *Six3-Cre*: *Bbs8 fl/fl* animals (*135*). A similar strategy was used to produce cone specific knockouts using Cre recombinase expressed under human red green pigment (HRGP) promoter (*120*).Oligonucleotides used in PCR to detect *Cre*

recombinase were 5’ CCT GGA AAA TGC TTC TGT CCG 3’ and 5’ CAG GGT GTT ATA AGC AAT CCC 3’. Primers used to detect floxed alleles were 5’ GGT GAC CAG AAG CAA GCA CAT A 3’ and 5’ GGC TGC TGT CTG GTT GAG TAA T 3’. Institutional Animal Care and Use Committee of the West Virginia University approved all experimental procedures involving animals conducted in this study.

Electroretinograpy (ERG)

ERGs were carried out on the UTAS Visual Diagnostic System with Big-Shot Ganzfeld with UBA-4200 amplifier and interface, and EMWIN 9.0.0 software (LKC Technologies, Gaithersburg, MD, USA). Prior to testing, mice were dark-adapted for 24 hours. Animals were anesthetized [2.0% isoflurane with 2.5 liters per minute (lpm) oxygen flow rate] for 10 minutes and eyes were topically dilated with a 1:1 mixture of tropicamide:phenylephrine hydrochloride. For ERG testing, mice were positioned on a heated platform with continuous flow of isoflurane through a nose cone [1.5% isoflurane with 2.5 liters per minute (lpm) oxygen flow rate]. A reference electrode was inserted subcutaneously in the scalp. ERG responses were recorded from both eyes with silver wire electrodes placed on top of each cornea, with contact being made with hypromellose solution (2% hypromellose in PBS) (Gonioscopic Prism Solution, Wilson Ophthalmic, Mustang, OK, USA). Scotopic (Rod-dominant) responses were obtained in the dark with flashes of LED white light at increasing flash intensities. For photopic response, animals were light adapted with rod-saturating white background light (30 cd $\cdot$ $m^{-}2$) for 10 minutes and cone responses were subsequently recorded.

Antibodies

The antibodies used in this study are described in *Supplementary Table I*.

Western Blot

Mice were euthanized by CO_2 inhalation followed by cervical dislocation and eyes were enucleated. For immunoblots, flash-frozen retinae dissected from enucleated eyes were sonicated in phosphate buffered saline [PBS: 137mM NaCl, 2.7 mM KCl, 4.3 mM $Na_2HPO_4 \cdot 7H_2O$, 1.4 mM KH_2PO_4, with protease inhibitor cocktail (Roche)]. Protein concentrations were measured using a NanoDrop spectrophotometer (Thermo Fisher Scientific, Inc.). Equal amounts of samples (100 μg total protein per well) were separated in a polyacrylamide SDS–PAGE gel and transferred onto polyvinylidene difluoride (PVDF) membranes (Immunobilon-FL, Millipore, Billerica). The membranes were then blocked with blocking buffer (Rockland Inc.) for 30 minutes at room temperature and further incubated with primary antibodies overnight at 4°C. Following incubation, membranes were washed in PBST (PBS with 0.1% Tween-20) three times for 5 minutes each at room temperature and incubated in secondary antibody, goat anti-rabbit Alexa 680 (or 800), rabbit anti-goat Alexa 680 or goat anti-mouse Alexa 680 (Invitrogen) for 45 minutes at room temperature. After washes with PBST, membranes were scanned using the Odyssey Infrared Imaging System (LI-COR Biosciences, Lincoln, NE, USA).

Immunocytochemistry

For immunofluorescence, enucleated eyes were submerged in 4% paraformaldehyde fixative for 5 minutes prior to removal of the cornea and lens. Eyecups were fixed for an additional hour, then washed in PBS three times for 5 minutes each, and incubated in 20% sucrose in PBS overnight at 4°C. Eyes were then incubated in 1:1 mixture of 20% sucrose in PBS:OCT (Cryo Optimal Cutting Temperature

Compound, Sakura) for 1 hour and flash-frozen in OCT. The cryosectioning was performed using Leica CM1850 Cryostat, and retinal sections of 16 μm and/or 10 μm (for ciliary staining) thickness were mounted on Superfrost Plus slides (Fisher Scientific). Retinal sections were mounted on slides, washed with PBST and incubated for 1 hour in blocking buffer at room temperature (PBS with 5% Goat Sera, 0.5% TritonX-100, 0.05% Sodium Azide). After blocking, retinal sections were incubated with primary antibodies at the dilutions described in *Supplementary Table I* at 4°C overnight. Afterwards, retinal sections were washed two times for 10 minutes with PBST and once for 5 minutes with PBS before incubation with secondary antibody at a 1:1000 dilution [DAPI nuclear stain 405, anti-Rabbit 488 (or 568), anti-mouse 488 (or 568)] for 1 h. For ciliary staining, enucleated eyes were fixed in 4% paraformaldehyde in PBS for 30 seconds and flash-frozen in OCT. Sectioning and staining were performed as stated above. Slides were mounted with ProLong Gold (Life Technologies) and cover slipped. Confocal imaging was performed at the WVU Microscope Imaging Facility with a Zeiss LSM 510 laser scanning confocal on a LSM Axioimager upright microscope using excitation wavelengths of 405, 488, 543 and 647 nm.

Ultrastructural analysis

Enucleated eyes were fixed (2% paraformaldehyde, 2.5% glutaraldehyde,0.1 M cacodylate buffer, pH 7.5) for 30 min prior to dissection and removal of the cornea and lens, followed by 48 h fixation at room temperature. Dissection, embedding and transmission electron microscopy was done according to previously established methods (*83, 136, 137*). For analyses of cone outer segment morphology, prior to fixation of enucleated eyes, mice underwent transcardial fixation perfusion with 2% paraformaldehyde, 2.5% glutaraldehyde, 0.1 M cacodylate buffer, pH 7.5.

Statistics

All data are presented as mean ± standard error margin. ERG data were analyzed by unpaired, two-tailed *t* test. For cilia measurements, 80-100 cilia were measured for each animal (n=3) and data were visualized with the ggplot2 package in R version 3.3.2. Image and densitometry analysis were performed using ImageJ 1.50i along with the Bio-Formats plugin (NIH).

ACKNOWLEDGEMENTS

The authors thank Zachary Wright, Caity Haring, Jessica Clemente and Dr. Eric Tucker (WVU) for help with data collection.

FUNDING

This work was supported by National Institutes of Health Grants R01 EY025536 (to VR and PS), R21 EY027707 (to VR), West Virginia Lions and Lions Club International Foundation.

CONFLICT OF INTEREST

The authors declare no conflict of interests.

REFERENCES

1 Ansley, S.J., Badano, J.L., Blacque, O.E., Hill, J., Hoskins, B.E., Leitch, C.C., Kim, J.C., Ross, A.J., Eichers, E.R., Teslovich, T.M. *et al.* (2003) Basal body dysfunction is a likely cause of pleiotropic Bardet-Biedl syndrome. *Nature*, **425**, 628-633.

2 Forsythe, E. and Beales, P.L. (2013) Bardet-Biedl syndrome. *Eur J Hum Genet*, **21**, 8-13.

3 Novas, R., Cardenas-Rodriguez, M., Irigoin, F. and Badano, J.L. (2015) Bardet-Biedl syndrome: Is it only cilia dysfunction? *FEBS Lett*, **589**, 3479-3491.

4 Zaghloul, N.A. and Katsanis, N. (2009) Mechanistic insights into Bardet-Biedl syndrome, a model ciliopathy. *J Clin Invest*, **119**, 428-437.

5 Heon, E., Kim, G., Qin, S., Garrison, J.E., Tavares, E., Vincent, A., Nuangchamnong, N., Scott, C.A., Slusarski, D.C. and Sheffield, V.C. (2016) Mutations in C8ORF37 cause Bardet Biedl syndrome (BBS21). *Hum Mol Genet*, **25**, 2283-2294.

6 Lindstrand, A., Frangakis, S., Carvalho, C.M., Richardson, E.B., McFadden, K.A., Willer, J.R., Pehlivan, D., Liu, P., Pediaditakis, I.L., Sabo, A. *et al.* (2016) Copy-Number Variation Contributes to the Mutational Load of Bardet-Biedl Syndrome. *Am J Hum Genet*, **99**, 318-336.

7 Nachury, M.V., Loktev, A.V., Zhang, Q., Westlake, C.J., Peranen, J., Merdes, A., Slusarski, D.C., Scheller, R.H., Bazan, J.F., Sheffield, V.C. *et al.* (2007) A core complex of BBS proteins cooperates with the GTPase Rab8 to promote ciliary membrane biogenesis. *Cell*, **129**, 1201-1213.

8 Zhang, Q., Yu, D., Seo, S., Stone, E.M. and Sheffield, V.C. (2012) Intrinsic protein-protein interaction-mediated and chaperonin-assisted sequential assembly of stable bardet-biedl syndrome protein complex, the BBSome. *J Biol Chem*, **287**, 20625-20635.

9 Loktev, A.V., Zhang, Q., Beck, J.S., Searby, C.C., Scheetz, T.E., Bazan, J.F., Slusarski, D.C., Sheffield, V.C., Jackson, P.K. and Nachury, M.V. (2008) A BBSome subunit links ciliogenesis, microtubule stability, and acetylation. *Dev Cell*, **15**, 854-865.

10 Berbari, N.F., Lewis, J.S., Bishop, G.A., Askwith, C.C. and Mykytyn, K. (2008) Bardet-Biedl syndrome proteins are required for the localization of G protein-coupled receptors to primary cilia. *Proc Natl Acad Sci U S A*, **105**, 4242-4246.

11 Tadenev, A.L., Kulaga, H.M., May-Simera, H.L., Kelley, M.W., Katsanis, N. and Reed, R.R. (2011) Loss of Bardet-Biedl syndrome protein-8 (BBS8) perturbs olfactory function, protein localization, and axon targeting. *Proc Natl Acad Sci U S A*, **108**, 10320-10325.

12 Pearring, J.N., Salinas, R.Y., Baker, S.A. and Arshavsky, V.Y. (2013) Protein sorting, targeting and trafficking in photoreceptor cells. *Prog Retin Eye Res*, **36**, 24-51.

13 Wensel, T.G., Zhang, Z., Anastassov, I.A., Gilliam, J.C., He, F., Schmid, M.F. and Robichaux, M.A. (2016) Structural and molecular bases of rod photoreceptor morphogenesis and disease. *Prog Retin Eye Res*, **55**, 32-51.

14 Young, R.W. (1967) The renewal of photoreceptor cell outer segments. *J Cell Biol*, **33**, 61-72.

15 Datta, P., Allamargot, C., Hudson, J.S., Andersen, E.K., Bhattarai, S., Drack, A.V., Sheffield, V.C. and Seo, S. (2015) Accumulation of non-outer segment proteins in the outer segment underlies photoreceptor degeneration in Bardet-Biedl syndrome. *Proc Natl Acad Sci U S A*, **112**, E4400-4409.

16 Goyal, S., Jager, M., Robinson, P.N. and Vanita, V. (2015) Confirmation of TTC8 as a disease gene for nonsyndromic autosomal recessive retinitis pigmentosa (RP51). *Clin Genet*, in press.

17 Riazuddin, S.A., Iqbal, M., Wang, Y., Masuda, T., Chen, Y., Bowne, S., Sullivan, L.S., Waseem, N.H., Bhattacharya, S., Daiger, S.P. *et al.* (2010) A splice-site mutation in a retina-specific exon of BBS8 causes nonsyndromic retinitis pigmentosa. *Am J Hum Genet*, **86**, 805-812.

18 Murphy, D., Singh, R., Kolandaivelu, S., Ramamurthy, V. and Stoilov, P. (2015) Alternative Splicing Shapes the Phenotype of a Mutation in BBS8 To Cause Nonsyndromic Retinitis Pigmentosa. *Mol Cell Biol*, **35**, 1860-1870.
19 Robson, J.G. and Frishman, L.J. (1998) Dissecting the dark-adapted electroretinogram. *Doc Ophthalmol*, **95**, 187-215.
20 Jin, H., White, S.R., Shida, T., Schulz, S., Aguiar, M., Gygi, S.P., Bazan, J.F. and Nachury, M.V. (2010) The conserved Bardet-Biedl syndrome proteins assemble a coat that traffics membrane proteins to cilia. *Cell*, **141**, 1208-1219.
21 Kim, J.C., Badano, J.L., Sibold, S., Esmail, M.A., Hill, J., Hoskins, B.E., Leitch, C.C., Venner, K., Ansley, S.J., Ross, A.J. *et al.* (2004) The Bardet-Biedl protein BBS4 targets cargo to the pericentriolar region and is required for microtubule anchoring and cell cycle progression. *Nat Genet*, **36**, 462-470.
22 Hong, D.H., Pawlyk, B., Sokolov, M., Strissel, K.J., Yang, J., Tulloch, B., Wright, A.F., Arshavsky, V.Y. and Li, T. (2003) RPGR isoforms in photoreceptor connecting cilia and the transitional zone of motile cilia. *Invest Ophthalmol Vis Sci*, **44**, 2413-2421.
23 Zhao, Y., Hong, D.H., Pawlyk, B., Yue, G., Adamian, M., Grynberg, M., Godzik, A. and Li, T. (2003) The retinitis pigmentosa GTPase regulator (RPGR)- interacting protein: subserving RPGR function and participating in disc morphogenesis. *Proc Natl Acad Sci U S A*, **100**, 3965-3970.
24 Liu, Q., Lyubarsky, A., Skalet, J.H., Pugh, E.N., Jr. and Pierce, E.A. (2003) RP1 is required for the correct stacking of outer segment discs. *Invest Ophthalmol Vis Sci*, **44**, 4171-4183.
25 Liu, Q., Zuo, J. and Pierce, E.A. (2004) The retinitis pigmentosa 1 protein is a photoreceptor microtubule-associated protein. *J Neurosci*, **24**, 6427-6436.
26 Omori, Y., Chaya, T., Katoh, K., Kajimura, N., Sato, S., Muraoka, K., Ueno, S., Koyasu, T., Kondo, M. and Furukawa, T. (2010) Negative regulation of ciliary length by ciliary male germ cell-associated kinase (Mak) is required for retinal photoreceptor survival. *Proc Natl Acad Sci U S A*, **107**, 22671-22676.
27 Arikawa, K. and Williams, D.S. (1993) Acetylated alpha-tubulin in the connecting cilium of developing rat photoreceptors. *Invest Ophthalmol Vis Sci*, **34**, 2145-2149.
28 Le, Y.Z., Ash, J.D., Al-Ubaidi, M.R., Chen, Y., Ma, J.X. and Anderson, R.E. (2004) Targeted expression of Cre recombinase to cone photoreceptors in transgenic mice. *Mol Vis*, **10**, 1011-1018.
29 Smith, T.S., Spitzbarth, B., Li, J., Dugger, D.R., Stern-Schneider, G., Sehn, E., Bolch, S.N., McDowell, J.H., Tipton, J., Wolfrum, U. *et al.* (2013) Light-dependent phosphorylation of Bardet-Biedl syndrome 5 in photoreceptor cells modulates its interaction with arrestin1. *Cell Mol Life Sci*, **70**, 4603-4616.
30 Abd-El-Barr, M.M., Sykoudis, K., Andrabi, S., Eichers, E.R., Pennesi, M.E., Tan, P.L., Wilson, J.H., Katsanis, N., Lupski, J.R. and Wu, S.M. (2007) Impaired photoreceptor protein transport and synaptic transmission in a mouse model of Bardet-Biedl syndrome. *Vision Res*, **47**, 3394-3407.
31 Nishimura, D.Y., Fath, M., Mullins, R.F., Searby, C., Andrews, M., Davis, R., Andorf, J.L., Mykytyn, K., Swiderski, R.E., Yang, B. *et al.* (2004) Bbs2-null mice have neurosensory deficits, a defect in social dominance, and retinopathy associated with mislocalization of rhodopsin. *Proc Natl Acad Sci U S A*, **101**, 16588-16593.
32 Scheidecker, S., Hull, S., Perdomo, Y., Studer, F., Pelletier, V., Muller, J., Stoetzel, C., Schaefer, E., Defoort-Dhellemmes, S., Drumare, I. *et al.* (2015) Predominantly Cone-System Dysfunction as Rare Form of Retinal Degeneration in Patients With Molecularly Confirmed Bardet-Biedl Syndrome. *Am J Ophthalmol*, **160**, 364-372 e361.

33 Nager, A.R., Goldstein, J.S., Herranz-Perez, V., Portran, D., Ye, F., Garcia-Verdugo, J.M. and Nachury, M.V. (2017) An Actin Network Dispatches Ciliary GPCRs into Extracellular Vesicles to Modulate Signaling. *Cell*, **168**, 252-263 e214.
34 Pazour, G.J., Baker, S.A., Deane, J.A., Cole, D.G., Dickert, B.L., Rosenbaum, J.L., Witman, G.B. and Besharse, J.C. (2002) The intraflagellar transport protein, IFT88, is essential for vertebrate photoreceptor assembly and maintenance. *J Cell Biol*, **157**, 103-113.
35 Salinas, R.Y., Pearring, J.N., Ding, J.D., Spencer, W.J., Hao, Y. and Arshavsky, V.Y. (2017) Photoreceptor discs form through peripherin-dependent suppression of ciliary ectosome release. *J Cell Biol*, **216**, 1489-1499.
36 Portran, D., Schaedel, L., Xu, Z., Thery, M. and Nachury, M.V. (2017) Tubulin acetylation protects long-lived microtubules against mechanical ageing. *Nat Cell Biol*, **19**, 391-398.
37 Xu, Z., Schaedel, L., Portran, D., Aguilar, A., Gaillard, J., Marinkovich, M.P., Thery, M. and Nachury, M.V. (2017) Microtubules acquire resistance from mechanical breakage through intralumenal acetylation. *Science*, **356**, 328-332.
38 Shida, T., Cueva, J.G., Xu, Z., Goodman, M.B. and Nachury, M.V. (2010) The major alpha-tubulin K40 acetyltransferase alphaTAT1 promotes rapid ciliogenesis and efficient mechanosensation. *Proc Natl Acad Sci U S A*, **107**, 21517-21522.
39 Blanks, J.C., Mullen, R.J. and LaVail, M.M. (1982) Retinal degeneration in the pcd cerebellar mutant mouse. II. Electron microscopic analysis. *J Comp Neurol*, **212**, 231-246.
40 Bosch Grau, M., Masson, C., Gadadhar, S., Rocha, C., Tort, O., Marques Sousa, P., Vacher, S., Bieche, I. and Janke, C. (2017) Alterations in the balance of tubulin glycylation and glutamylation in photoreceptors leads to retinal degeneration. *J Cell Sci*, **130**, 938-949.
41 LaVail, M.M., Blanks, J.C. and Mullen, R.J. (1982) Retinal degeneration in the pcd cerebellar mutant mouse. I. Light microscopic and autoradiographic analysis. *J Comp Neurol*, **212**, 217-230.
42 Mattapallil, M.J., Wawrousek, E.F., Chan, C.C., Zhao, H., Roychoudhury, J., Ferguson, T.A. and Caspi, R.R. (2012) The Rd8 mutation of the Crb1 gene is present in vendor lines of C57BL/6N mice and embryonic stem cells, and confounds ocular induced mutant phenotypes. *Invest Ophthalmol Vis Sci*, **53**, 2921-2927.
43 Furuta, Y., Lagutin, O., Hogan, B.L. and Oliver, G.C. (2000) Retina- and ventral forebrain-specific Cre recombinase activity in transgenic mice. *Genesis*, **26**, 130-132.
44 Kirschman, L.T., Kolandaivelu, S., Frederick, J.M., Dang, L., Goldberg, A.F., Baehr, W. and Ramamurthy, V. (2010) The Leber congenital amaurosis protein, AIPL1, is needed for the viability and functioning of cone photoreceptor cells. *Hum Mol Genet*, **19**, 1076-1087.
45 Ku, C.A., Chiodo, V.A., Boye, S.L., Hayes, A., Goldberg, A.F., Hauswirth, W.W. and Ramamurthy, V. (2015) Viral-mediated vision rescue of a novel AIPL1 cone-rod dystrophy model. *Hum Mol Genet*, **24**, 670-684.
46 Wright, Z.C., Singh, R.K., Alpino, R., Goldberg, A.F., Sokolov, M. and Ramamurthy, V. (2016) ARL3 regulates trafficking of prenylated phototransduction proteins to the rod outer segment. *Hum Mol Genet*, **25**, 2031-2044.

Supplementary Material

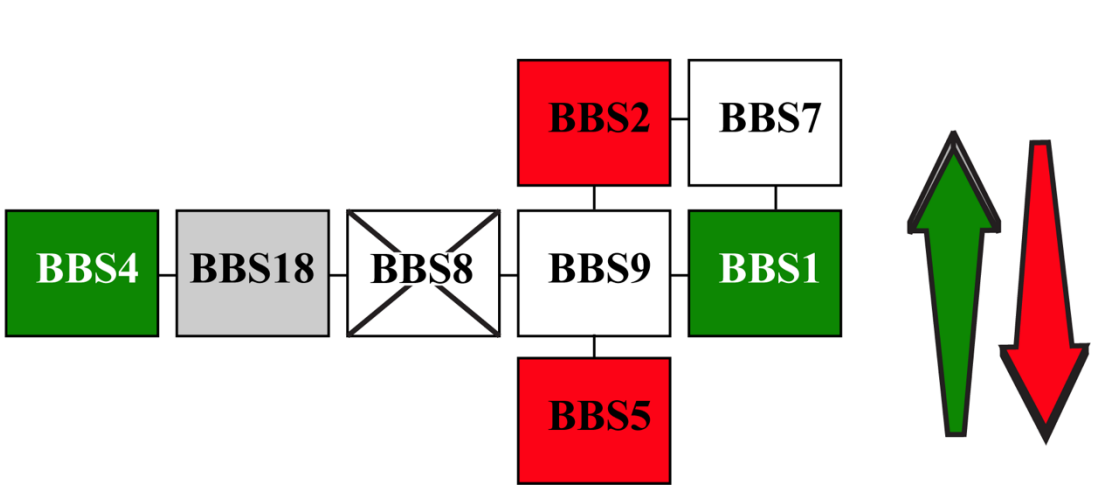

Supplementary Figure 1. Scheme showing changes in BBS subunits in the absence of BBS8.

Scheme displaying changes in BBS subunit levels in the absence of BBS8 (Red = decrease, Green = increase, White = no change, Gray = untested).

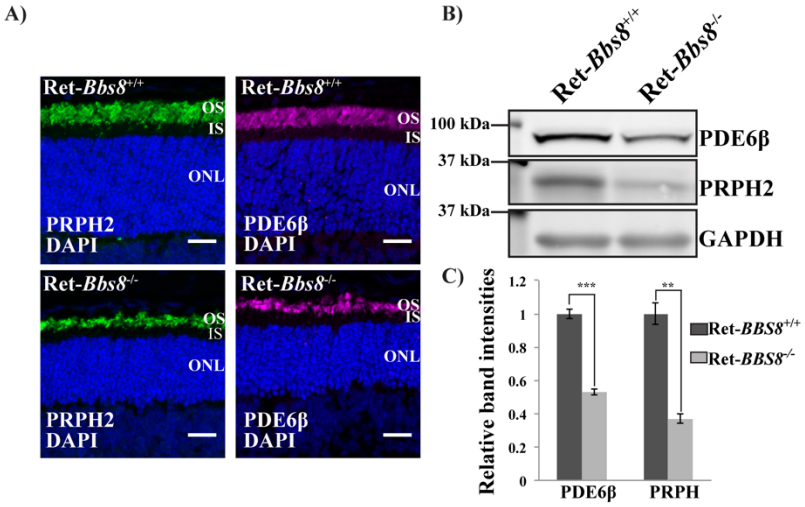

Supplementary Figure 2. Normal trafficking of OS-resident proteins in the retina lacking BBS8.

(A) Staining for peripherin-2/rds (PRPH2, green) and phosphodiesterase (PDE6β, cyan), DAPI , 4',6-diamidino-2-phenylindole (Blue); marks the nuclei. (B) Representative immunoblot of P12 retinal lysates from Ret-*Bbs8* $^{-/-}$ and littermate controls. (C) Quantification of retinal isolates from Ret-*Bbs8* $^{-/-}$ and littermate controls (PRPH2 : $P = 0.0008$, PDE6β : $P = 0.0002$). Scale bars: 20µm.

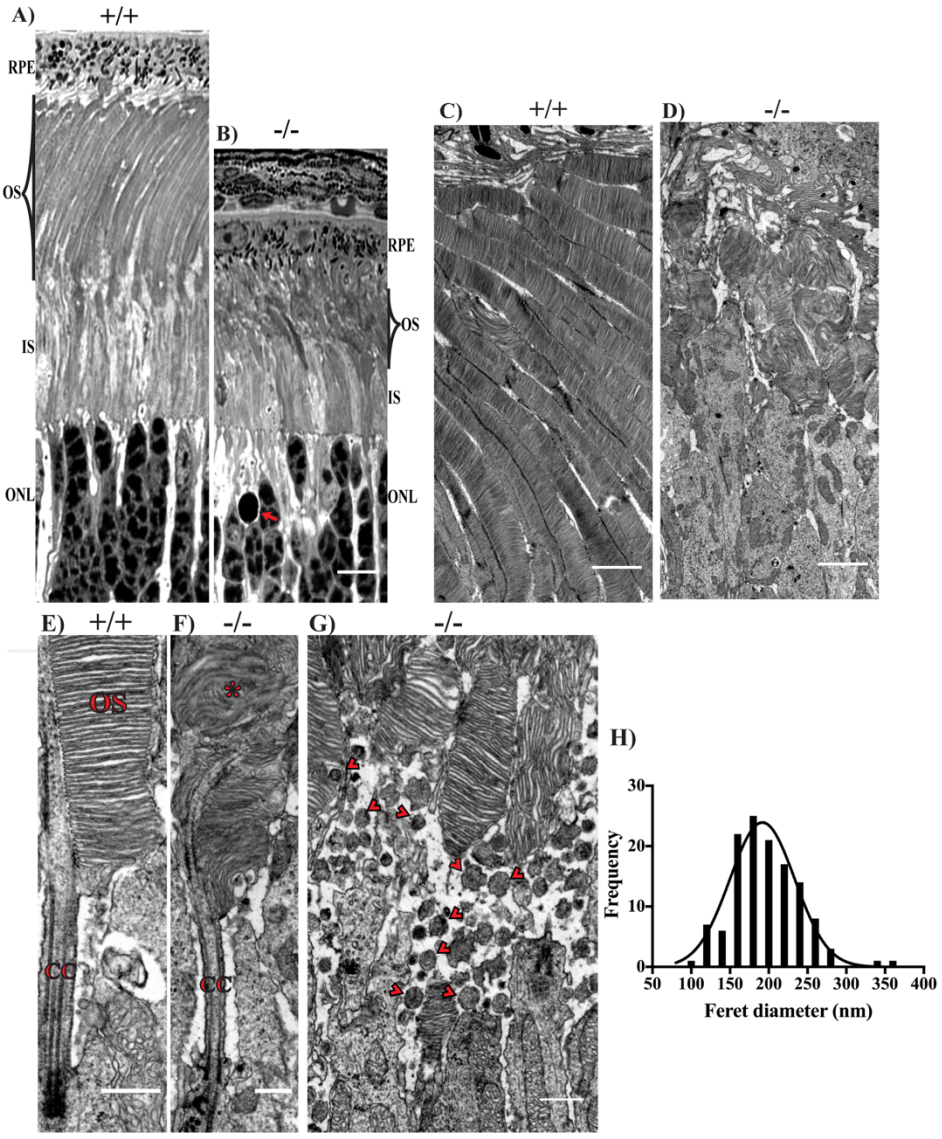

Supplementary Figure 3. Morphology of photoreceptors at P18.

(A) Toluidine blue-stained semi-thin retinal sections from *Bbs8*$^{+/+}$ showing normally organized retinal layers. Scale bar: 5 µm. (B) *Bbs8*$^{-/-}$ retinal section with reduced IS and OS layers and pyknotic nuclei

(arrow). (C) Organized and developed mature photoreceptor OS in *Bbs8*$^{+/+}$. Scale bar: 2 μm. (D) Reduced rod OS density with disordered and shortened photoreceptor OS in *Bbs8*$^{-/-}$. Scale bar: 2 μm. (E) Normally stacked OS disc membranes and connecting cilia (CC) in *Bbs8*$^{+/+}$ (CC average = 1.6μm, N=3). (F) Dysmorphic OS (asterisk) in *Bbs8*$^{-/-}$ (CC average = 1.7μm, N=3). (G) Extracellular vesicles (arrows) in *Bbs8*$^{-/-}$ retina. Scale bar: 500nm. (H) Gaussian histogram of Feret diameter measurements (nm) of extracellular vesicles found in *Bbs8*$^{-/-}$ animals (N = 126 from two animals).

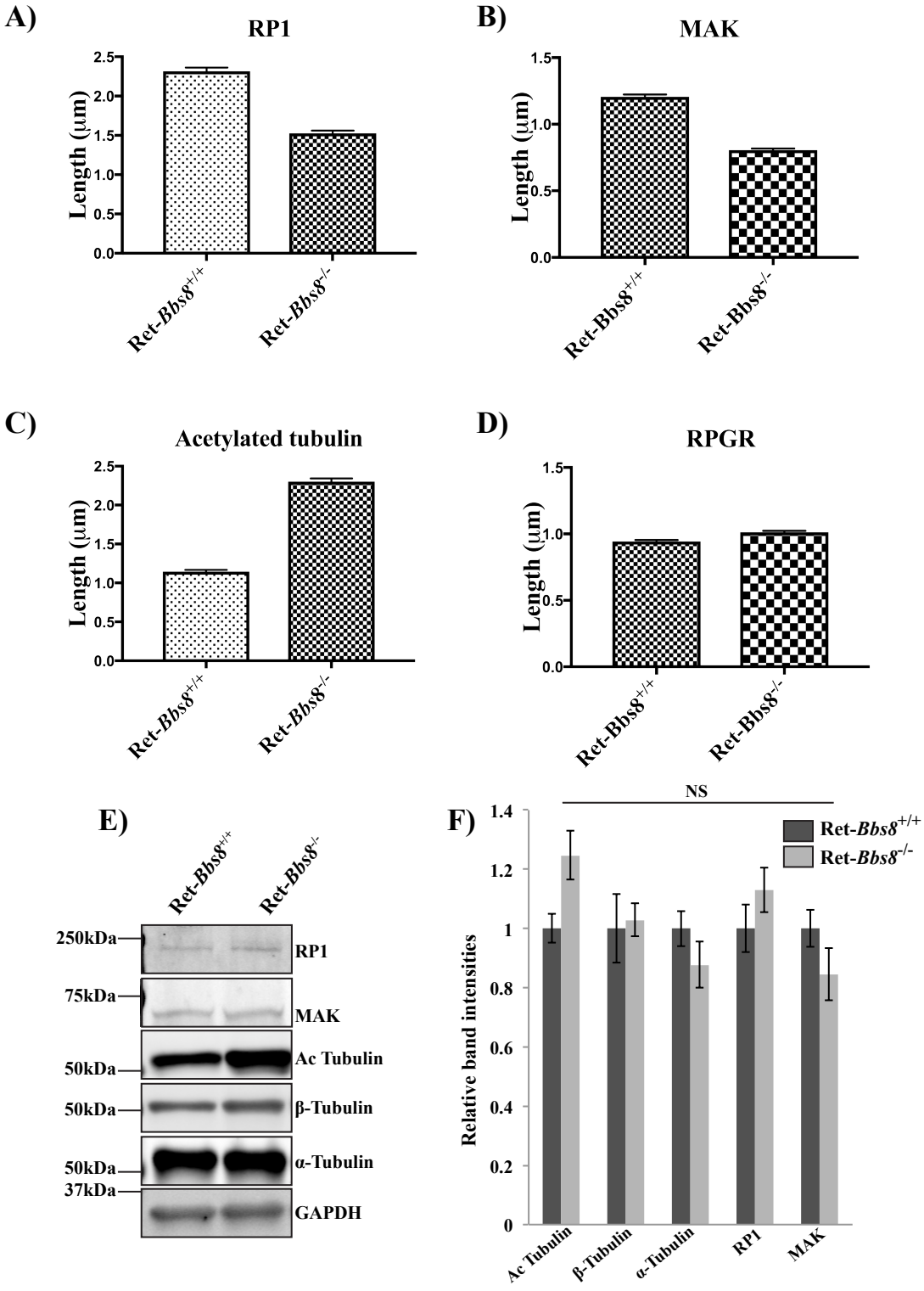
A)
RP1
Length (μm)
2.5
2.0
1.5
1.0
0.5
0.0
Ret-Bbs8+/+
Ret-Bbs8-/-
B)
MAK
Length (μm)
1.5
1.0
0.5
0.0
Ret-Bbs8+/+
Ret-Bbs8-/-
C)
Acetylated tubulin
Length (μm)
2.5
2.0
1.5
1.0
0.5
0.0
Ret-Bbs8+/+
Ret-Bbs8-/-
D)
RPGR
Length (μm)
1.5
1.0
0.5
0.0
Ret-Bbs8+/+
Ret-Bbs8-/-
E)
Ret-Bbs8+/+
Ret-Bbs8-/-
250kDa
RP1
75kDa
MAK
50kDa
Ac Tubulin
50kDa
β-Tubulin
50kDa
α-Tubulin
37kDa
GAPDH
F)
NS
Ret-Bbs8+/+
Ret-Bbs8-/-
Relative band intensities
1.4
1.2
1
0.8
0.6
0.4
0.2
0
Ac Tubulin
β-Tubulin
α-Tubulin
RP1
MAK

Supplementary Figure 4. Length measurements of ciliary zones in retina lacking BBS8 at P10. (A-D) Graphs depicting the calculated mean for the length measurements of Retinitis Pigmentosa-1 (RP1), Male Germ Cell Associated Kinase (MAK), acetylated tubulin, and retinitis pigmentosa GTPase regulator (RPGR) in retina lacking BBS8 compared to littermate controls at P10. Error bars represent SEM, $P = 0.0001$. (E) Representative immunoblots of P10 retinal protein samples stained against ciliary markers in retina lacking BBS8 compared to wild-type littermate controls. (F) Quantification of protein levels from Ret-*Bbs8*$^{-/-}$ and Ret-*Bbs8*$^{+/+}$ retinal isolates (NS = no significance).

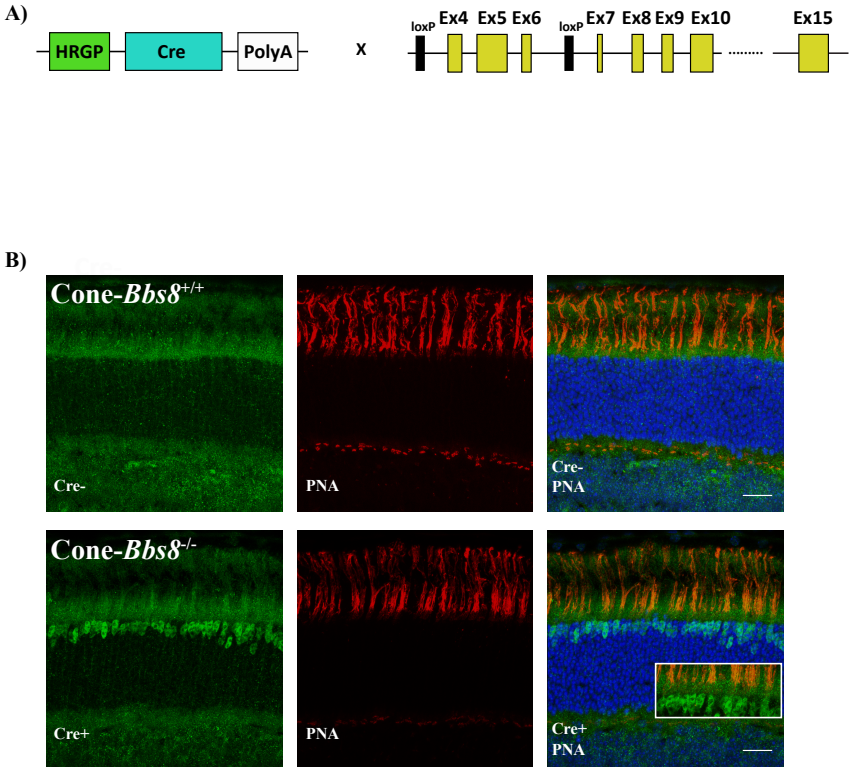

Supplementary Figure 5. Generation of animal model lacking BBS8 exclusively in cone photoreceptor cells. (A) Schematic representation delineating the creation of cone-specific conditional BBS8 knockout animals. Mice expressing Cre recombinase under the human red/green pigment promoter (HRGP) were crossed with *Bbs8* floxed animals. (B) Retinal cross-sections of Cone-*Bbs8*$^{+/+}$

and Cone-*Bbs8*$^{-/-}$ at post natal day 30, stained against Cre recombinase (green), Peanut agglutinin (PNA, red) as the cone marker, and DAPI (blue, marking the nuclei). Scale bar: 20µm.

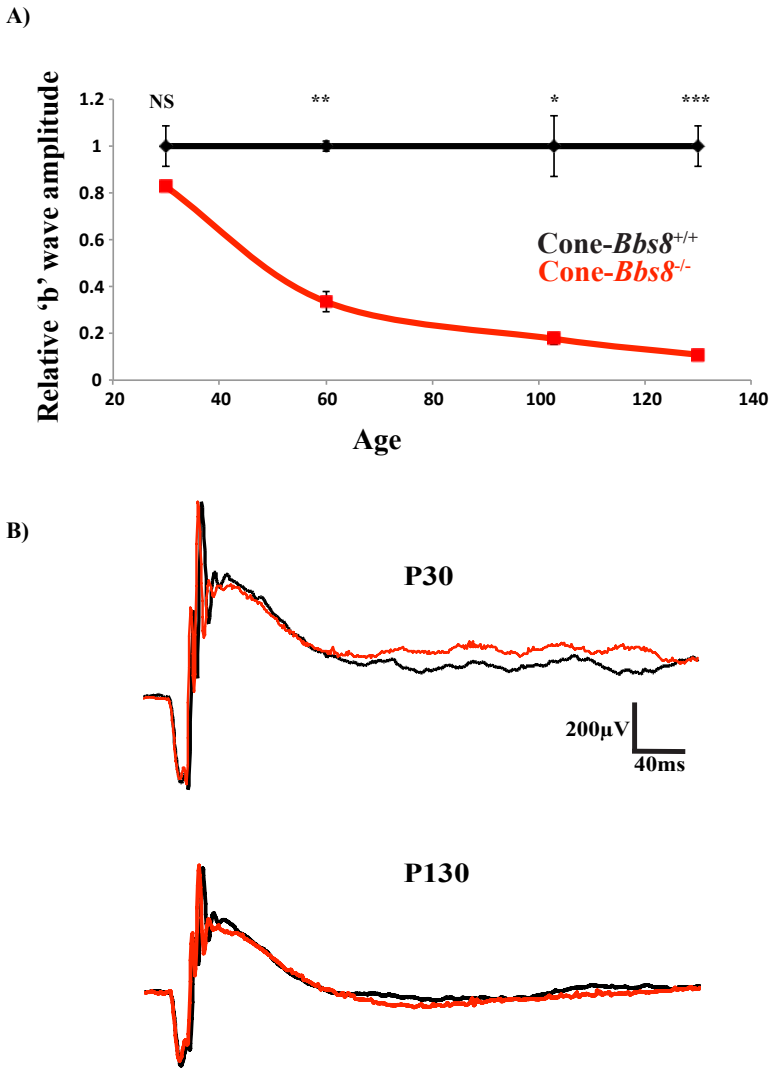

Supplementary Figure 6. Progressive loss of cone photoreceptor function in Cone-*Bbs8*$^{-/-}$ animals. (A) Graph illustrating the relative photopic (cone) "b"-wave amplitude measured at the light intensity 0.69 log cd s/m^2 at various ages. (B) Representative scotopic (rod) electroretinograms (ERGs) at -0.8 log cd s/m^2, showing no observable difference in rod photoresponse in Cone-*Bbs8*$^{-/-}$ animals compared to their wild-type

littermate controls. *P = 0.0035, **P = 0.002, ***P = 0.0006.

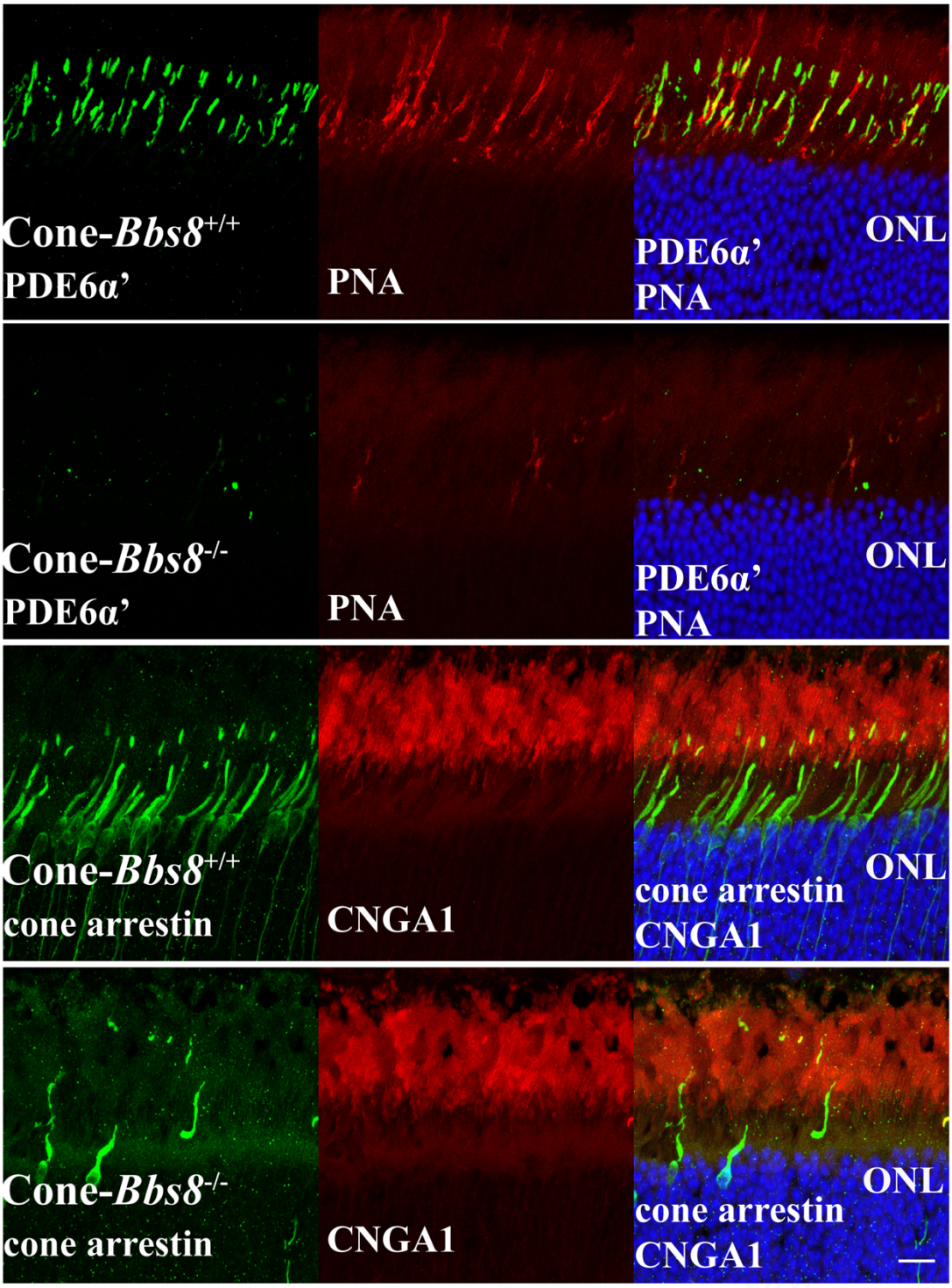

Supplementary Figure 7. Degeneration of cone photoreceptors in mice lacking BBS8. (A). Retinal cross-sections from 4 month old animals stained against cone PDE6α' (cone Phosphodiesterase-6α'), cone arrestin, PNA (peanut agglutinin), CNGA1 (Cyclic Nucleotide Gated Channel α 1), and DAPI (blue) in Cone-*Bbs8*$^{-/-}$ compared to wild-type littermate controls. Scale bar: 20μm.

Antibody	Source	Dilution
Rabbit anti-BBS5	Proteintech 14569-1-AP	1:2000
Rabbit anti-BBS2	Proteintech 11188-2-AP	1:1000
Rabbit anti-BBS7	Proteintech 13458-1-AP	1:2000
Rabbit anti-BBS9	Proteintech 14460-1-AP	1:1000
Mouse anti-BBS5	UC Davis,N304B/11	1:2000
Goat anti-BBS1	Santa Cruz,N-20	1:1000
Rabbit anti-BBS4	Santa Cruz sc-67201	1:1000
Goat anti-BBS8	Santa Cruz, P-20	1:1000
Rabbit anti-PDE6β	Pierce Lab	1:2000
Mouse anti-GAPDH	Fitzgerald 10R-G109a	1:10,000
Mouse anti-GRK1	Thermo Fisher MA1-720	1:2000
Mouse anti-CNGA1	UC Davis/NIH NeuroMab Facility	1:1000
Chicken anti-RP1	gift from Dr. Eric Pierce, Ocular Genomics Institute, Harvard University	1:500
Mouse anti-acetylated tubulin	Santa Cruz 6-11B-1	1:500
Mouse anti-alpha tubulin	Sigma T9026	1:4000
Mouse anti-beta tubulin	Sigma T8328	1:4000
Rabbit anti-Syntaxin3	Proteintech 15556	1:1000
Guinea pig anti-MAK	Wako 012-26441	1:500
Chicken anti-Rootletin	gift from Dr. Tiansen Li, National Eye Institute	1:500
Rabbit anti-RPGR	gift from Dr. Tiansen Li (NEI)	1:500
Rabbit anti-RDS-c (Peripherin)	gift from Dr. Gabriel Travis, University of California, Los Angeles, CA	1:2000

Mouse anti-1D4 (Rhodopsin)	gift from Dr. Ted Wensel, Baylor College of Medicine	1:500
Rabbit anti-opsin red/green	AB5405,EMD Millipore, Billerica, MA, USA	1:2000
Biotinylated Peanut Agglutinin (PNA)	Vector Laboratories, Burlingame, Ca	1:1000
Rabbit anti-cone arrestin	AB15282, EMD Millipore, Billerica, MA,USA	1:2000
4′,6-diamindino-2-phenylindole,(DAPI)	Invitrogen	1:1000
Propidium Iodide	EMD Millipore, Billerica, MA, USA	1:2000
Rabbit anti-Cre	EMD Millipore -69050	1:2000

Supplementary Table 1. List of antibodies used in this study

3

Title: ARL13B, a Joubert Syndrome-associated protein, is critical for retinogenesis and elaboration of photoreceptor outer segments

Abbreviated title: ARL13B and photoreceptor development

Authors: Tanya L. Dilan[1,2], Abigail R. Moye[1,2#], Ezequiel M. Salido[1#], Thamaraiselvi Saravanan[1], Kolandaivelu Saravanan [1,2], Andrew F.X. Goldberg[4], Visvanathan Ramamurthy[1,2,3*]

Published: *Journal of Neuroscience 2019* 39(8):1347-1364. doi: 10.1523/JNEUROSCI.1761-18.2018.

Affilitions:[1] Departments of Ophthalmology[1] and Biochemistry[2], and WVU Rockefeller Neuroscience Institute[3], West Virginia University, Morgantown, WV 26506, USA and [4]Eye Research Institute, Oakland University, Rochester, MI 48309, USA

[#] These authors contributed equally to this work

Corresponding author (s): Visvanathan Ramamurthy, Departments of Ophthalmology and Biochemistry; Eye Institute, One Medical Center Drive, West Virginia University, Morgantown, WV 26506-9193, USA. Email: ramamurthyv@wvumedicine.org Tel: 304 598 6940; Fax: 304 598 6928.

Keywords: Blindness, Joubert Syndrome; photoreceptors; protein trafficking; outer segment; IFT

Competing interests: The author(s) declare no competing interests.

Acknowledgments: The authors thank Dr. Tamara Caspary at Emory and Dr. Peter Mathers at WVU for providing animals used in this study. The authors would like to thank Dr. Mike Schaller for aiding in

preparation of this manuscript, Victoria Kimler (Eye Research Institute, Oakland University) and Mateo Dilan (WVU) for help with data collection. This work was supported by National Institutes of Health Grants RO1 EY028035, R01 EY025536, R21 EY027707, West Virginia Lions and Lions Club International Foundation.

Abstract

Mutations in the Joubert syndrome-associated small GTPase, ARL13B, are linked to photoreceptor impairment and vision loss. To dissect the role of ARL13B in the development, function and maintenance of ciliated photoreceptors, we generated a pan-retina knockout (*Six3*-Cre) and a rod photoreceptor-specific inducible conditional knockout (*Pde6g*-Cre^{ERT2}*)* of ARL13B using murine models. Embryonic deletion of ARL13B led to defects in retinal development with reduced cell proliferation. In the absence of ARL13B, photoreceptors failed to develop outer segment (OS) membranous discs and axonemes, resulting in loss of function and rapid degeneration. Additionally, the majority of photoreceptor basal bodies did not dock properly at the apical edge of the inner segments. The removal of ARL13B in adult rod photoreceptor cells, after maturation of OS, resulted in loss of photoresponse, vesiculation in the OS, and progressive photoreceptor cell death. Interestingly, prior to changes in photoresponse, removal of ARL13B led to mislocalization of rhodopsin, prenylated phosphodiesterase-6 (PDE6), and intraflagellar transport protein-88 (IFT88). Our findings show that ARL13B is required at multiple stages of retinogenesis, including early postnatal proliferation of retinal progenitor cells, development of photoreceptor cilia, and morphogenesis of photoreceptor OS discs. Lastly, our results establish a need for ARL13B in photoreceptor maintenance and protein trafficking.

Introduction

ADP ribosylation factor–like GTPase 13B (*Arl13b*) is a member of the Arf-like Ras superfamily of small GTPases. Small GTPases serve as molecular "switches" that cycle between GDP-bound "off" and GTP-bound "on" conformations (*75*). In their GTP-bound conformation, also known as the active state, small GTPases elicit a wide variety of cellular responses by binding to different effector protein's (*75, 138*). ARL13B is a larger protein among the Arf/Arl family of small GTPases and lacks a highly conserved glutamine residue that is critical for the proteins intrinsic GTPase activity (*90, 139, 140*). Additionally, ARL13B is doubly palmitoylated at the N-terminus region of the protein and it is highly enriched within the cilium, a microtubule-based organelle protrusion that acts as a signaling hub for the extracellular environment (*10, 78, 141*). The aforementioned lipid modification plays a critical role in ARL13B's ciliary localization, stability and function (*79*).

Mutations in the *Arl13b* gene are linked to Joubert Syndrome, an autosomal recessive 'ciliopathy' characterized by hypotonia, ataxia, intellectual disability, obesity and retinal dystrophy (*92, 142*). Moreover, removal of *Arl13b* leads to defective ciliogenesis in the kidney duct of zebrafish models and in murine renal epithelia (*84, 143*). In mice, a null allele of *Arl13b* (*hennin* mutant) leads to embryonic lethality, markedly shorter nodal cilia and structural defects in the ciliary axoneme (*78*). Interestingly, ARL13B is needed for the formation of the eye, with *hennin* mutant embryos exhibiting traits of anophthalmia (*78*). Previous studies have reported that ARL13B acts as a ciliary length regulator by its unique ability to induce ciliary membrane protrusions (*88, 144*). However, the role of ARL13B in axonemal extension, a process critical for cilia formation, remains unclear.

In addition to its role in the development of cilia, ARL13B is a guanine-nucleotide exchange factor (GEF) that activates ARL3, another small GTPase (*81, 145*). Mutations in the *ARL3* gene are linked to Retinitis Pigmentosa (vision loss) in humans (*2*). Recent work where either ARL3 is ablated or when a GTP-locked mutant form of ARL3 is expressed in rod photoreceptors suggests that ARL3 through its interaction with PRBPδ and UNC119 binds prenylated and myristoylated protein cargoes, respectively, and aid in their trafficking (*90, 146*). (*82, 147*). Defects in ARL3 led to mistrafficking of prenylated PDE6, as well as accumulation of lipidated transducin in the photoreceptor inner segment (IS) (*82, 147*). Additionally, these animals suffered from progressive loss of photoreceptor cells (*82, 147*). The critical role of ARL3 in transport of lipidated photoreceptor outer segment (POS) proteins points to a likely important role for its GEF, ARL13B in these processes. Therefore, to better understand the role of ARL13B in trafficking of lipidated proteins and in photoreceptor development, in this study, we conditionally ablated ARL13B in the developing retina and selectively removed ARL13B in mature rod photoreceptor cells.

Results

ARL13b is present in the photoreceptor outer segments

ARL13B is highly enriched within primary cilia and has been used extensively as a marker in cilia studies (*78, 148*). To determine the localization of ARL13B in photoreceptor cells, we performed immunohistochemistry using different commercially available antibodies (Fig. 1A and data not shown).

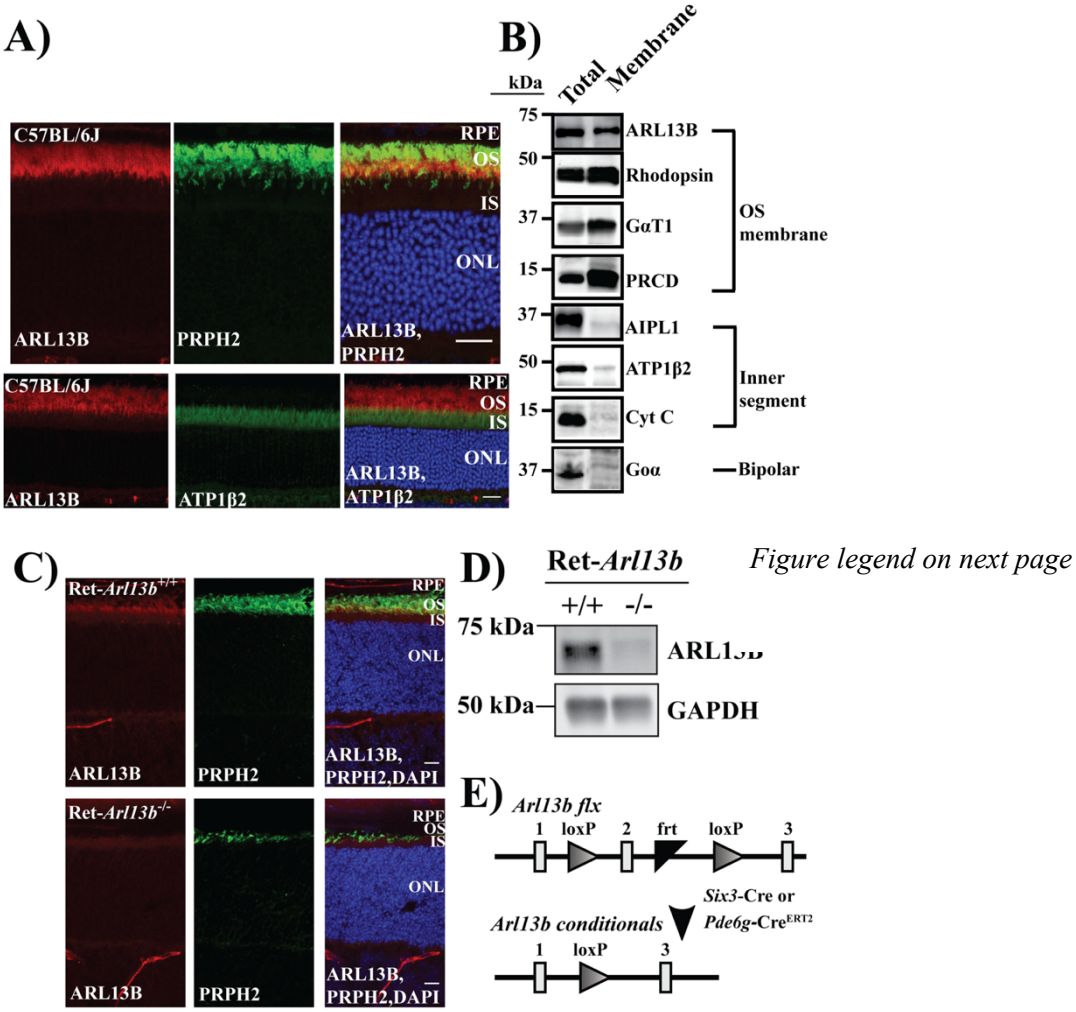

Figure legend on next page

We used antibodies against peripherin-2 (PRPH2) and Sodium-Potassium ATPase (ATP1β2) to mark the photoreceptor outer and inner segment respectively (Fig. 1A, Top and Bottom panels). ARL13B

Figure 1: Validation of animal model and localization of ARL13B in murine retina

A-B) Immunolocalization of ARL13B in the murine retina. A) *(Top panel)* Retinal cross sections of P30 wild-type animals (C57BL/6J) stained against ARL13B (red) and Peripherin-2 (PRPH2), an OS marker, stained in green. *(Bottom panel)* Retinal cross sections of P30 wild-type animals (C57BL/6J) stained against ARL13B (red) and Sodium-Potassium ATPase (ATP1β2), an IS marker, stained in green. Scale bar: 20μm. B) Immunoblot showing sub-cellular localization of ARL13B in photoreceptors. Rod outer segment (ROS) membrane fractions were isolated as described in materials and methods. Total fraction represents the retinal lysate that was the starting material for ROS isolation. The proteins found in specific photoreceptor compartments were used for validation of the isolated ROS including; outer segment proteins (Rhodopsin, GαT1: Rod transducin-α subunit, PRCD: Progressive Rod-Cone Degeneration Protein), inner segment proteins (AIPL1: Aryl Hydrocarbon Receptor Interacting Protein Like-1, ATP1β2: Sodium-Potassium ATPase β2 subunit, Cyt C: Cytochrome c and bipolar cell protein, Goα. C-E) Validation of Ret-*Arl13b*$^{-/-}$ animal models by immunofluorescence and immunoblot analysis. C) Retinal cross sections probed for ARL13B from Ret-*ARL13B*$^{-/-}$ (*Six3*-Cre *Arl13b*$^{-/-}$) and wild-type littermate controls at P10. D) Validation of animal model by immunoblotting. Retinal lysates from Ret-*Arl13b*$^{-/-}$ (*Six3*-Cre: *Arl13b*$^{flx/flx}$) and their wild type littermate controls at P10 probed against ARL13B and Glyceraldehyde 3-phosphate dehydrogenase (GAPDH) that served as a loading control (n=3). E) Scheme depicting the generation of conditional *Arl13b* animal models. *LoxP* flanks exon 2 of *Arl13b*. Following Cre expression from either *Six3* or *Pde6g* promoter, exon 2 of *Arl13b* is removed in a tissue and/or cell specific manner.

was concentrated at the proximal end of the photoreceptor outer segments (Fig. 1A). To independently confirm the presence of ARL13B in the outer segments, we isolated photoreceptor membrane from adult wild-type retina. To validate our membrane preparation, we probed for the presence of established markers of inner segment and outer segment proteins (Fig. 1B) (*149-151*). As expected, photoreceptor inner segment proteins were absent in the isolated ROS membrane fractions (i.e: AIPL1= Aryl Hydrocarbon Receptor Interacting Protein Like 1; Cyt C= Cytochrome C; ATP1β2 = Sodium-Potassium ATPase subunit β2). Similarly, Goα, a protein localized to ON bipolar cells, that are downstream to photoreceptors, was not present in the membrane fraction (*152*). Interestingly, we found ARL13B in both the total and membrane fractions. Additionally, we found enrichment of photoreceptor OS membrane-resident proteins in the ROS membrane fraction compared to the total fraction (i.e: Rhodopsin; GαT1 = Transducin-α subunit, PRCD = Progressive Rod-Cone Degeneration Protein) further validating our membrane preparation. Taken together, our results show ARL13B is predominantly localized to the photoreceptor outer segments. Furthermore, our results suggest ARL13B is associated with photoreceptor ROS membranes.

Generation of *Arl13b* animal models

To determine the role of ARL13B in the retina, we generated a pan-retina *Arl13b* knockout using *Cre-loxP* recombination technology. *Arl13b* floxed animals contained *loxP* sites flanking exon 2 (Fig. 1C)

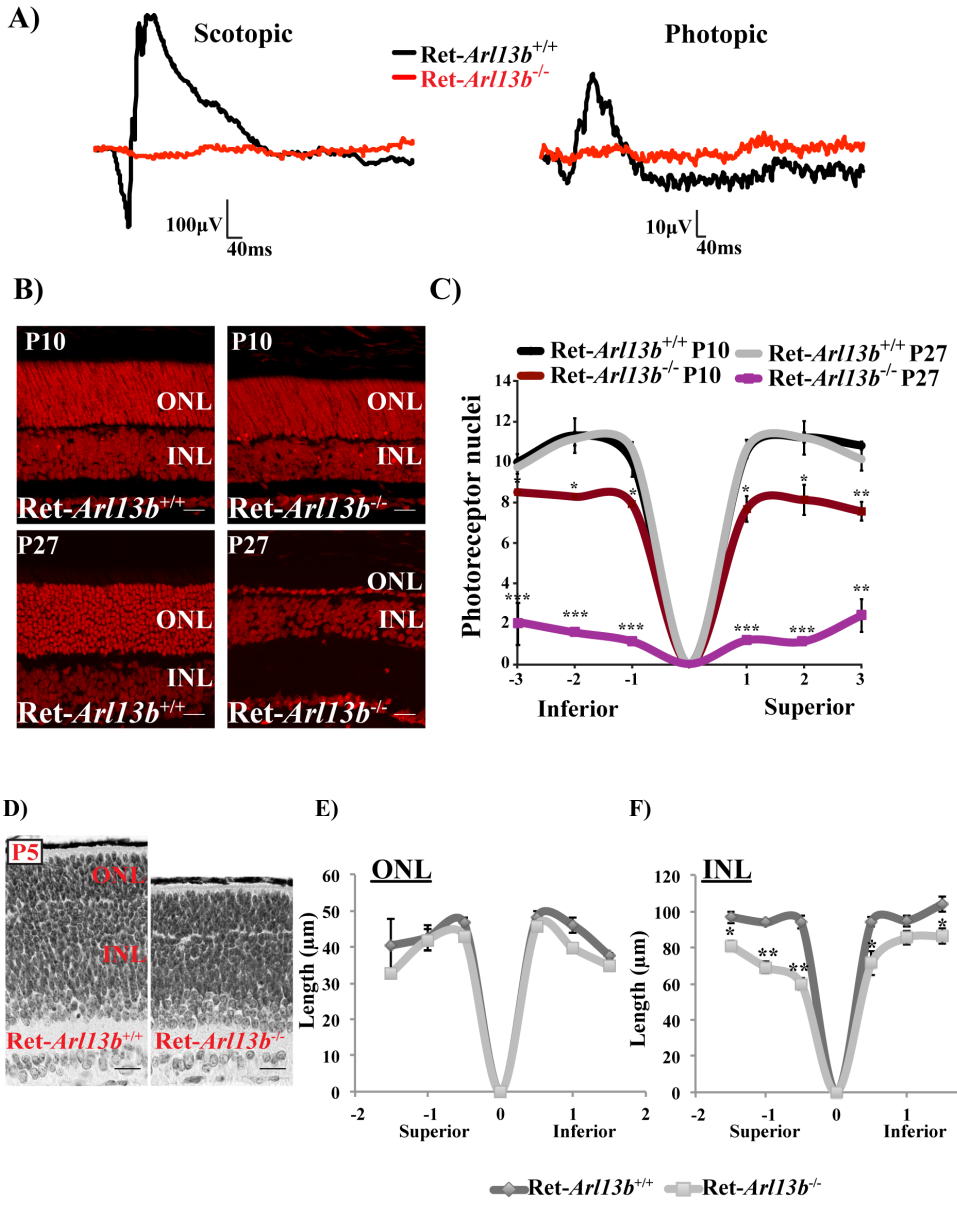

Figure legend on next page

Figure 2: Reduced retinal thickness and rapid photoreceptor degeneration in ARL13B null retinas

A) Representative scotopic (-0.8 log cd*s/m^2) and photopic (0.7 log cd*s/m^2) electroretinograms (ERGs) of Ret-*Arl13b*$^{-/-}$ (*red*) and littermate control (*black*) at P15. B) Retinal cross sections stained with Propidium Iodide at P10 and P27. Scale bar: 20μm. C) Quantification of the ONL thickness (cell nuclei) at different sites along the retina from the inferior to superior regions between Ret-*Arl13b*$^{-/-}$ and wild-type littermate controls at P10 and P27. Data are represented as mean ± SEM (n=3, unpaired two-tailed t-test; ***$P \leq 0.0001$; **$P \leq 0.001$; *$P \leq 0.01$). D) Light microscopy of Hematoxylin and Eosin (H&E) stained cross sections of Ret-*Arl13b*$^{-/-}$ mutant and wild-type littermate control at P5. Graphs depicting length measurements of the developing outer nuclear layer (ONL) (*Panel* E) and inner nuclear layer (INL) (*Panel* F) from Ret-*Arl13b*$^{-/-}$ mutants and their wild-type littermate controls (**P =0.001, *P= 0.01; n=3).

(*153*). *Arl13b* floxed animals were crossed with a *Cre* recombinase driver-line under the retina and forebrain specific promoter *Six3,* with excision taking place at embryonic day 9.5 [23]. We next verified the validity of our animal model by probing for ARL13B using immunohistochemistry and immunoblotting (Fig. 1C-D). As expected, ARL13B was absent in *Six3*-Cre: *Arl13b*$^{flx/flx}$ (Ret-*Arl13b*$^{-/-}$) animals compared to their littermate controls, *Arl13b*$^{flx/flx}$ or *Six3*-Cre: *Arl13*b$^{flx/+}$ (Ret-*Arl13b*$^{+/+}$) (Fig. 1C-D). In agreement with previous findings, we found that ARL13B exhibits an anomalous SDS-PAGE mobility, running at ~60kDa, rather than the 48kDa molecular weight predicted by its amino acid sequence (*78, 90*). At postnatal day 10, the majority (more than 90%) of ARL13B protein was lost in Ret-*Arl13b*$^{-/-}$ mutants (Fig. 1D).

ARL13B is essential for postnatal retinal development

To examine the impact of ARL13B deletion on photoreceptor function, we performed Electroretinography tests (ERG). ERG measures the electric potential generated by the retinal cells in response to a light stimulus. The activity by photoreceptors and depolarization of bipolar cells results in the generation of "a"- and "b"- waves, respectively (*154, 155*). At P15, after mice open their eyes, in

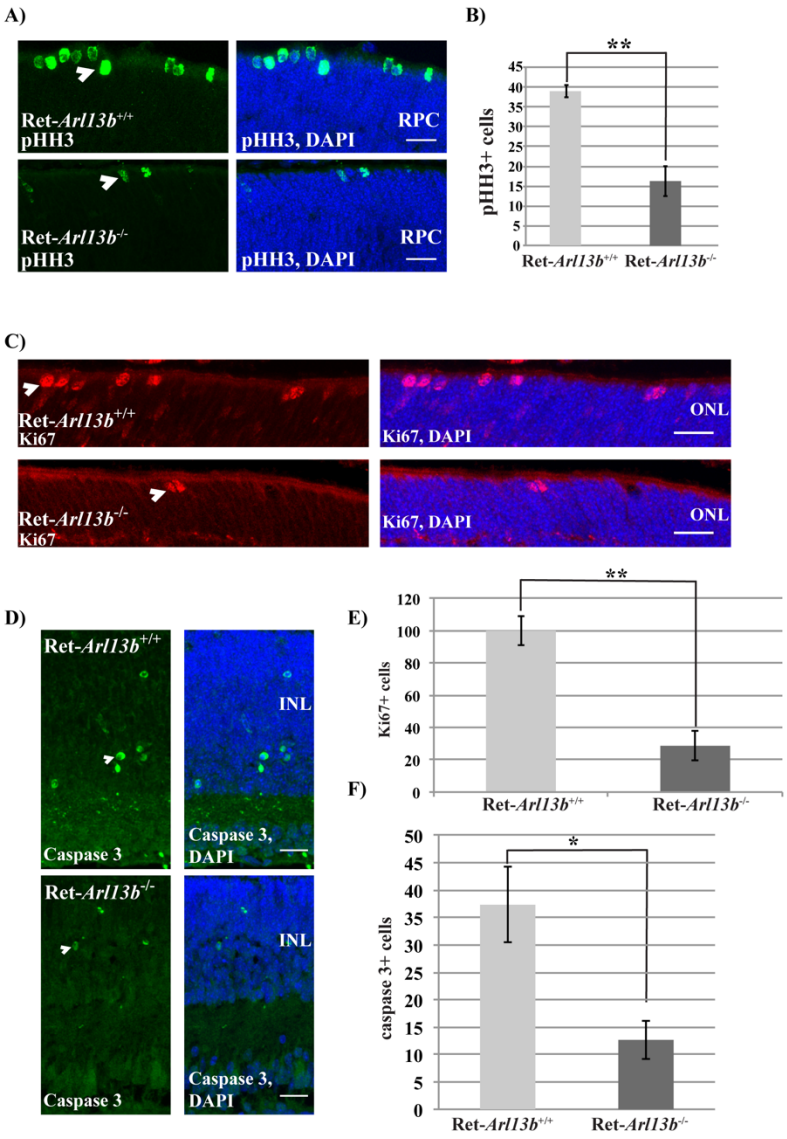

Figure 3: Defective retinal development in the absence of ARL13B

A) Retinal cross sections of Ret-*Arl13b*$^{-/-}$ and wild-type littermate controls stained against the proliferation marker phospho-histone-H3 (pHH3 in green; marked by arrowheads) at P5. Scale bar: 20µm. B) Quantifications of phospho-histone H3-positive cells across the retina from Ret-*Arl13b* null animals and littermate controls at P5. Data are represented as mean± SEM (n=3, Students t- test; **P = 0.005) (RPC = retinal progenitor cells). C) Retinal cross sections from Ret-*Arl13b*$^{-/-}$ and littermate controls stained with proliferation marker Ki-67 at P5 (Red, marked by arrowheads). Scale bar: 20µm, ONL: outer nuclear layer identified by 4′,6-diamidino-2-phenylindole (DAPI in blue) staining. D) Retinal cross sections from Ret-*Arl13b*$^{-/-}$ and littermate controls stained with apoptotic marker caspase-3 at P5 (Green, marked by arrowheads). Scale bar: 20µm, INL: inner nuclear layer identified by DAPI staining.). E) Quantification of Ki-67 positive cells identified in panel C. Data are represented as mean ± SEM (n =3, unpaired two-tailed t-test; ** P = 0.005). F) Quantification of caspase-3 positive cells identified in panel D. Data are represented as mean ± SEM (n =3, unpaired two-tailed t-test; * P = 0.05).

Ret-*Arl13b*$^{-/-}$ animals we observed a severe loss of rod (scotopic) and cone (photopic) photoreceptor

function (Fig. 2A).

The observed loss of photoreceptor function could be due to photoreceptor cell death. Thus, we counted photoreceptor nuclei at P10 and P27 (Fig. 2B and 2C). At P10, we observed a reduction in photoreceptor nuclei in retina lacking ARL13B (Fig. 2C; Ret-*Arl13b*$^{+/+}$ = 10.6±0.32 vs. Ret-*Arl13b*$^{-/-}$ = 6.8±0.21 rows of nuclei, P = 0.0006; n= 3). By P27, we detected rapid photoreceptor degeneration with extensive loss occurring in the central retina (Fig. 2C; Ret-*Arl13b*$^{+/+}$ = 10.9±0.18 vs. Ret-*Arl13b*$^{-/-}$ = 1.24±0.12 rows of nuclei, P = 0.0001; n= 3) compared to the peripheral edges of the retina (Fig. 2C; Ret-*Arl13b*$^{+/+}$ = 9.9±0.16 vs. Ret-*Arl13b*$^{-/-}$ = 2.2±0.13 rows of nuclei, P = 0.0001; n= 3). The retinal thickness was also reduced in the developing retina at P5 (Fig. 2D-F).

Due to the early loss of photoreceptor nuclei in Ret-*Arl13b*$^{-/-}$ mutants and the role for ARL13B in proliferation, we further investigated whether the loss of ARL13B would affect retinal proliferation at early stages of development (Fig. 3) (*156*). We stained cross sections of Ret-*Arl13b*$^{-/-}$ and littermate wild-type controls at P5 for phospho-histone H3 (pHH3), a late G2 to M phase marker that primarily labels mitotic progenitors and Ki-67, a marker found to primarily label late G1 to M phase proliferating cells (Fig. 3A and 3C) (*157-159*). As expected, pHH3 positive cells were detected around the outer edges of the retina in both Ret-*Arl13b*$^{-/-}$ and wild-type littermate controls at P5 (Figure 3A) (*157*). Interestingly, the number of pHH3 positive cells was decreased by 58% in retina lacking ARL13B (Fig. 3B; Ret-*Arl13b*$^{+/+}$ = 39±1.5 vs. Ret-*Arl13b*$^{-/-}$ = 16.3±3.7, P = 0.005; n= 3). We observed a similar reduction in proliferation (71.4%) with Ki-67 staining in Ret-*Arl13b*$^{-/-}$ animals compared to wild-type littermate controls (Fig. 3E; Ret-*Arl13b*$^{+/+}$ = 100±8.9 vs. Ret-*Arl13b*$^{-/-}$ = 28.3±9.7, P = 0.005; n=3).

When we tested for apoptosis using activated caspase-3, we also observed reduced staining in the retina lacking ARL13B (Fig. 3D and 3F; Ret-*Arl13b*$^{+/+}$ = 37.3±6.8 vs. Ret-*Arl13b*$^{-/-}$ = 13.0±3.4, $P = 0.03$; n=3). These results indicate that the initial development and function of photoreceptor cells is severely affected in the absence of ARL13B.

Robust reduction of photoreceptor OS-resident proteins in the absence of ARL13B

Based on previous studies that implicate ARL13B as the GEF for ARL3, and the known role for ARL3 in trafficking of prenylated PDE6, we investigated if loss of ARL13B perturbed the movement of PDE6 into the outer segments (OS) (*81, 145*). We probed for PDE6 by immunohistochemistry using retinal cross sections from Ret-*Arl13b*$^{-/-}$ and their wild-type littermate controls at P10 (Fig. 4A-B). PDE6β was found properly localized to the OS (Fig. 4A), however at reduced levels in retina lacking ARL13B, which were later confirmed by immunoblot (73% reduction for PDE6β, $P = 0.001$, n= 3; Fig. 4D and 4E). The staining for PDE6 was not uniform; in some areas of the retina, PDE6 staining was completely absent in Ret-*Arl13b*$^{-/-}$ animals (Fig. 4B). Although the majority of Rhodopsin protein was found targeted to the OS, we detected mislocalized Rhodopsin in the photoreceptor ONL in Ret-*Arl13b*$^{-/-}$ animals (Fig. 4A-B). Additionally, non-prenylated Peripherin-2 was found properly targeted to the photoreceptor OS in retina lacking ARL13B at P10 (Fig. 4C). In agreement with our results from immunohistochemistry, we observed an overall reduction of photoreceptor OS-resident proteins in the absence of ARL13B at P10 by immunoblotting (Fig. 4D and 4E). Specifically, we found 70% and 60% reduction of Transducin (GαT1) and Peripherin-2 (PRPH2) respectively in Ret-*Arl13b*$^{-/-}$ animals at P10 (GαT1, $P = 0.03$; PRPH2, $P = 0.004$, n= 3; Fig. 4D and 4E). Lastly, similar to PDE6, we found a trend

in decreased relative protein levels of the prenylated protein, Rhodopsin Kinase-1 (GRK1), in Ret-*Arl13b*$^{-/-}$ at P10 (Fig. 4D and 4E). In summary, ARL13B deletion led to a reduction in the majority of OS-resident proteins.

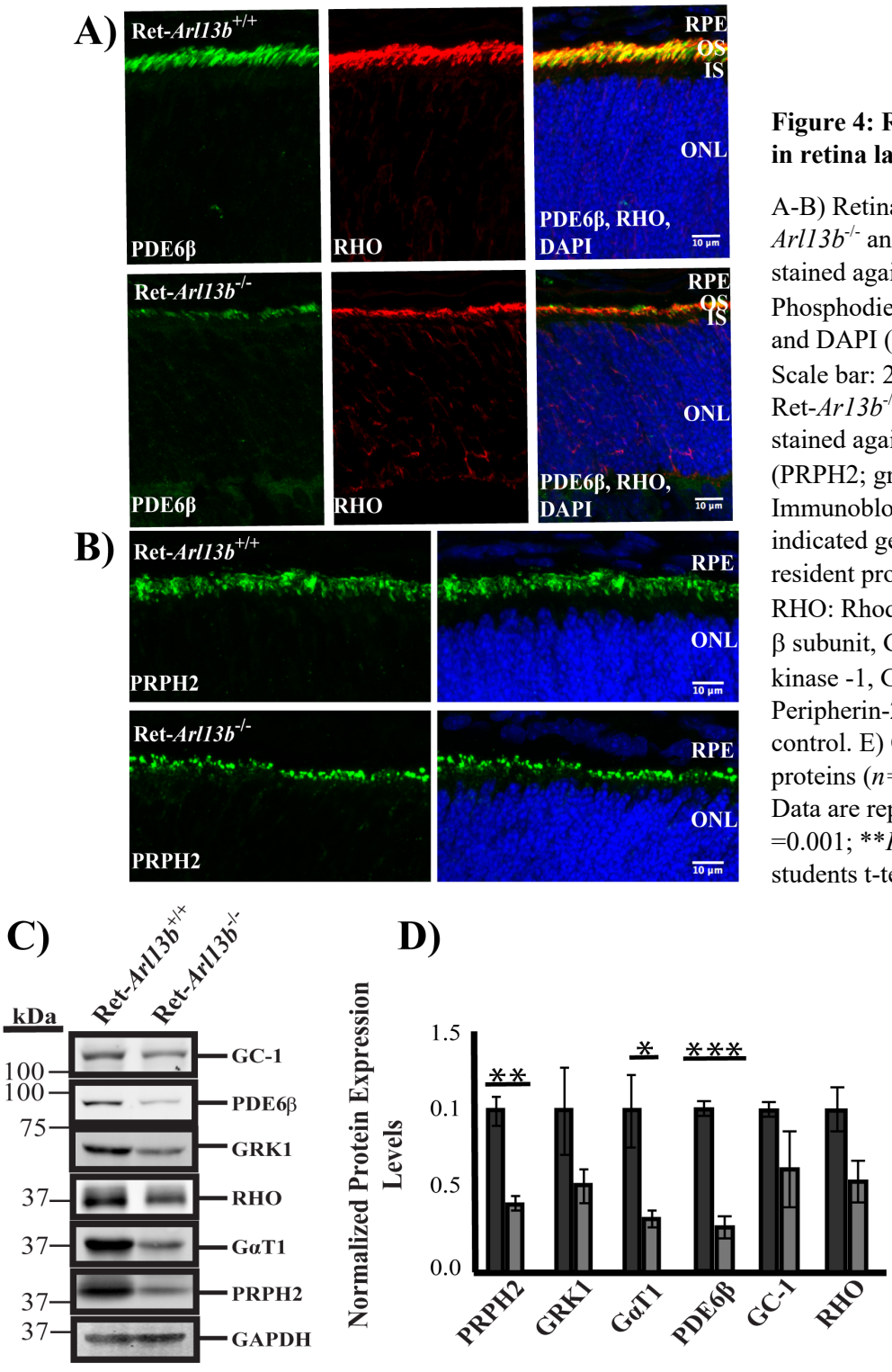

Figure 4: Reduced expression of OS proteins in retina lacking ARL13B

A-B) Retinal cross sections from P10 Ret-*Arl13b*$^{-/-}$ and wild-type littermate controls stained against Rhodopsin (red), Phosphodiesterase-6 β subunit (PDE6β: green) and DAPI (4',6-diamidino-2-phenylindole). Scale bar: 20μm. C) Retinal cross sections of Ret-*Ar13b*$^{-/-}$ and littermate wild-type controls stained against OS-resident protein Peripherin-2 (PRPH2; green) at P10. Scale bar: 10μm. D) Immunoblot of P10 retinal lysates from indicated genotypes, probed for different OS-resident proteins (GC-1: Guanylate Cyclase-1, RHO: Rhodopsin, PDE6β: Phosphodiesterase-6 β subunit, GRK1: G protein-coupled receptor kinase -1, GαT1: Rod Transducin-α, PRPH2: Peripherin-2). GAPDH serves as loading control. E) Quantification of outer segment (OS) proteins (n=3), normalized against GAPDH. Data are represented as mean± SEM ***P =0.001; **P =0.004, *P =0.03 as determined by students t-test.

ARL13B is required for photoreceptor outer segment biogenesis

Staining for several OS-resident proteins including Peripherin-2 in retina lacking ARL13B revealed shorter OS's suggesting a defect in OS structure (Fig. 4). Therefore, we performed Transmission Electron Microscopy (TEM) to conduct ultrastructural analyses of the retina from Ret-*Arl13b*$^{-/-}$ and littermate controls (Fig. 5). At P10, electron micrographs revealed OS's, which displayed well-ordered stacked discs in wild-type littermate controls (Fig. 5A and 5C). In contrast, TEM analysis of P10 ARL13B-null retina revealed a complete absence of recognizable OS's (Fig. 5B). We observed a few 'OS rudiments' in the retina lacking ARL13B, however they were highly vesiculated and lacked the characteristic stacked discs (Fig. 5D-F). Interestingly, we observed the presence of extracellular vesicles (ectosomes) with uniform diameter in the sub-retinal space of Ret-*Arl13B*$^{-/-}$ mutants at P10 (202 ± 54 nm; mean ± SD; Fig. 5G and 5H red arrowheads). These results illustrate a crucial role for ARL13B in the elaboration of photoreceptor outer segments and stacked disc membranes.

Figure 5: ARL13B is needed for normal development of photoreceptor outer segments

A) TEM image of the photoreceptor outer segment-Retinal pigment epithelium (OS-RPE) interface, from a wild-type littermate control, showing properly developing OSs, possessing numerous well-ordered membranous discs. Scale bar: 500nm. B) TEM image of the photoreceptor OS-RPE interface, from a P10 Ret-*Arl13b*$^{-/-}$animal, showing IS-OS boundary for photoreceptors to be significantly affected compared to littermate controls. Scale bar: 500nm. C) (*Left Panel*) Wild-type littermate control, showing normal photoreceptor CC and OSs, compared to a TEM image from a Ret-*Arl13b*$^{-/-}$ (*D-F*) retina, displaying a vesicle-filled OS rudiment. Scale bars: 500nm. (BB= basal body, OLM=outer limiting membrane, IS-inner segment, CC = connecting cilium, OS = outer segment). G) Electron micrograph of P10 Ret-*Arl13b*$^{-/-}$ cross-sections, red arrowheads showing the accumulation of extracellular vesicles in the sub-retinal space. Scale bar: 500nm. H) Gaussian histogram of Feret diameters for extracellular vesicles in Ret-*Arl13b*$^{-/-}$ retinas (n = 204 pooled from three animals).

Figure on next page

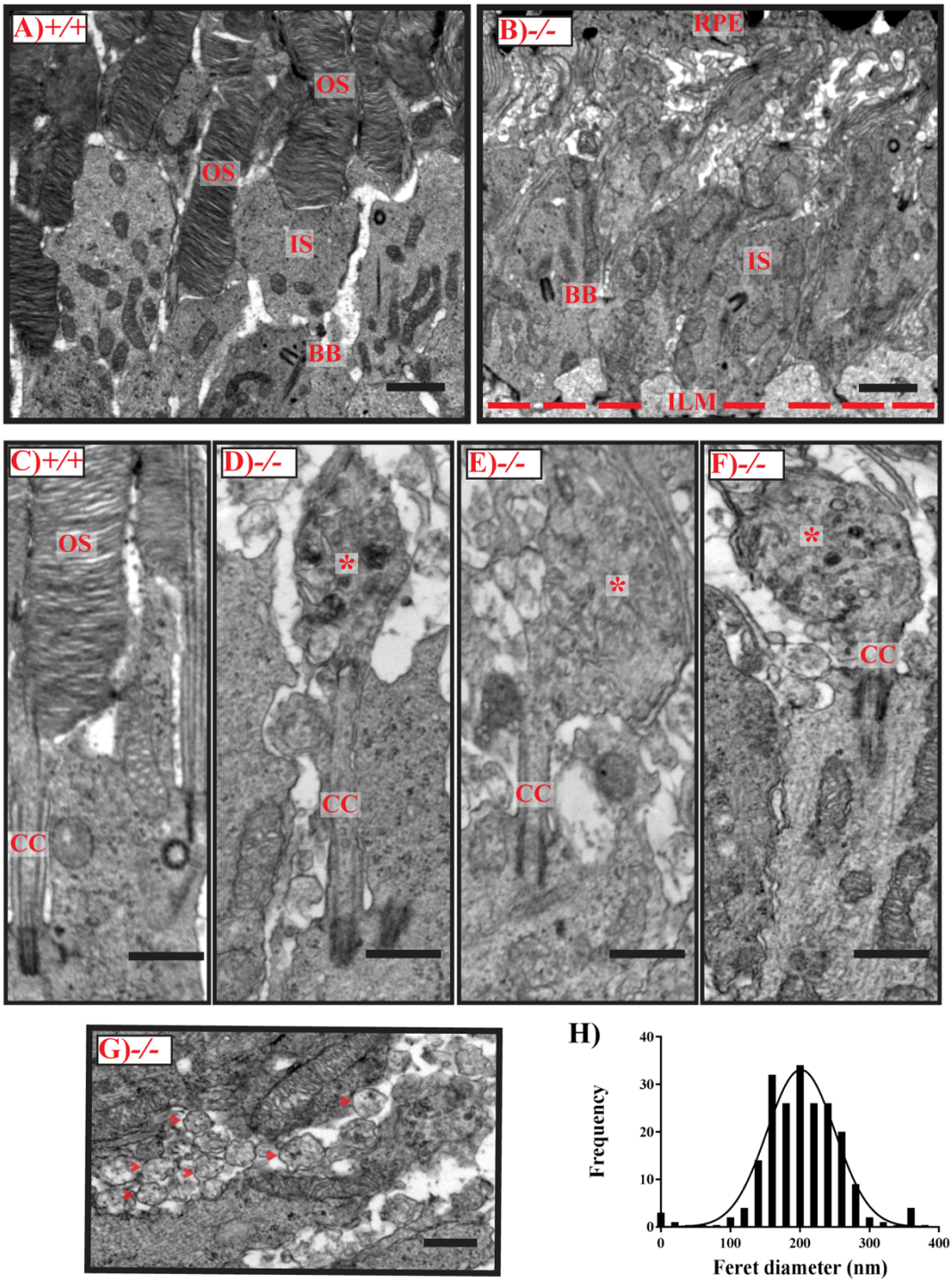

Basal body positioning and ciliary extension are disrupted in ARL13B-null retina

Loss of ARL13B leads to reduced numbers of primary cilia and dysregulation of ciliary length (i.e. shorter cilia) (*78, 88*). To evaluate the effects of ARL13B deletion on photoreceptor cilia, we performed immunohistochemistry in lightly fixed retinal cross sections using various ciliary markers at P10, a common approach used to characterize photoreceptor cilia length (*32, 160*)(Fig. 6). At P10, Rootletin

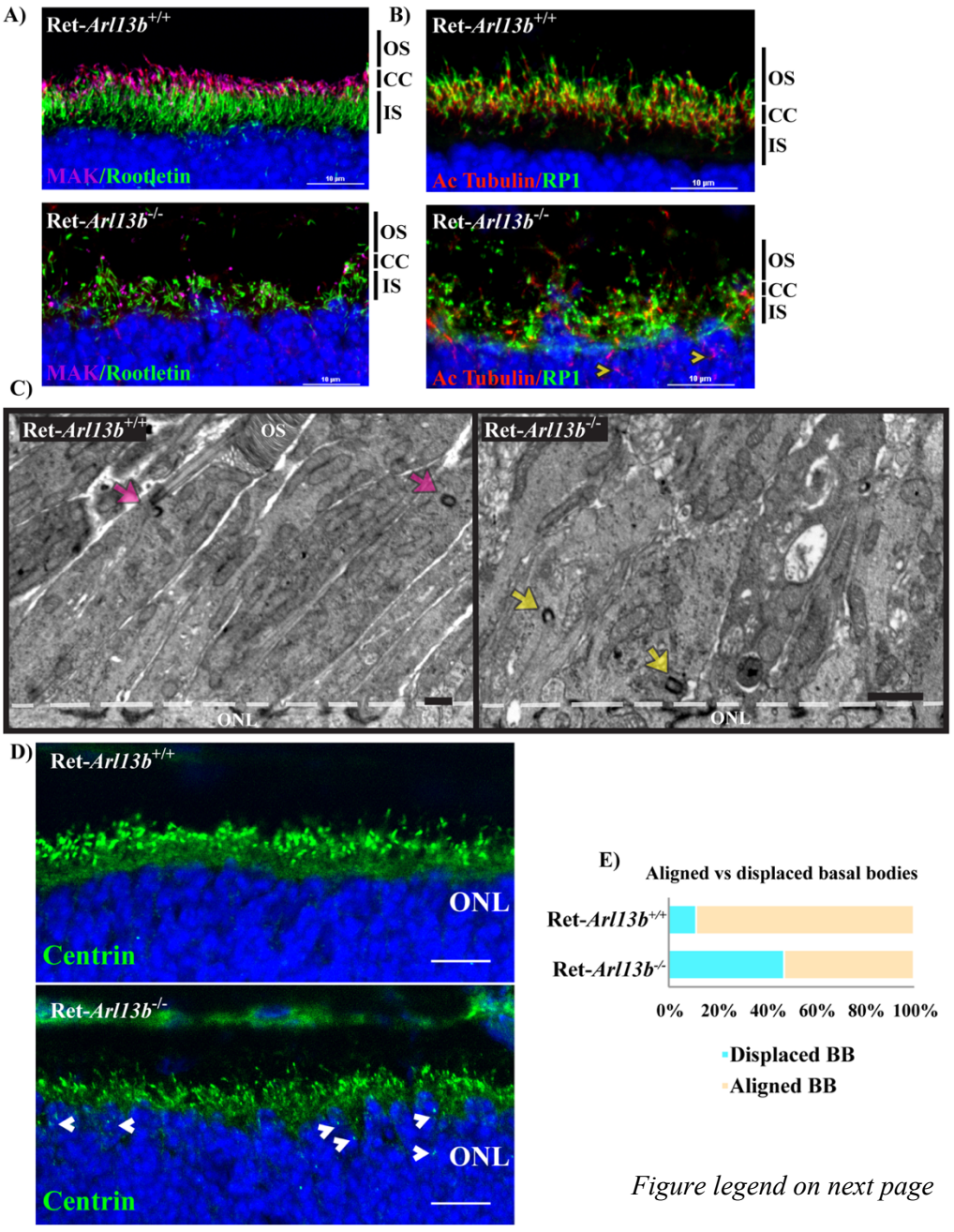

Figure legend on next page

Figure 6: Severe ciliary defects in retina lacking ARL13B

A) Retinal cross sections of Ret-*Arl13b*$^{-/-}$ and wild-type littermate controls stained against axonemal marker MAK (cyan; male germ cell-associated kinase) and inner segment (IS) marker Rootletin (green). B) Immunofluorescence images of Ret-*Arl13b*$^{-/-}$ and littermate controls showing staining against additional axonemal marker Retinitis Pigmontosa-1 (RP1; green) and connecting cilium marker acetylated tubulin (red). Scale bars: 10μm. C) (*Left panel*) TEM images of wild-type littermate controls showing properly docked mother and daughter centrioles (basal body) (cyan arrows). (*Right panel*) Electron micrographs of P10 Ret-*Arl13b*$^{-/-}$ mutants showing displaced solitary basal bodies (yellow arrows). Scale bars: 1μm. (OS: outer segment, ONL: outer nuclear layer). D) Representative immunofluorescence staining of Centrin (green) in Ret-*Arl13b*$^{+/+}$ and Ret-*Arl13B*$^{-/-}$, the latter showing signs of displaced basal bodies (white arrowheads). Scale bar: 10μm. Graphs depicting the percent of normal mother and daughter centrioles also known as basal bodies versus the observation of just one solitary centriole in retina lacking ARL13B at P10 (Ret-*Arl13b*$^{+/+}$ = 59 (Solitary centriole) /121 Total versus Ret-*Arl13b*$^{-/-}$= 167 (Solitary centriole)/ 237 Total; n=3, unpaired two-tailed t-test, P = 0.0002). E) Graphs depicting the percent of docked basal bodies versus displaced basal bodies in retina lacking ARL13B at P10 (Ret-*Arl13b*$^{+/+}$ = 14 (Displaced BBs)/121 Total versus Ret-*Arl13b*$^{-/-}$= 111 (Displaced BBs)/ 237 Total; n=3, unpaired two-tailed t-test, P = 0.0002).

staining (Fig. 6A left panel; Rootletin in green) revealed shorter ciliary rootlets in Ret-*Arl13b*$^{-/-}$ animals compared to littermate controls, suggesting shorter photoreceptor inner segments, which was confirmed through ultrastructural analysis. The axonemal marker, Male germ cell-associated kinase (MAK) was expressed in a punctate fashion and was mislocalized to the inner segment in Ret-*Arl13b*$^{-/-}$ retinas (Fig. 6A; MAK in cyan). To independently verify these defects in the axoneme, we assessed the localization of Retinitis Pigmentosa-1 (RP1), a microtubule-associated protein (MAP) primarily found in the photoreceptor axoneme (*161*). We also co-stained with acetylated tubulin, a hallmark of long-lived microtubules primarily found along the photoreceptor connecting cilia/transition zone and the base of the photoreceptor axoneme (Fig. 6B) (*160, 162, 163*). As expected, RP1 was present in photoreceptor axonemes in wild-type littermate controls. However, in photoreceptors lacking ARL13B, RP1 was found in a punctate pattern and was mislocalized to the IS. Interestingly, acetylated tubulin was mislocalized to the outer nuclear layer of Ret-*Arl13b*$^{-/-}$ animals (ONL; Fig. 6B yellow arrowheads). Ultrastructural analysis (at P10) revealed that basal bodies in the knockout retina were displaced and often found within the ISs adjacent to the outer limiting membrane (Fig. 6C and Fig. 6E, Ret-*Arl13b*$^{+/+}$ =

12% vs. Ret-*Arl13b*$^{-/-}$ = 47% Displaced BBs; *n*=3, P = 0.0002). To corroborate the observed defects in basal body positioning, we probed for Centrin in

Ret-*Arl13b*$^{-/-}$ and littermate controls (Fig. 6D). Centrin is commonly used basal body marker in photoreceptors, where it associates with centrioles and to a lesser extent the inner face of the microtubule doublets of the connecting cilium (Wolfrum et al., 2002). We observed centrin staining adjacent to the top layer of photoreceptor nuclei as well as closer to the basal side of the inner segment in retina lacking ARL13B (Fig. 6D, white arrowheads). Altogether, our results suggest ARL13B plays a role in axonemal/ciliary extension, potentially by an effect on photoreceptor basal body positioning.

ARL13B is essential for rod photoreceptor maintenance

Our studies using embryonic deletion of ARL13B in the murine retina establish the essential need for ARL13B in early development of photoreceptor cilia and outer segment morphogenesis in mice. However, rapid photoreceptor degeneration, disrupted OS elaboration, and the fact that ARL13B was ablated in other retinal cell types prevented us from establishing a direct role for ARL13B in photoreceptors. In addition, we wanted to investigate if ARL13B's function is restricted to the early phase of photoreceptor development, or if it also plays a critical role in the maintenance of fully developed photoreceptors. In order to tackle some of these questions, we depleted ARL13B in mature adult murine rod photoreceptor neurons through the use of a tamoxifen-inducible *Cre-LoxP* system. The *Cre*-recombinase (Cre^{ERT2}) is expressed under the rod-specific phosphodiesterase-6 gamma subunit (*Pde6g)* promoter (*164*).We crossed this line with *Arl13b* floxed animals to generate a rod-specific

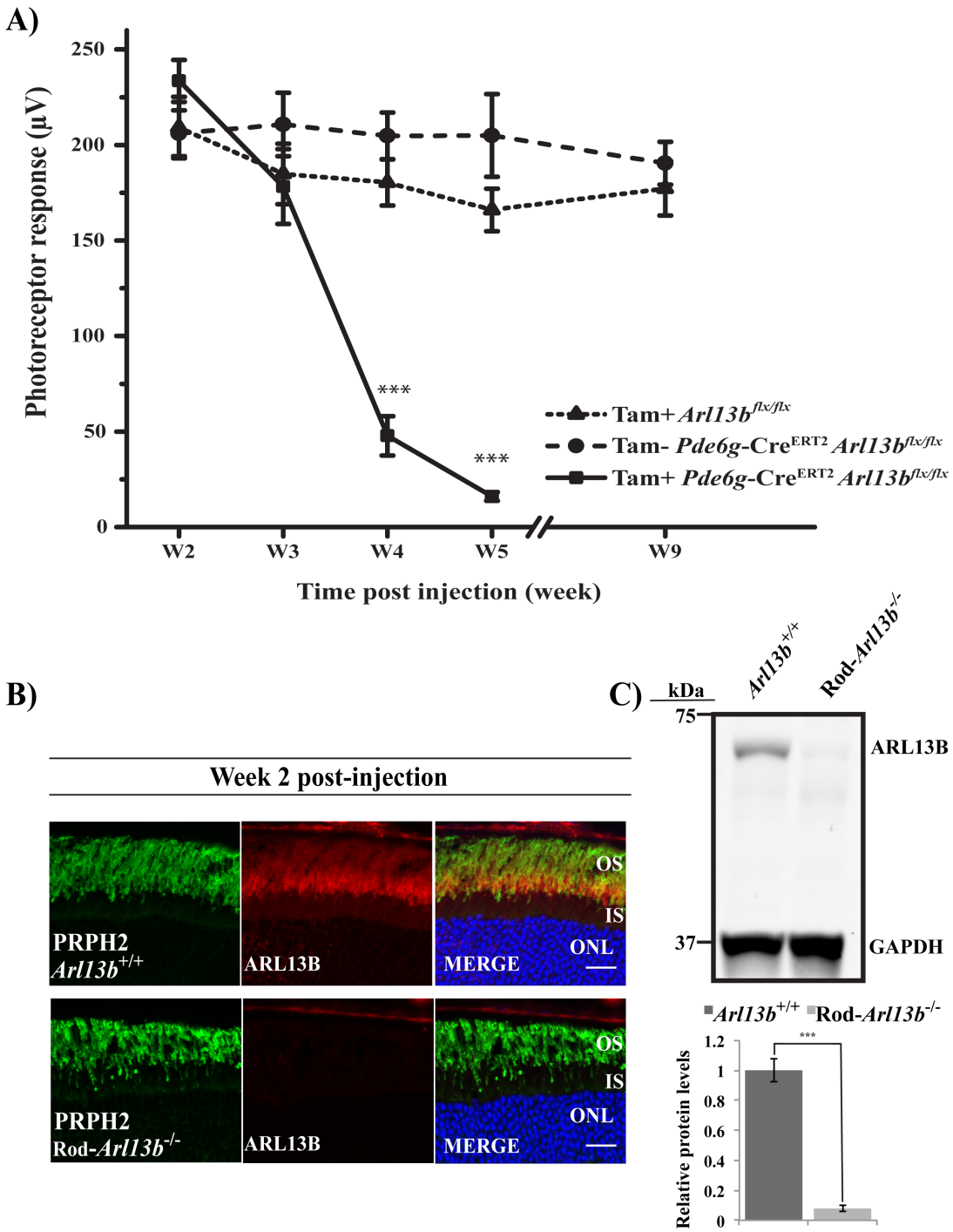

Figure 7: Progressive decline of rod photoreceptor function after removal of ARL13B in mature rod photoreceptors. A) Loss of rod photoreceptor response measured by "a" wave response plotted against time in weeks after tamoxifen injections (Tam+ = tamoxifen injected). Data are represented as mean± SEM (n=6, two-way ANOVA; *** P= 0.005). B) Immunohistochemistry of retinal cross sections of Rod-*Arl13b*$^{-/-}$ (Tam+ *Pde6g*-Cre^{ERT2}-*Arl13b*$^{flx/flx}$) and wild-type littermate controls (Tam+ *Arl13b*$^{flx/flx}$) showing significant loss of ARL13B at 2 weeks post tamoxifen injections. Peripherin-2 (PRPH2; green) marks the OS. Scale bars: 20µm. C) (*Top*) Representative immunoblot of Rod-*Arl13b*$^{-/-}$ (Tam+ *Pde6g*-Cre^{ERT2}-*Arl13b*$^{flx/flx}$) and wild-type littermate control retinal lysates (Tam+ *Arl13b*$^{flx/flx}$) of animals 2 weeks after tamoxifen-induced ARL13B deletion probed for ARL13B. GAPDH serves as loading control. C) (*Bottom*) Quantification of ARL3B protein (n=3), normalized against GAPDH. Data are represented as mean± SEM ***P =0.0003; as determined by students t-test.

Pde6g-Cre^{ERT2}-*Arl13b*$^{flx/flx}$ mutants (Tam+ Rod-*Arl13b*$^{-/-}$) and their wild-type littermate controls, including experimental animals to which tamoxifen was not administered (i.e. Tam- *Pde6g*-Cre^{ERT2}-*Arl13b*$^{flx/flx}$; Fig. 7A). However, a reduction in scotopic (rod) photoresponse occurred at 3 weeks leading to complete ablation of photoresponse after 5 weeks PI. (Fig. 7A). The photopic photoresponses were also severely affected 5 weeks PI (data not shown). To eliminate the possibility that tamoxifen could lead to photoreceptor toxicity, thus affecting ERG responses, we administered tamoxifen in wild-type littermate controls and observed no changes in rod photoresponse up to 5 and 9 weeks post IP injection (Fig. 7A). We confirmed significant reduction of ARL13B in Rod-*Arl13b*$^{-/-}$ animals (Tam+ *Pde6g*-Cre^{ERT2}-*Arl13b*$^{flx/flx}$) by immunohistochemical analysis on retinal cross sections obtained 2 weeks after tamoxifen injections and by immunoblotting (Fig. 7B and Fig. 7C; 90% reduction for ARL13B, $P = 0.0003$, $n=3$). Our results show that absence of ARL13B in adult rods leads to rapid decline in photoreceptor viability and function.

ARL13B is required for trafficking of Rhodopsin

Due to ARL13B's role as a GEF for ARL3, we speculated that prenylated cargo would be mislocalized after removal of ARL13B. At two weeks post-tamoxifen injections, when rod photoresponse was unaltered (Fig. 7A), Tam+ Rod-*Arl13b*$^{-/-}$ retinal cross sections stained against PDE6β revealed small puncta in the photoreceptor IS (Fig. 8A arrowheads). This finding is reminiscent of PDE6β accumulation in ARL3 dominant-active transgenic animal models (Wright et al., 2016). However, this defect was specific for PDE6, as we observed normal OS localization of prenylated Rhodopsin kinase (GRK1) (data not shown). Interestingly, at two weeks post-tamoxifen injections, Rhodopsin was

mislocalized to the IS and ONL (Fig. 8A). However, we observed no mislocalization of rod Transducin or CNGA1 (data not shown). Furthermore, ultrastructural analysis of Tam+ Rod-*Arl13b*$^{-/-}$ two weeks after tamoxifen-induced deletion of ARL13B, showed accumulation of vesicles within the photoreceptor outer segments (Fig. 8B, red arrows), reminiscent of what was seen in Ret-*Arl13B*$^{-/-}$ photoreceptors. More strikingly, 5 weeks after tamoxifen-induced deletion of ARL13B, the majority of photoreceptors

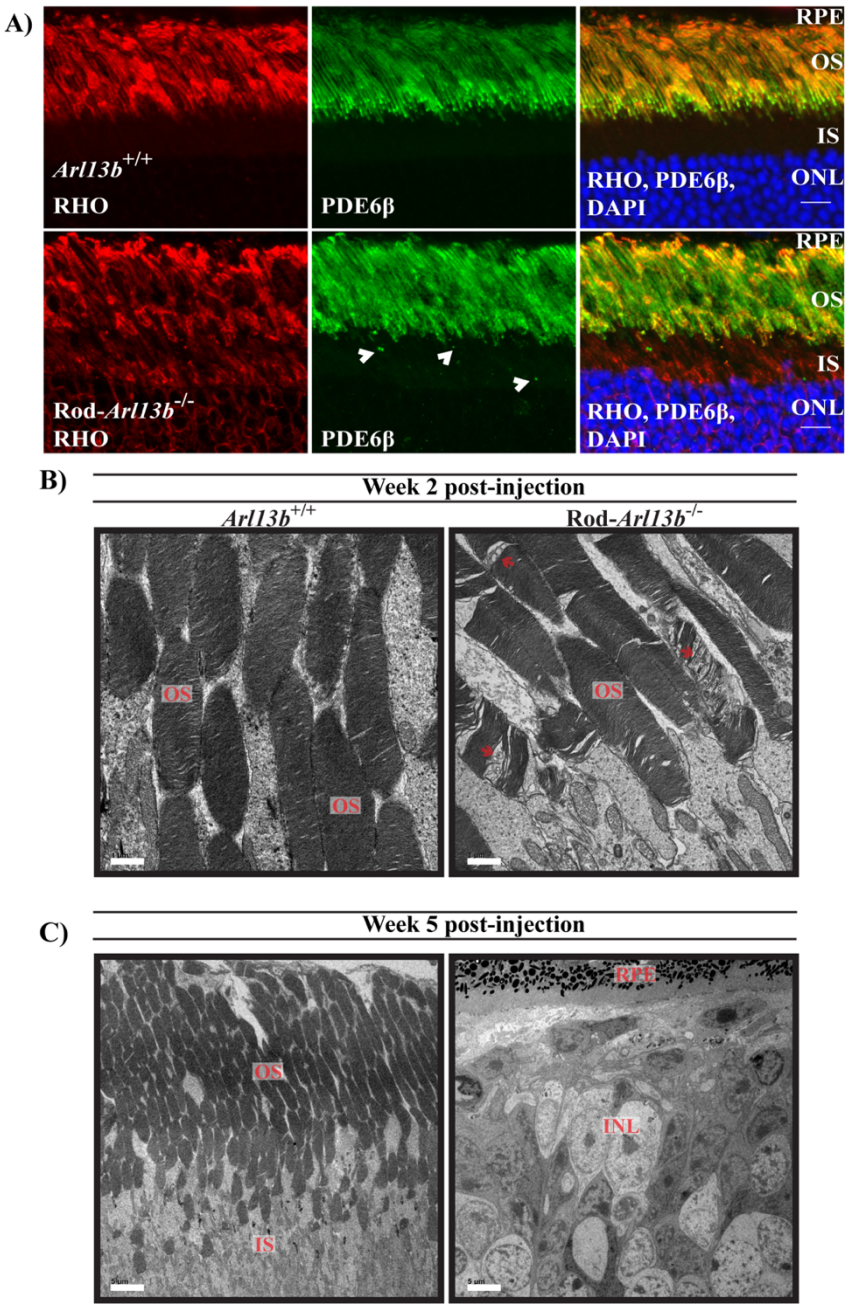

Figure 8: Rhodopsin is mislocalized after deletion of ARL13B in mature rod photoreceptors.

A) Retinal cross sections of Rod-*Arl13b*$^{-/-}$ and wild-type littermate controls 2 weeks post-tamoxifen injection stained with antibodies against Rhodopsin (red) and Phosphodiesterase-6 (PDE6β, green). Punctate pattern of mislocalized PDE6β is indicated by white arrowheads. B) (*Left panel*) Electron micrographs of Rod-*Arl13b*$^{-/-}$ and wild-type littermate controls two weeks after tamoxifen injections showing normal elaborated OS (*Left panel*) and the initial stages of vesicle formation within OS (*Right panel*, red arrows) after ARL13B deletion. Scale bar: 1µm. C) TEM images of wild-type littermate controls (*Left panel*) and Rod-*Arl13b*$^{-/-}$ (*Right panel*) showing severe photoreceptor degeneration five weeks after tamoxifen-induced ARL13B ablation. Scale bar: 5µm.

cells were lost (Fig. 8C). Taken together, our data shows ARL13B is needed for the maintenance of normal trafficking of OS proteins in adult rod photoreceptor cells.

ARL13B is needed for the maintenance of rod photoreceptor axoneme and IFT88 transport

To further investigate the role of ARL13B in photoreceptor axonemal structure, we performed immunofluorescence imaging of lightly fixed retinal cross sections of Tam+ Rod-*Arl13b*$^{-/-}$ animals at two weeks post-tamoxifen injections and their wild-type littermate controls. We observed no significant changes in the immunostaining for both tubulin glutamylation (1.24 μm ± 0.02, n = 300 in littermate controls; 1.31 μm ± 0.01, n = 311 in Rod-*Arl13b*$^{-/-}$; P = 0.004) and acetylation (1.54 μm ± 0.02, n = 309 in littermate controls; 1.66 μm ± 0.02, n = 358 in Rod-*Arl13b*$^{-/-}$; P = 0.0002) after two weeks post tamoxifen injections (Fig. 9A-B). Interestingly, length measurements taken for immunostaining of RP1 protein, a microtubule-associated protein known to stain the photoreceptor axoneme, showed a significant length reduction in Tam+ Rod-*Arl13b*$^{-/-}$ mutants after two weeks post-tamoxifen injections (Fig. 9A; 3.38μm ± 0.05, n = 322 in littermate controls; 1.9μm ± 0.03, n = 320 in Rod-*Arl13b*$^{-/-}$; P = 0.0001). To further corroborate our findings, immunohistochemical analysis of MAK, a kinase normally found enriched in the photoreceptor axoneme, revealed significantly reduced immunostaining after two weeks post-tamoxifen injections in Tam+ Rod-*Arl13b*$^{-/-}$ retina (Fig. 9C; 2.80 μm ± 0.05, n = 305 in littermate controls; 1.62 μm ± 0.03, n = 313 in Rod-*Arl13b*$^{-/-}$; P = 0.0001) (*160*).

In primary cilia, the bidirectional transport of proteins is mediated by the intraflagellar transport complex (IFT). Previous reports show accumulation of IFT-A and IFT-B proteins, specifically IFT88 and IFT40 subunits at the ciliary tip in ARL13B-null RPE cell lines (*165*). To establish whether the IFT complex is affected in photoreceptors lacking ARL13B, we performed immunohistochemical analysis of retinal cross sections of Tam+ Rod-*Arl13b*$^{-/-}$ animals two weeks post-tamoxifen injections and their wild type littermate controls (Fig. 9B). In wild-type photoreceptors, IFT88 labeled both the proximal inner segment and distal outer segment ends of the photoreceptor connecting cilia (Fig. 9B white arrowheads) (*48*). Interestingly, similar to the phenotype observed in RPE cell lines, IFT88 accumulated in the distal segment of the photoreceptor connecting cilia with loss of immnunoreactivity at the proximal segment of the photoreceptor connecting cilia (Fig. 9B white arrows). In addition, we observed mislocalization of IFT88 to the inner segment two weeks after ARL13B ablation (Fig. 9B). These results suggest that retrograde trafficking of IFT88-dependent cargoes could be affected in the absence of ARL13B. Overall, our results show ARL13B is needed for the maintenance of photoreceptor axonemes in the adult retina.

Figure 9: Altered axonemal length after elimination of ARL13B.

A) (*Left panel*) Immunofluorescence staining of cross sections from Rod-*Arl13b*$^{-/-}$ and wild-type littermate controls with axonemal marker Retinitis Pigmentosa-1 (RP1; green) two weeks post-tamoxifen injections. (Acetylated tubulin = connecting cilium marker, red). Scale bars: 10μm. (*Right panel*) Violin plots representing overall distribution of length measurements for RP1 and acetylated tubulin (*n*= 300 cilia pooled from 3 animals). B) (*Left panel*) Immunohistochemistry of cross sections from Rod-*Arl13b*$^{-/-}$ and wild-type littermate controls depicting intraflagellar transport protein IFT88 and connecting cilia marker glutamylated tubulin at two weeks post-tamoxifen injections. Scale bars: 10μm. *Top red box* = Representative immunofluorescence staining of IFT88 in wild-type retinal sections observed as two puncta at the basal and apical sides of the connecting cilium zone (arrowheads). In contrast with *bottom red box* = Representative immunofluorescence staining of IFT88 in Rod-*Arl13b*$^{-/-}$ animals two weeks post-tamoxifen injections, observed as single puncta in the apical side of the connecting cilium zone. Scale bars: 2μm. B) (*Right panel*) Violin plots representing overall distribution of length measurements for glutamylated tubulin (*n*= 300 pooled from 3 animals). C) (*Left panel*) Retinal cross sections from Rod-*Arl13b*$^{-/-}$ (Tamoxifen injected *PDE6g-Cre*^{ERT2}-*Arl13b*$^{flx/flx}$ animals) and wild-type littermate controls stained with antibody against axonemal marker MAK (cyan; male germ cell-associated kinase) and inner segment (IS) marker Rootletin (green). Scale bar: 10μm. (OS: outer segment, CC: connecting cilia, IS: inner segment). (*Right panel*) Violin plots representing overall distribution of length measurements for MAK (*n*= 300 cilia pooled from 3 animals).

Figure on next page

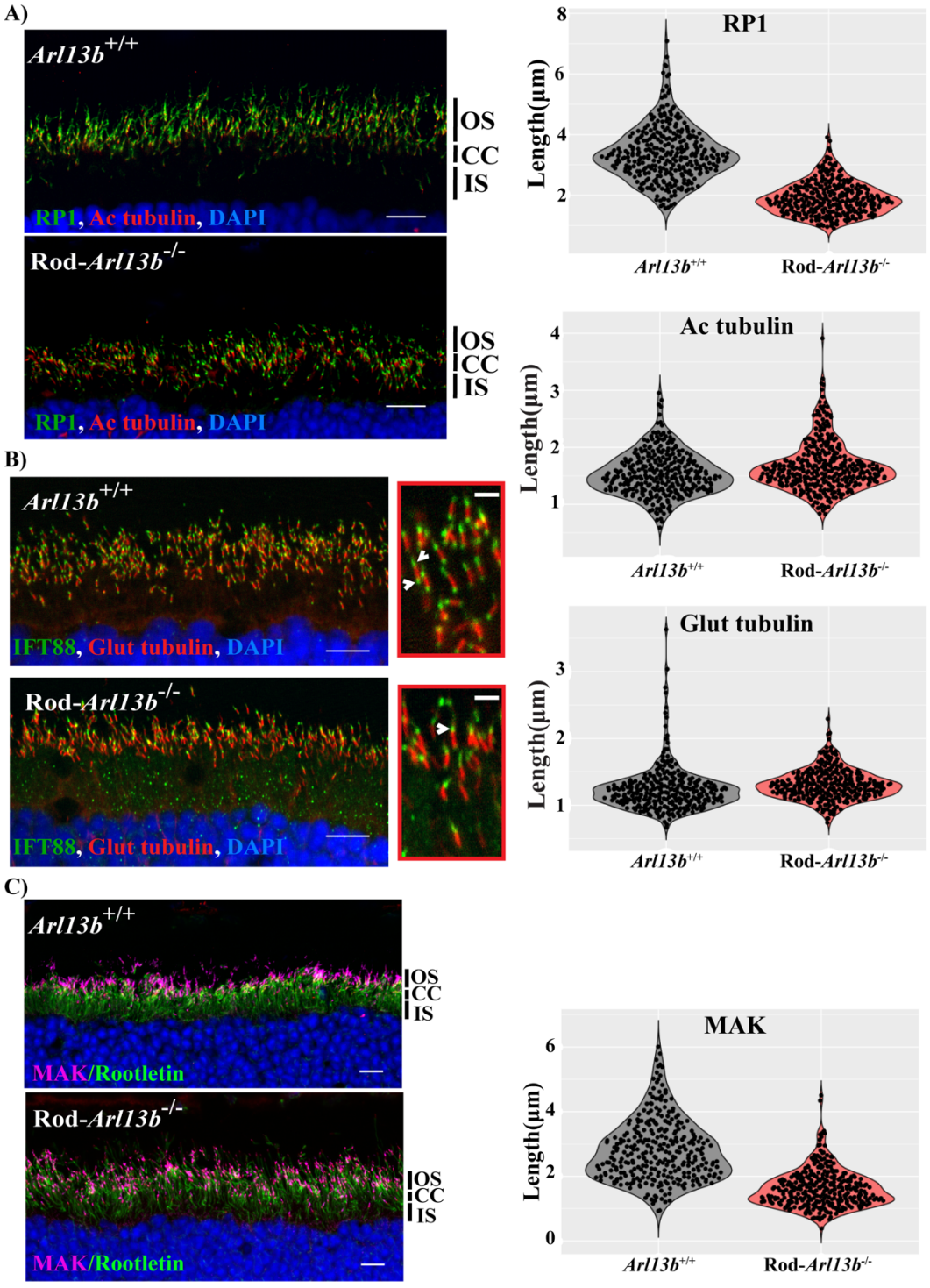
A)
Arl13b+/+
OS
CC
IS
RP1, Ac tubulin, DAPI
Rod-Arl13b-/-
OS
CC
IS
RP1, Ac tubulin, DAPI
RP1
Length(μm)
8
6
4
2
Arl13b+/+
Rod-Arl13b-/-
B)
Arl13b+/+
IFT88, Glut tubulin, DAPI
Rod-Arl13b-/-
IFT88, Glut tubulin, DAPI
Ac tubulin
Length(μm)
4
3
2
1
Arl13b+/+
Rod-Arl13b-/-
Glut tubulin
Length(μm)
3
2
1
Arl13b+/+
Rod-Arl13b-/-
C)
Arl13b+/+
OS
CC
IS
MAK/Rootletin
Rod-Arl13b-/-
OS
CC
IS
MAK/Rootletin
MAK
Length(μm)
6
4
2
0
Arl13b+/+
Rod-Arl13b-/-

Discussion

In this study, we sought to better understand the role of ARL13B in photoreceptor cells. Intriguingly, global ablation of ARL13B in mice leads to embryonic lethality and anophthalmia (*78*). Furthermore, a Joubert Syndrome (JS) patient with a loss of function missense mutation of ARL13B (Y86C) displayed the classical JS symptoms as well as retinal impairment and vision loss (*92*). To explore the role of ARL13B in photoreceptor neurons, we generated pan-retina and rod-specific inducible-knockout murine models. Embryonic deletion of ARL13B led to proliferation defects in the developing retina. Ablation of ARL13B also resulted in defective morphogenesis of outer segment discs and rapid photoreceptor loss. In support of these findings, photoresponses were absent at any age tested in this animal model. Additionally, pan-retina ARL13B knockouts displayed higher ratios of displaced basal bodies compared to wild-type littermates. The deletion of ARL13B in adult rod photoreceptors resulted in abrogation of photoreceptor function and severe retinal degeneration. We observed impaired transport of Rhodopsin and prenylated PDE6β, as well as the accumulation of intraflagellar transport complex protein-88 (IFT88). Overall, our models show the need for ARL13B throughout the development and maintenance of photoreceptor cells. During the preparation of this manuscript, a similar study was performed on ARL13B in murine photoreceptors (*166*). Our investigation was able to reproduce the main findings of the alternate study as well as introduce novel findings on the role of ARL13B in ciliated photoreceptor neurons. Figure 10 contains an overall schematic summary of the most important results observed in ARL13B-null retina at different stages.

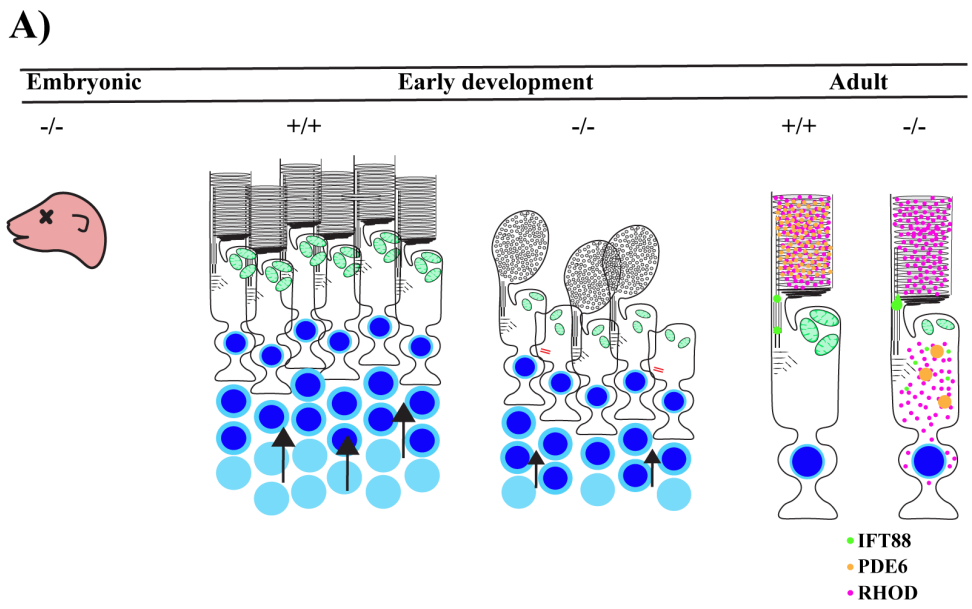

Figure 10: Summary of role for ARL13B in the retina

A) Scheme illustrating the need for ARL13B at different time points throughout murine retinal development: A complete knockout (*hennin mutants*) exhibited Anophthlamia; Embryonic deletion of ARL13B in the retina resulted in decreased photoreceptor proliferation, basal body mislocalization, aberrant or no OS disc formation accompanied by vesiculation, and impaired cilium growth; In fully developed rod photoreceptor cells (P60), 2 weeks after ARL13B-induced ablation, growth of the axoneme was impaired, IFT88 stalled, PDE6 and Rhodopsin mislocalized to the IS. B) Scheme illustrating the potential roles for ARL13B in photoreceptor neurons. 1) Proliferation signaling and/or detection, 2) Basal body polarization, 3) Repression of extracellular vesicles during OS disc formation, and 4) Regulator of protein trafficking in ciliated photoreceptors.

The embryonic removal of ARL13B did not affect retinal lamination. However, we detected reduced proliferation of retinal progenitor cells (RPCs), using two independent markers (Fig. 3) resulting in reduced retinal thickness and photoreceptor nuclei layers at P5 (Fig. 2). The study from Hanke-Gogokhia and co-authors did not report any changes in murine retinal development in the absence of ARL13B. At present, the reason behind the differences in our findings is not clear. Additionally, we also observed reduction in natural retinal apoptosis at P5. We attribute reduction in apoptosis due to the

lower number of proliferating cells present in ARL13B-null retina. These findings suggest that the defect in the absence of ARL13B is in proliferation of precursors, not in a stimulation of their death. Of note our results are supported by studies that showed slower proliferation rates in *hennin* mutant embryos and immortalized mouse embryonic fibroblast (HNN) cell lines, respectively (*167*). Several lines of evidence have demonstrated that Sonic Hedgehog pathway (SHH) is an extrinsic regulator of progenitor cell proliferation and differentiation in the neural retina (*168-170*). At present, the mechanism behind reduced cell proliferation in the absence of ARL13B is not understood. However, previous reports have found that absence of ARL13B and subsequent dysregulated SHH signaling leads to defects in neural tube patterning of ARL13B mutant embryos (*86, 88, 171*). It is therefore possible that the defects in proliferation we observed in Ret-$Arl13b^{-/-}$ mutants could be in part due to dysregulated SHH detection by the RPCs that are still undergoing division during early postnatal development. Conversely, abnormal cell proliferation was not observed in the neural tube of $Arl13b^{hennin}$ mutants during embryogenesis (*78*). One possible explanation for the difference is the type of assay employed in each study used to determine proliferation. Additionally, it is possible that the proliferation defects detected in the absence of ARL13B are likely dependent on the tissue, time of development, and the organism studied. It is worth emphasizing the phenotypic variance of ARL13B deletion observed across tissues and organisms. For instance, ARL13B deletion in the retina of zebrafish models leads to a slower photoreceptor degeneration phenotype compared to the rapid cell death observed in murine models (*172*). Taken together, our results show ARL13B to be an essential player in murine retinal development.

In photoreceptors, the initial ciliary compartment begins at the connecting cilia with the ciliary axoneme extending into the OS (*104*). Cilia development (ciliogenesis) is similar between primary cilia and

photoreceptors in that both start with the mother and daughter centriole (basal bodies) adhering to what is termed a 'ciliary vesicle' that docks to the apical plasma membrane, thus allowing microtubule extension (axonemal extension) to commence (*32, 104*). In the absence of ARL13B we observed a higher incidence of basal bodies that failed to dock to the apical side of the photoreceptor inner segment in the developing retina (Fig. 6A-E). Interestingly, we also observed a higher proportion of either the daughter centriole missing ('solitary' basal bodies) across all mutant animals tested in comparison to littermate controls (data not shown). However, we cannot discount the possibility that the this finding could be due to the plane of acquisition when performing TEM. It is likely that the aberrations in basal body positioning observed in photoreceptors lacking ARL13B is a contributing factor to the impaired ciliogenesis (or outer segment development) observed in ARL13B-null photoreceptors (Fig. 5).

The mechanisms behind photoreceptor outer segment morphogenesis remain one of the most perplexing topics in photoreceptor biology. ARL13B-null retina displayed little to no OS development; connecting cilia produced only OS rudiments that contained membrane vesicles but no membranous discs (Fig. 5). We attribute the loss of ERG responses to the absence of the membranous discs that host the phototransduction cascade machinery necessary for visual transduction (Fig. 2). Previous reports have found that ARL13B associates with membranes via palmitoyl lipid anchors in primary cilia and our data shows enrichment of ARL13B in rod outer segment membranes (Fig. 1) (*79, 141*). Interestingly, ARL13B contains a "VxPx" motif in its C-termini (*86*). This motif is also present in various OS-resident proteins including Rhodopsin and Peripherin-2 and it is thought to be essential for their targeting to the OS (*104, 173, 174*). Additionally, ARL13B has been shown to be required for elongation of primary cilia through aiding in ciliary membrane protrusion by an unknown mechanism (*144*). These findings suggest that ARL13B could play an important structural/morphological role in generation of the OS by

its association with photoreceptor membranes (Fig. 1). In the absence of ARL13B we observed abundant formation of extracellular vesicles (ectosomes), similar to those observed in Peripherin-2 and BBS8-null retina (Fig. 5)(*175, 176*). It is thought that the ectosome-suppressing pathway promoted by Peripherin-2 permits the formation of photoreceptor OS discs (*175, 177*). It is possible that ARL13B, along with other key players (i.e. Peripherin-2, BBSome proteins), act synergistically in photoreceptor OS development by suppressing the 'ectosome-release' pathway and aiding in ciliary membrane protrusion. Current studies are focused on further characterizing the involvement of ARL13B in OS morphogenesis and determining the subcellular localization of ARL13B within the photoreceptor OS.

Embryonic deletion of ARL13B resulted in proliferation defects, aberrant photoreceptor ciliogenesis, and disrupted OS morphogenesis. Previous reports studied the role of ARL13B in the adult retina, more specifically in photoreceptor maintenance via tamoxifen-induced deletion of ARL13B throughout all cell-types with the use Cre^{ER}-driver line under the control of ubiquitous promoter (Hanke-Gogokhia et al., 2017). To eliminate any confounding effects from global deletion of ARL13B in adult mice we ablated ARL13B, specifically, in mature rod photoreceptors *by* $Cre^{(ERT2)}$-driven by rod *Pde6g* promoter. Remarkably, removal of ARL13B in adult rods led to abolished photoreceptor function five weeks after ARL13B ablation (Fig. 7). Additionally, two weeks after ARL13B deletion, when rod photoresponse is comparable between ARL13B-null rods and wild type littermate controls, we observed vesicles accumulating within the photoreceptor OS (Fig. 8B). Moreover, two weeks after removal of ARL13B we observed mislocalization of Rhodopsin to the photoreceptor IS and ONL, as well as accumulation of intraflagellar transport protein-88 (IFT88) to the apical tip of the connecting cilia (Fig. 8A and Fig. 9B). The bidirectional transport of protein cargoes along the ciliary axoneme is mediated by the intraflagellar transport complex (IFT), which is composed of two multi-protein sub-complexes, IFT-A and IFT-B

(*178, 179*). The IFT complex also aids in the elongation of the ciliary axoneme by concentrating tubulin to the ciliary tip (*180*). ARL13B directly interacts with members of the IFT-B sub-complex, which mediates the anterograde transport of proteins from the base to the ciliary tip (*165, 181*). Our findings suggest possible alterations of ciliary protein trafficking (i.e. Rhodopsin) and/or impaired retrograde transport in ARL13B-null photoreceptors. It is possible the axonemal defects (i.e. shortening) we observed 2 weeks after rod-specific tamoxifen-induced deletion of ARL13B is a result of the mislocalization of IFT88 (Fig. 9). Mice carrying a mutation in the IFT88 subunit (*Tg737*/*Ift88*) have been reported to develop vesiculated photoreceptor outer segments, extracellular vesicle formation (ectosomes) and Rhodopsin mislocalization (*48*). The phenotypes observed in ARL13B-depleted adult rod photoreceptors resemble the reported phenotypes of *Tg737/Ift88* animals. Nevertheless, we cannot solely attribute the abnormalities observed in our ARL13B animal models to defects in the IFT complex. Previous reports show ARL13B aids as the GEF for ARL3 (*81*). Active ARL3 is needed for the release of PDE6δ-bound prenylated cargo proteins including PDE6 to the photoreceptor OS (*147*). It is likely that the defects observed in ARL13B-deficient retinas, such as PDE6 mislocalization, are a result of mis-regulation of ARL3 activity (Fig. 8A). It is important to note that localization of OS-resident proteins such as GRK1, CNGA1 or Transducin was unaffected (data not shown). The primary defect in the ARL13B-null retina was the impaired OS development. Interestingly, we also observed areas of selective loss of PDE6 in the retina where the majority of opsin was localized to the OS (Fig. 4B). These findings lend support to the idea that GEF activity of ARL13B is needed for trafficking and/or biosynthesis of prenylated PDE6 (Hanke-Gogokhia et al., 2017). In conclusion, our study documents the essential role for ARL13B in early photoreceptor development, function and maintenance. Therefore, identification of the phenotypical events that ARL13B and its multiple protein interactors participate in photoreceptor neurons is a subject that will be addressed in future studies.

Materials and Methods

Mice, genotyping and animal husbandry

Arl13b$^{flx/flx}$ line that contain *LoxP* sites flanking exon 2 were backcrossed with C57BL/6J (Jackson laboratory, Stock No. 000664) for five generations. *Arl13b*$^{flx/flx}$ animals were then crossed with *Six3*-cre or *Pde6g*-Cre^{ERT2} to generate retina-specific (*Six3*-Cre) and rod-specific conditional ablation of *Arl13b* (*135, 153*). All experiments used littermates as controls. For inducible deletion of *Arl13b* in rod photoreceptors using the *Pde6g*-Cre^{ERT2} line, tamoxifen (Sigma-Aldrich #T5648-1G) was injected intraperitoneally (IP) at concentrations of 100 µg/g body weight for 3 consecutive days (1 injection/day) as previously described (*164*). PCR primers used to detect floxed alleles were 5'- CGA CCA TCA CAA GTG TCA CC-3' and 5'-AGG ACG GTT GAG AAC CAC TG-3'. Oligonucleotides used in PCR to detect *Cre* recombinase were 5' CCT GGA AAA TGC TTC TGT CCG 3' and 5' CAG GGT GTT ATA AGC AAT CCC 3'. Oligonucleotides used in PCR to verify the presence of *Pde6g*-Cre^{ERT2} driver line were 5'- GGT CAG ATT CCA GTG TGT GG - 3' and 5'- GTT TAG CTG GCC CAA ATG TTG - 3'. All animals used in this study are free of *rd1* and *rd8* alleles (*134, 182*).

The animals were maintained under 12-h light / 12-h dark light cycles with food and water provided *ad libitum*. All experimental procedures involving animals in this study were approved by the Institutional Animal Care and Use Committee of West Virginia University.

Electroretinography (ERG)

Electroretinograms were performed on the UTAS Visual Diagnostic System with Big-Shot Ganzfeld using a UBA-4200 amplifier and interface, and EMWIN 9.0.0 software (LKC Technologies, Gaithersburg, MD, USA). Prior to ERG testing, mice were dark-adapted for 24 hours. Mice were anesthetized [2.0% isoflurane with 2.5 liters per minute (lpm) oxygen flow rate] for 10 minutes and eyes were topically dilated with a 1:1 mixture of tropicamide:phenylephrine hydrochloride. For ERG procedure, mice were placed on a heated platform with continuous flow of isoflurane through a nose cone [1.5% isoflurane with 2.5 liters per minute (lpm) oxygen flow rate]. A reference electrode was introduced subcutaneously in the scalp and ERG responses were recorded from both eyes with silver wire electrodes placed on top of each cornea, with contact being facilitated with hypromellose solution (2% hypromellose in Phosphate Buffer Solution/PBS) (Gonioscopic Prism Solution, Wilson Ophthalmic, Mustang, OK, USA). Scotopic photoresponses were acquired under dark conditions with flashes of LED white light at increasing flash intensities. For photopic photoresponses, animals were light-adapted with rod-saturating white background light (30 cd.m-2) for 10 minutes and cone photoresponses were subsequently recorded.

Immunohistochemistry

For immunohistochemical experiments, eyes were enucleated and immersed in 4% paraformaldehyde fixative (4% PFA in Phosphate Buffered Saline [PBS: 137mM NaCl, 2.7 mM KCl, 4.3 mM $Na_2HPO_4 \cdot 7H_2O$, 1.4 mM KH_2PO_4,]) for 30 min prior to the removal of the cornea and lens. Following removal of cornea and lens, enucleated eyes were fixed for an additional 30 min, washed in PBS three times for 5 min each, and incubated in 20% sucrose in PBS overnight at 4°C on a nutator. Following overnight incubation, eyecups were placed in a 1:1 mixture of 20% sucrose in PBS and OCT (Cryo Optimal Cutting Temperature Compound, Sakura) for 1 hr and flash-frozen in OCT. For ciliary staining,

enucleated eyes were fixed in 4% paraformaldehyde in PBS for 30 sec and flash-frozen in OCT. Cryosectioning was performed using Leica CM1850 Cryostat, and retinal sections of 16 µm and/or 12 µm (for ciliary staining) thickness were mounted on Superfrost Plus slides (Fisher Scientific). Mounted Retinal sections were washed with PBST (PBS with 5% Goat Sera, 0.5% TritonX-100, 0.05% Sodium Azide) 2 times for 5 minutes each and incubated for 1 hr in blocking buffer at room temperature (PBST: PBS with 5% Goat Sera, 0.5% Tween 20, 0.05% Sodium Azide). After blocking, retinal sections were incubated with primary antibodies at the dilutions described in *Table I* at 4°C overnight. For ciliary staining, incubation with primary antibodies was done for 3-4 hrs at room temperature. After primary antibody incubation, retinal sections were washed with PBST 2 times for 5 min and once with PBS for 5 min before incubation with secondary antibodies [anti-rabbit 488 (or 568), anti-mouse 488 (or 568), anti-guinea pig 680, anti-chicken488] for 1hr. Nuclei were stained with DAPI nuclear stain 405. Slides were mounted with ProLong Gold (Life Technologies) and cover-slipped. Confocal imaging was performed with the Nikon's C2si+ system laser scanning confocal microscope using excitation wavelengths of 405, 488, 543 and 647 nm. Micrographs were captured using the same exposure time settings among all groups.

Immunoblotting

Mice were euthanized by CO_2 inhalation followed by cervical dislocation, eyes were enucleated and retina was dissected following previously established protocols (*183*). For immunoblots, flash-frozen retinae were sonicated in phosphate buffered saline [PBS with protease inhibitor cocktail (Roche)]. Protein concentrations were measured using a spectrophotometer (Thermo Fisher Scientific, Inc.) and the RC DC protein assay (Bio-Rad Laboratories, Inc.). Equal amounts of samples (100 µg total protein per well) were separated in a polyacrylamide SDS–PAGE gel and transferred onto polyvinylidene

difluoride (PVDF) membranes (Immobilon-FL, Millipore, Billerica). Membranes were subsequently incubated in blocking buffer (Odyssey Blocking Buffer, LI-COR Biosciences) for 45 min at room temperature and further incubated with primary antibodies overnight at 4°C on a bidirectional rotator. Following primary antibody incubation (*Table I)*, membranes were washed in PBST (PBS with 0.1% Tween-20) three times for 5 min each at room temperature and incubated in secondary antibody, goat anti-rabbit Alexa 680 (or 800), rabbit anti-goat Alexa 680 or goat anti-mouse Alexa 680 (Invitrogen) for 30 min at room temperature. After washes with PBST, membranes were scanned using the Odyssey Infrared Imaging System (LI-COR Biosciences, Lincoln, NE, USA).

Photoreceptor ultrastructure

Eyes were enucleated and fixed in freshly made 2% paraformaldehyde, 2.5% glutaraldehyde, 0.1M cacodylate buffer, pH 7.5 for 30 minutes before removal of cornea and lens. Enucleated eyes were additionally fixed as mentioned above for 48 hours at room temperature under rotation (nutator). Subsequent dissection, embedding and transmission electron microscopy were performed as previously described (*184*).

Rod outer segment membrane isolation

The isolation of rod outer segment (ROS) membranes was performed using previously described protocols with modifications (*150, 151*). ROS membranes were prepared using 20 murine retinae obtained from adult wild-type animals. Briefly, the retinal tissue suspended in 300 µl of 8% (vol/vol) OptiPrep (Sigma-Aldrich) in Ringer's buffer (10 mM Hepes, 130 mM NaCl, 3.6 mM KCl, 2.4 mM $MgCl_2$, 1.2 mM $CaCl_2$, and 0.02 mM EDTA, pH 7.4), was vortexed at maximum speed, followed by

centrifugation at 250 x *g* for 1 min. The supernatant was collected. The pellet was re-suspended in 300 µl of solution containing 8% OptiPrep in Ringer's buffer. The vortexing and centrifugation steps were repeated as described above for five times. The pooled supernatant samples were layered on a 10–30% (vol/vol) continuous gradient of OptiPrep in 12 ml of Ringer's buffer The gradient was centrifuged for 50 min at 26,500 x *g* at 4 °C using a Beckman ultracentrifuge (Optima LE-80K; SW-41Ti). Intact ROS membranes were found at two thirds away from the top. The ROS membrane band was recovered by aspiration using a pasteur pipette and diluted with threefold Ringer's buffer. The resulting suspension was centrifuged for 3 min at 650 x *g*. To retrieve ROS membranes, the supernatant was collected and placed in a 1.5ml ultracentrifuge tube (Beckman 9.5 X 38mm) and centrifuged for 30 min at 26,500 x *g* using a table top Beckman ultracentrifuge (Optima TLX; rotor-TLA55). The resulting pellet contained the isolated ROS membranes.

Experimental design and Statistical Analysis

All quantitative analysis was performed on age-matched *Arl13b* littermate wild-type controls *and knockout animals.* For immunohistochemical analysis, at least 4 sections were imaged per sample and data were derived from at minimum $n > 3$ independent experiments. Statistical analyses were performed using GraphPad Prism software version 7.0. Data are presented as mean ± standard error margin. Unpaired Student's t tests were conducted to compare measured values between control and mutant samples. Scotopic and photopic electroretinography (ERG) responses were analyzed with two-way ANOVA and then applied Tukey post-hoc test for comparison of means between groups with p-value <0.05. For cilia measurements, 80-100 cilia were measured for each animal ($n=3$) and data were visualized with the ggplot2 package in R version 3.3.2. Image and densitometry analysis were

performed using ImageJ-FIJI 1.50i along with the Bio-Formats plugin (NIH). Sex differences were assessed for each outcome measure, with no significant change observed.

References

Arikawa K, Williams DS (1993) Acetylated alpha-tubulin in the connecting cilium of developing rat photoreceptors. Investigative Ophthalmology & Visual Science 34:2145-2149.

Bay SN, Long AB, Caspary T (2018) Disruption of the ciliary GTPase Arl13b suppresses Sonic hedgehog overactivation and inhibits medulloblastoma formation. Proc Natl Acad Sci U S A 115:1570-1575.

Bishop AL, Hall A (2000) Rho GTPases and their effector proteins. Biochem J 348 Pt 2:241-255.

Cantagrel V et al. (2008) Mutations in the cilia gene ARL13B lead to the classical form of Joubert syndrome. Am J Hum Genet 83:170-179.

Caspary T, Larkins CE, Anderson KV (2007) The graded response to Sonic Hedgehog depends on cilia architecture. Dev Cell 12:767-778.

Cevik S, Hori Y, Kaplan OI, Kida K, Toivenon T, Foley-Fisher C, Cottell D, Katada T, Kontani K, Blacque OE (2010) Joubert syndrome Arl13b functions at ciliary membranes and stabilizes protein transport in Caenorhabditis elegans. The Journal of Cell Biology 188:953-969.

Cevik S et al. (2013) Active transport and diffusion barriers restrict Joubert Syndrome-associated ARL13B/ARL-13 to an Inv-like ciliary membrane subdomain. PLoS Genet 9:e1003977.

Cherfils J, Zeghouf M (2013) Regulation of small GTPases by GEFs, GAPs, and GDIs. Physiol Rev 93:269-309.

Dakubo GD, Wallace VA (2004) Hedgehogs and retinal ganglion cells: organizers of the mammalian retina. Neuroreport 15:479-482.

Deretic D, Schmerl S, Hargrave PA, Arendt A, McDowell JH (1998) Regulation of sorting and post-Golgi trafficking of rhodopsin by its C-terminal sequence QVS(A)PA. Proceedings of the National Academy of Sciences of the United States of America 95:10620-10625.

Dilan TL, Singh RK, Saravanan T, Moye A, Goldberg AFX, Stoilov P, Ramamurthy V (2018) Bardet–Biedl syndrome-8 (BBS8) protein is crucial for the development of outer segments in photoreceptor neurons. Human Molecular Genetics 27:283-294.

Furuta Y, Lagutin O, Hogan BL, Oliver GC (2000) Retina- and ventral forebrain-specific Cre recombinase activity in transgenic mice. Genesis 26:130-132.

Gimenez E, Montoliu L (2001) A simple polymerase chain reaction assay for genotyping the retinal degeneration mutation (Pdeb(rd1)) in FVB/N-derived transgenic mice. Laboratory animals 35:153-156.

Goldberg AF, Ritter LM, Khattree N, Peachey NS, Fariss RN, Dang L, Yu M, Bottrell AR (2007) An intramembrane glutamic acid governs peripherin/rds function for photoreceptor disc morphogenesis. Invest Ophthalmol Vis Sci 48:2975-2986.

Gotthardt K, Lokaj M, Koerner C, Falk N, Giessl A, Wittinghofer A (2015) A G-protein activation cascade from Arl13B to Arl3 and implications for ciliary targeting of lipidated proteins. Elife 4.

Hanke-Gogokhia C, Wu Z, Gerstner CD, Frederick JM, Zhang H, Baehr W (2016) Arf-like Protein 3 (ARL3) Regulates Protein Trafficking and Ciliogenesis in Mouse Photoreceptors. J Biol Chem 291:7142-7155.

Hanke-Gogokhia C, Wu Z, Sharif A, Yazigi H, Frederick JM, Baehr W (2017) The guanine nucleotide exchange factor, Arf-like protein 13b, is essential for assembly of the mouse photoreceptor transition zone and outer segment. Journal of Biological Chemistry.
Harris JA, Van De Weghe JM, Kubo T, Witman GB, Lechtreck K (2018) Diffusion rather than IFT provides most of the tubulin required for axonemal assembly. bioRxiv.
Hendzel MJ, Wei Y, Mancini MA, Van Hooser A, Ranalli T, Brinkley BR, Bazett-Jones DP, Allis CD (1997) Mitosis-specific phosphorylation of histone H3 initiates primarily within pericentromeric heterochromatin during G2 and spreads in an ordered fashion coincident with mitotic chromosome condensation. Chromosoma 106:348-360.
Hori Y, Kobayashi T, Kikko Y, Kontani K, Katada T (2008) Domain architecture of the atypical Arf-family GTPase Arl13b involved in cilia formation. Biochemical and Biophysical Research Communications 373:119-124.
Horner VL, Caspary T (2011) Disrupted dorsal neural tube BMP signaling in the cilia mutant Arl13b(hnn) stems from abnormal Shh signaling. Developmental biology 355:43-54.
Hua K, Ferland RJ (2017) Fixation methods can differentially affect ciliary protein immunolabeling. Cilia 6:5.
Ismail SA, Chen YX, Miertzschke M, Vetter IR, Koerner C, Wittinghofer A (2012) Structural basis for Arl3-specific release of myristoylated ciliary cargo from UNC119. EMBO J 31:4085-4094.
Ivanova AA, Caspary T, Seyfried NT, Duong DM, West AB, Liu Z, Kahn RA (2017) Biochemical characterization of purified mammalian ARL13B protein indicates that it is an atypical GTPase and ARL3 guanine nucleotide exchange factor (GEF). J Biol Chem 292:11091-11108.
Koch SF, Tsai YT, Duong JK, Wu WH, Hsu CW, Wu WP, Bonet-Ponce L, Lin CS, Tsang SH (2015) Halting progressive neurodegeneration in advanced retinitis pigmentosa. J Clin Invest 125:3704-3713.
Larkins CE, Aviles GD, East MP, Kahn RA, Caspary T (2011) Arl13b regulates ciliogenesis and the dynamic localization of Shh signaling proteins. Mol Biol Cell 22:4694-4703.
Lechtreck KF (2015) IFT-Cargo Interactions and Protein Transport in Cilia. Trends Biochem Sci 40:765-778.
Li Y, Tian X, Ma M, Jerman S, Kong S, Somlo S, Sun Z (2016) Deletion of ADP Ribosylation Factor-Like GTPase 13B Leads to Kidney Cysts. J Am Soc Nephrol 27:3628-3638.
Liu Q, Zuo J, Pierce EA (2004) The Retinitis Pigmentosa 1 Protein Is a Photoreceptor Microtubule-Associated Protein. The Journal of neuroscience : the official journal of the Society for Neuroscience 24:6427-6436.
Lu H, Toh MT, Narasimhan V, Thamilselvam SK, Choksi SP, Roy S (2015) A function for the Joubert syndrome protein Arl13b in ciliary membrane extension and ciliary length regulation. Dev Biol 397:225-236.
Malicki JJ, Johnson CA (2017) The Cilium: Cellular Antenna and Central Processing Unit. Trends Cell Biol 27:126-140.
Mariani LE, Bijlsma MF, Ivanova AI, Suciu SK, Kahn RA, Caspary T (2016) Arl13b regulates Shh signaling from both inside and outside the cilium. Molecular biology of the cell 27:3780-3790.
Mattapallil MJ, Wawrousek EF, Chan CC, Zhao H, Roychoudhury J, Ferguson TA, Caspi RR (2012) The Rd8 mutation of the Crb1 gene is present in vendor lines of C57BL/6N mice and embryonic stem cells, and confounds ocular induced mutant phenotypes. Invest Ophthalmol Vis Sci 53:2921-2927.
Miertzschke M, Koerner C, Spoerner M, Wittinghofer A (2014) Structural insights into the small G-protein Arl13B and implications for Joubert syndrome. Biochem J 457:301-311.

Molday RS, Goldberg AFX (2017) Peripherin diverts ciliary ectosome release to photoreceptor disc morphogenesis. The Journal of Cell Biology.
Mongan M, Wang J, Liu H, Fan Y, Jin C, Kao WY, Xia Y (2011) Loss of MAP3K1 enhances proliferation and apoptosis during retinal development. Development 138:4001-4012.
Moshiri A, McGuire CR, Reh TA (2005) Sonic hedgehog regulates proliferation of the retinal ciliary marginal zone in posthatch chicks. Dev Dyn 233:66-75.
Nickell S, Park PS-H, Baumeister W, Palczewski K (2007) Three-dimensional architecture of murine rod outer segments determined by cryoelectron tomography. The Journal of Cell Biology 177:917-925.
Noga V (1998) Alpha subunit of Go localizes in the dendritic tips of ON bipolar cells. Journal of Comparative Neurology 395:43-52.
Nozaki S, Katoh Y, Terada M, Michisaka S, Funabashi T, Takahashi S, Kontani K, Nakayama K (2017) Regulation of ciliary retrograde protein trafficking by the Joubert syndrome proteins ARL13B and INPP5E. J Cell Sci 130:563-576.
Omori Y, Chaya T, Katoh K, Kajimura N, Sato S, Muraoka K, Ueno S, Koyasu T, Kondo M, Furukawa T (2010) Negative regulation of ciliary length by ciliary male germ cell-associated kinase (Mak) is required for retinal photoreceptor survival. Proceedings of the National Academy of Sciences 107:22671-22676.
Pazour GJ, Baker SA, Deane JA, Cole DG, Dickert BL, Rosenbaum JL, Witman GB, Besharse JC (2002) The intraflagellar transport protein, IFT88, is essential for vertebrate photoreceptor assembly and maintenance. The Journal of Cell Biology 157:103-114.
Pearring JN, Salinas RY, Baker SA, Arshavsky VY (2013) Protein sorting, targeting and trafficking in photoreceptor cells. Prog Retin Eye Res 36:24-51.
Pinto LH, Invergo B, Shimomura K, Takahashi JS, Troy JB (2007) Interpretation of the mouse electroretinogram. Documenta ophthalmologica Advances in ophthalmology 115:127-136.
Portran D, Schaedel L, Xu Z, Théry M, Nachury MV (2017) Tubulin acetylation protects long-lived microtubules against mechanical aging. Nature cell biology 19:391-398.
Pruski M, Rajnicek A, Yang Z, Clancy H, Ding YQ, McCaig CD, Lang B (2016) The ciliary GTPase Arl13b regulates cell migration and cell cycle progression. Cell Adh Migr 10:393-405.
Quinteros Q, Benedetto ML, Maldonado MM, E ACVdP, Contin MA (2016) Electroretinography: A biopotential to assess the function/dysfunction of the retina. Journal of Physics: Conference Series 705:012053.
Rakshit T, Senapati S, Sinha S, Whited AM, Park PSH (2015) Rhodopsin Forms Nanodomains in Rod Outer Segment Disc Membranes of the Cold-Blooded Xenopus laevis. PLOS ONE 10:e0141114.
Ramamurthy V, Niemi GA, Reh TA, Hurley JB (2004) Leber congenital amaurosis linked to AIPL1: A mouse model reveals destabilization of cGMP phosphodiesterase. Proceedings of the National Academy of Sciences of the United States of America 101:13897-13902.
Roy K, Jerman S, Jozsef L, McNamara T, Onyekaba G, Sun Z, Marin EP (2017) Palmitoylation of the ciliary GTPase ARL13b is necessary for its stability and its role in cilia formation. J Biol Chem 292:17703-17717.
Salinas RY, Pearring JN, Ding J-D, Spencer WJ, Hao Y, Arshavsky VY (2017) Photoreceptor discs form through peripherin-dependent suppression of ciliary ectosome release. The Journal of Cell Biology 216:1489-1499.
Sedmak T, Wolfrum U (2010) Intraflagellar transport molecules in ciliary and nonciliary cells of the retina. J Cell Biol 189:171-186.

Skiba NP, Spencer WJ, Salinas RY, Lieu EC, Thompson JW, Arshavsky VY (2013) Proteomic identification of unique photoreceptor disc components reveals the presence of PRCD, a protein linked to retinal degeneration. J Proteome Res 12:3010-3018.
Song P, Dudinsky L, Fogerty J, Gaivin R, Perkins BD (2016) Arl13b Interacts With Vangl2 to Regulate Cilia and Photoreceptor Outer Segment Length in Zebrafish. Invest Ophthalmol Vis Sci 57:4517-4526.
Strom SP, Clark MJ, Martinez A, Garcia S, Abelazeem AA, Matynia A, Parikh S, Sullivan LS, Bowne SJ, Daiger SP, Gorin MB (2016) De Novo Occurrence of a Variant in ARL3 and Apparent Autosomal Dominant Transmission of Retinitis Pigmentosa. PLOS ONE 11:e0150944.
Su C-Y, Bay SN, Mariani LE, Hillman MJ, Caspary T (2012) Temporal deletion of Arl13b reveals that a mispatterned neural tube corrects cell fate over time. Development (Cambridge, England) 139:4062-4071.
Suga A, Sadamoto K, Fujii M, Mandai M, Takahashi M (2014) Proliferation Potential of Müller Glia after Retinal Damage Varies between Mouse Strains. PLOS ONE 9:e94556.
Sun Z, Amsterdam A, Pazour GJ, Cole DG, Miller MS, Hopkins N (2004) A genetic screen in zebrafish identifies cilia genes as a principal cause of cystic kidney. Development 131:4085-4093.
Tam BM, Moritz OL, Papermaster DS (2004) The C terminus of peripherin/rds participates in rod outer segment targeting and alignment of disc incisures. Mol Biol Cell 15:2027-2037.
Taschner M, Lorentzen E (2016) The Intraflagellar Transport Machinery. Cold Spring Harb Perspect Biol 8.
Thomas S, Cantagrel V, Mariani L, Serre V, Lee JE, Elkhartoufi N, de Lonlay P, Desguerre I, Munnich A, Boddaert N, Lyonnet S, Vekemans M, Lisgo SN, Caspary T, Gleeson J, Attie-Bitach T (2015) Identification of a novel ARL13B variant in a Joubert syndrome-affected patient with retinal impairment and obesity. Eur J Hum Genet 23:621-627.
Wall DS, Mears AJ, McNeill B, Mazerolle C, Thurig S, Wang Y, Kageyama R, Wallace VA (2009) Progenitor cell proliferation in the retina is dependent on Notch-independent Sonic hedgehog/Hes1 activity. J Cell Biol 184:101-112.
Wright ZC, Singh RK, Alpino R, Goldberg AFX, Sokolov M, Ramamurthy V (2016) ARL3 regulates trafficking of prenylated phototransduction proteins to the rod outer segment. Human Molecular Genetics 25:2031-2044.
Zhang Q, Li Y, Zhang Y, Torres VE, Harris PC, Ling K, Hu J (2016) GTP-binding of ARL-3 is activated by ARL-13 as a GEF and stabilized by UNC-119. Scientific Reports 6:24534.

4

Discussion and Future Perspectives

As mentioned in Chapter 1, the outer segment is a modified ciliary compartment that houses all of the protein machinery needed for visual transduction. The stacked-membranous disc architecture of the outer segment (OS) represents a deviation from the architecture of traditional primary cilia. Another key distinction rests with the fact that photoreceptor outer segments are constantly renewing their cellular components, which means that new membranous discs must be continually synthesized, and populated throughout the lifetime of the organism (*9*). The mechanistic steps and the identity of the key proteins involved in the formation of the OS membranous disc, the maintenance of the OS, and the transport of proteins from their sites of synthesis in the inner segment (IS) to the OS remain poorly understood. The long-term goal of this study was to better understand the role of two ciliary proteins, BBS8 and ARL13B, in assisting photoreceptor outer segment morphogenesis, maintenance, and function. These two proteins are linked to retinitis pigmentosa (vision loss), highly enriched in the photoreceptor OS, and have no known role in the phototransduction cascade. In the following sub-

chapters, we will discuss the main findings, additional preliminary findings, and future experimental avenues that could be explored for studying both of these ciliary proteins in the context of vision.

4.1 Phenotypic similarities and differences between ARL13B and BBS8 mutants:

4.1.1 Retinogenesis

Since global ablation of ARL13B is embryonically lethal, we generated a conditional murine model using a *Cre* recombinase driver-line under the *Six3* promoter (Chapter 3). The *Six3*-Cre driver-line ablates ARL13B in the retina and ventral forebrain at embryonic day 9.5 (*185*). Contrary to ARL13B, global deletion of BBS8 did not result in embryonic lethality (Chapter 2). To study the role of BBS8 in photoreceptor cells, we recovered a BBS8 global knockout (BBS8-null) mouse model from sperm obtained from the UC Davis KOMP repository. This line contains a stop cassette that knocks-in a β-galactosidase reporter after exon 2, terminating *Bbs8* gene transcription (Chapter 2). Due to low litter numbers caused by fertility issues with the line (a symptom of BBS), we opted to generate a similar model as ARL13B, where we delete BBS8 in the retina at embryonic day 9.5 (Chapter 3). Both BBS8 and ARL13B mutant models presented with a significant reduction in retinal photoresponse at the earliest age tested (P15) (Chapters 2 and 3). In spite of this similarity, early deletion of ARL13B resulted in defects in the proliferation of retinal progenitor cells at P5, leading to the loss of 2-3 nuclei layers by the age of P10 (Chapter 3). In contrast, nuclei layers in BBS8-null retina were comparable to wild-type littermate controls at P10. Several lines of evidence have shown the Sonic Hedgehog signaling pathway to regulate cell proliferation and differentiation in the developing retina (*186-189*). Furthermore, the link between primary cilia and Sonic Hedgehog (SHH) signaling was first formed when researchers began to observe mutant models of ciliary proteins displaying defective patterning of the mouse embryo, as well

as other phenotypes that are characteristic of defects in Sonic hedgehog signaling (*190, 191*). Corbit and colleagues went on to demonstrate that mammalian Smoothened (Smo), a seven-transmembrane protein essential for SHH signaling, is expressed within the primary cilium, its ciliary expression is regulated by SHH pathway activity (*192*). Within the murine retina, SHH ligand is produced in the retinal ganglion cells (RGC's) and is required for the maintenance of SHH target gene expression in proliferating retinal cells (RPC's) both *in vivo* and in retinal explants (*188, 193*). All retinal cells, except for astrocytes, are derived from these multipotential retinal precursor cells (RPC's)(*194-196*). We hypothesize that the defects we observe in the proliferation of RPC's (Chapter 3), is due to defective Sonic hedgehog detection and/or secretion due to aberrant ciliogenesis in the absence of ARL13B. To test this hypothesis, a two-prong approach can be implemented: 1) Determine whether retinal ganglion cell-derived SHH secretion, which acts to maintain RPC homeostasis (*197*), is impaired in ARL13B-null retina, and 2) Determine whether SHH detection by RPC's is impaired in ARL13B-null retina. The major downstream targets of the SHH pathway are the Gli1 and Gli2 transcription factors, which activate target gene expression in response to Smo signaling (*198, 199*). To determine if SHH detection by RPC's is impaired (caused by aberrant ciliogenesis) in ARL13B-null retina, we can measure the relative protein expression of Gli1 and Gli3 in embryonic retinal explants stimulated with SHH ligand (*200*). Alternatively, to determine whether the initial proliferation defects are originating from poor SHH secretion from retinal ganglion cells, our ARL13B floxed animals can be crossed to a *Cre* recombinase under a retinal ganglion cell-specific promoter (i.e., *Chrnb3*-Cre) (*201*).

In addition to defects in retinogenesis, our preliminary studies also showed defective retinal angiogenesis in the absence of ARL13B, a result not observed in retina lacking BBS8 (Figure 4.1.1). The retinal vasculature network is comprised of three interconnected layers of retinal vessels that are entrenched among retinal neurons. The superficial layer lies adjacent to the ganglion cell layer, and the intermediate and deep retinal vascular networks run along each side of the inner nuclear layer (INL) (Figure 4.1.1a). Lastly, the choroidal vessels are located beneath the retinal pigmented epithelium (RPE) and supply oxygen and nutrients to the outer portion of the retina (Figure 4.1.1a). In ARL13B-null retina, we observe the retardation of capillary development in the intermediate layer compared to littermate controls (Figure 4.1.1b right and left panels). Unlike ARL13B mutants, the intermediate layer of the vasculature network of another retinitis pigmentosa murine model, *Rd1*$^{-/-}$; which is characterized by a mutation in Pde6β that leads to rapid and severe photoreceptor degeneration, is comparable to

Figure 4.1.1 Vascular changes in retina lacking ARL13B A) A schematic cross-section of the retinal vasculature lining the inner surface of the retina and the choroid vessels. B) *(Left panel)* Confocal sections of the superficial, intermediate, and deep vascular layer in ARL13B-null retina and WT littermate controls at P18 (stained for Isolectin, n=3). (*Right panel*) 3D-reconstructed image showing retardation of intermediate capillaries in mutant animals compared to wild-type controls. Collaboration with Dr. Sujata Rao Cleveland Clinic.

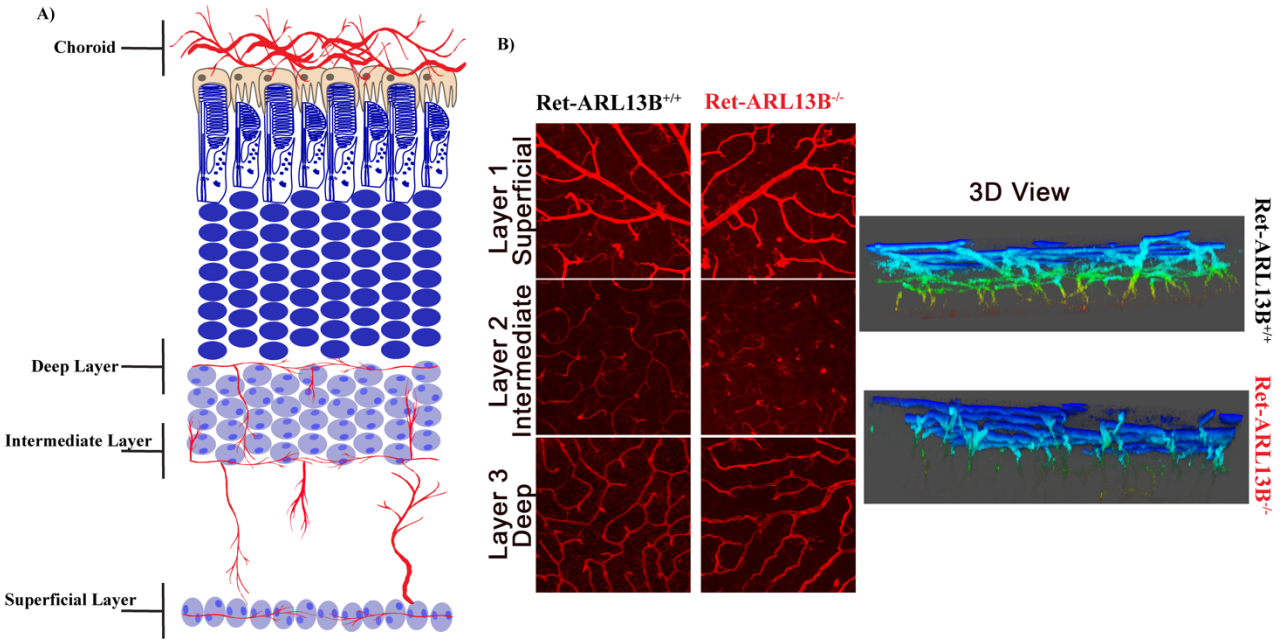

littermate controls and shows no retardation of intermediate blood capillaries (*202*). The *Rd1* models do display retardation of retinal vascular development in the vasculature deep layer (layer adjacent to the photoreceptor neurons) (*202*). At present, the connection between photoreceptor degeneration and vasculature angiogenesis is not well understood; however, recent papers support a role for cilia in developmental angiogenesis (*203*). Goetz and colleagues demonstrated that alterations in ciliogenesis impair endothelial calcium levels and perturb vascular morphogenesis (*204*). At present, it is unclear if the defects observed in the vasculature intermediate layer of ARL13B-null retina is a response to changing neuronal activity at the onset of neurodegeneration or defective ciliary signaling crosstalk between retinal neurons and vasculature endothelia. Teasing out the origin of the observed vasculature deficit in ARL13B-null retina could be an interesting avenue for future work.

4.1.2 Outer segment morphogenesis

Ultrastructural analysis of both BBS8- and ARL13B- null retina showed proper basal body docking and connecting cilia/ transition zone development. Although ARL13B did have a higher percentage of displaced basal bodies compared to littermate controls (Chapter 3 and Chapter 4). Interestingly, embryonic deletion of BBS8 resulted in photoreceptors which formed outer segments and their membranous-stacked discs. However, once formed, the outer segments became highly dysmorphic over time. In contrast, ARL13B deletion prevented the formation of outer segments; where the OS did form, they resembled highly vesiculated rudiments. These results suggest that ARL13B is needed for the initial formation of photoreceptor outer segments, while BBS8 is not needed for OS development per

se—the structural defects observed are most likely a secondary effect from the breakdown of protein clearance that arises from BBS8 loss (see Chapter 2 or continue to Chapter 4.1.3).

In Chapters 2 and 3, we presented through ultrastructure analysis, that BBS8 and ARL13B mutant mice accumulate extracellular vesicles directly adjacent to their dysmorphic OS rudiments. We made this striking observation at both ages tested (P10 and P18), where we observed large amounts of extracellular material in the subretinal space. In both IMCD3- and mouse embryonic fibroblast (MEF) cell lines lacking BBS subunits, ciliary GPCR's accumulated at the ciliated tip and were removed by ectocytosis, forming extracellular vesicles (ectovesicles or EV's) (*65*). These extracellular vesicles were similar to the ciliary ectosomes, which had been described for other ciliated cells (*65, 205, 206*). The average Feret diameter of ciliary EVs was just over 100 nm in cell culture studies, while the average Feret diameter of both ARL13B- and BBS8-null retina was around 202 nm and 145nm, respectively. We hypothesize photoreceptor extracellular vesicle formation is a response to protein accumulation and is conserved across cilia. Indeed, photoreceptor ectovesicles were once thought to be an artifact of EM sample preparation—only recently have they been linked to a ciliary process (*207*). At present, we have only observed these ectovesicles form in some models of retinitis pigmentosa (i.e., Peripherin-2, ARL13B, BBS8, IFT88 mutants). Identifying the contents of these ciliary vesicles (do they carry accumulated GPCR's?) and determining if are they utilized by photoreceptor cells to 'communicate' with neighboring cells during healthy states could be a topic for future studies.

4.1.2 Development of ciliary structures: the microtubule axoneme, tubulin post-translational modifications, and the Intraflagellar transport protein complex

Microtubule axoneme and tubulin post-translational modifications

Although the ciliary axoneme and connecting cilia both form in ARL13B- and BBS8- null retina, as evidenced by ultrastructural analysis, the axoneme is shorter in the mutants compared to wild-type littermate controls. In the case of BBS8-null retina, the microtubule axoneme is shorter, and there is an increase in tubulin acetylation (Chapter 2). Meanwhile, hyperacetylation was not observed in ARL13B-null retina. The tubulin found in the ciliary axoneme and connecting cilia undergoes several posttranslational modifications (PTMs), including tubulin acetylation (*208*). Perturbations in tubulin PTMs have been linked to cilia dysfunction; however, it is unclear how microtubule PTMs are regulated in photoreceptor cilia (*118, 209, 210*). In our BBS8-null mice, we observe an increase in acetylated tubulin stained zones along the connecting cilia (Chapter 3), which suggests two possible scenarios: 1) Independent from the BBSome complex, BBS18, the linker subunit between BBS4 and BBS8 (*211*), is a known regulator of microtubule acetylation through its direct interaction with histone deacetylase 6 (HDAC6) (*209*). HDAC6 is known for its role in α-tubulin deacetylation and ciliary disassembly (*212-214*). Our results also confirm that in the absence of BBS8, there are dynamic changes to the other BBS partner subunits. One possible scenario for the increased tubulin acetylation is that BBS18 could be upregulated in photoreceptors lacking BBS8, causing dysregulation of HDAC6 and subsequently microtubule acetylation. 2) Interestingly, α-Tubulin N-acetyltransferase-1 (αTAT1) is considered the enzyme responsible for acetylation of α -tubulin in ciliated organisms, and it has been shown to interact directly with the BBSome complex (*215-217*). We cannot presently exclude the possibility that the observed increased in microtubule acetylation in BBS8-null retina could be due to increased ciliary localization of αTAT1 under a dynamic BBSome.

To test if BBS8 ablation leads to upregulation and/or downregulation of microtubule acetylation, future studies should focus on measuring relative protein levels of BBS18 (which was not performed during our initial examination), HDAC6 and αTAT1 in retina lacking BBS8 by Western blot and compare them to their wild-type littermate controls. Complementary studies exploring the temporal dynamics of gene expression of the previously mentioned proteins by performing qPCR and quantifying the mRNA levels in BBS8-KO retina would also be useful in determining if the potential changes in protein abundance are occurring at the posttranslational level. Importantly, the activity of HDAC6 and αTAT1 is not the only factor that dictates their regulation of microtubule stability; subcellular distribution also plays an important role in substrate selection (*218, 219*). The BBSome complex interacts with both HDAC6 and αTAT1 (*57, 209, 217*), so one possible scenario is that BBS8 ablation leads to the improper subcellular localization of these tubulin PTM enzymes. Therefore, determining the subcellular localization of HDAC6 and αTAT1 by immunofluorescence in BBS8-KO retina should also be done in conjunction with the previously mentioned studies. Due to recent findings linking tubulin isoforms to retinal diseases and dynamic changes of tubulin PTM's in response to retinal disease (*118, 220, 221*), understanding the relationship between photoreceptor cilia and their cytoskeletal regulation in the pathogenesis of Bardet-Biedl Syndrome could provide important insights to further dissect and understand the 'tubulin code'.

Intraflagellar transport complex

As mentioned in Chapter 1, the intraflagellar transport protein complex ('IFT trains') plays an essential role in axonemal extension and regulation by aiding in the transport of tubulin into cilia. The IFT complex is comprised of at least 20 different proteins and dissociates into two sub-complexes; IFT-A and IFT-B (*36, 37*). Interestingly, when ARL13B was ablated in rod photoreceptors in adult animals with the use of a tamoxifen-inducible *Cre*-driver line (*Pde6g*-Cre^{ERT2}), we observed mislocalization of intraflagellar transport protein-88 (IFT88) from the basal side of the connecting cilia (WT littermates) to the photoreceptor inner segment two weeks after ARL13B deletion (Chapter 3 and Figure 4.1.2). IFT88

Figure 4.1.2 ARL13B and IFT88 subcellular localization within photoreceptors A) Adapted from Sedmak et al., 2010, electron micrograph of anti-IFT88 immunolabeling in both the apical side of the connecting cilia/ transition zone and the mother centriole region (basal area) of the murine photoreceptor cilia. B) Our preliminary studies of anti-ARL13B immunolabeling in the murine photoreceptor cilia, pink arrows indicate ARL13B density in the mother centriole, the same region IFT88 is densely concentrated (A) (Collaboration with Dr. Hemant Khanna at UMASS). C) Immunofluorescence of retinal cross-sections of tamoxifen-inducible ARL13B mouse models two weeks after ARL13B deletion, showing lack of IFT88 at the basal zone of the connecting cilia/transition zone, the same region that houses the mother centriole.

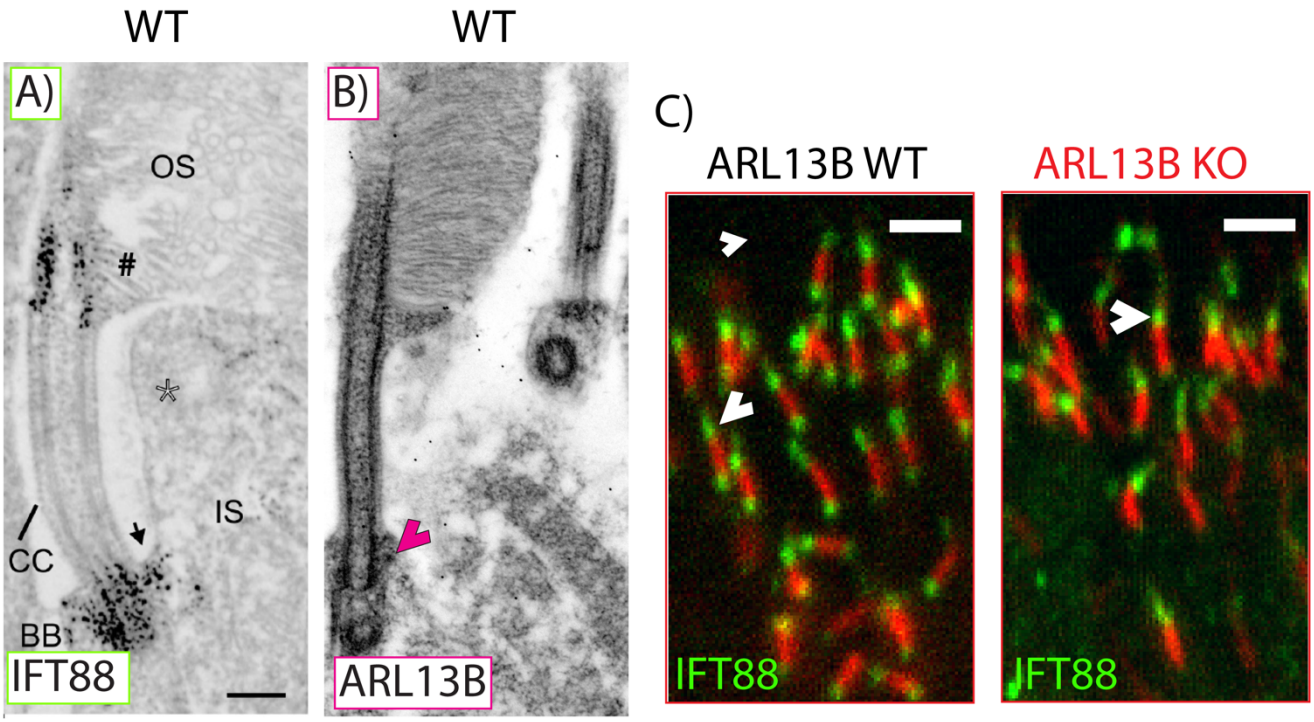

is a member of the IFT-B complex, which is involved in anterograde (base to ciliary tip) protein transport. We further determined the sub-ciliary effects of ARL13B deletion on the localization of other members of the IFT-B complex (IFT20, IFT27) as well as the IFT-A complex protein IFT140 in photoreceptor cilia (Figure 4.1.3). Interestingly, we observed no defects in the other IFT proteins tested. Our preliminary findings do not exclude the possibility that other IFT members (from the ~20 IFT proteins) are still affected.

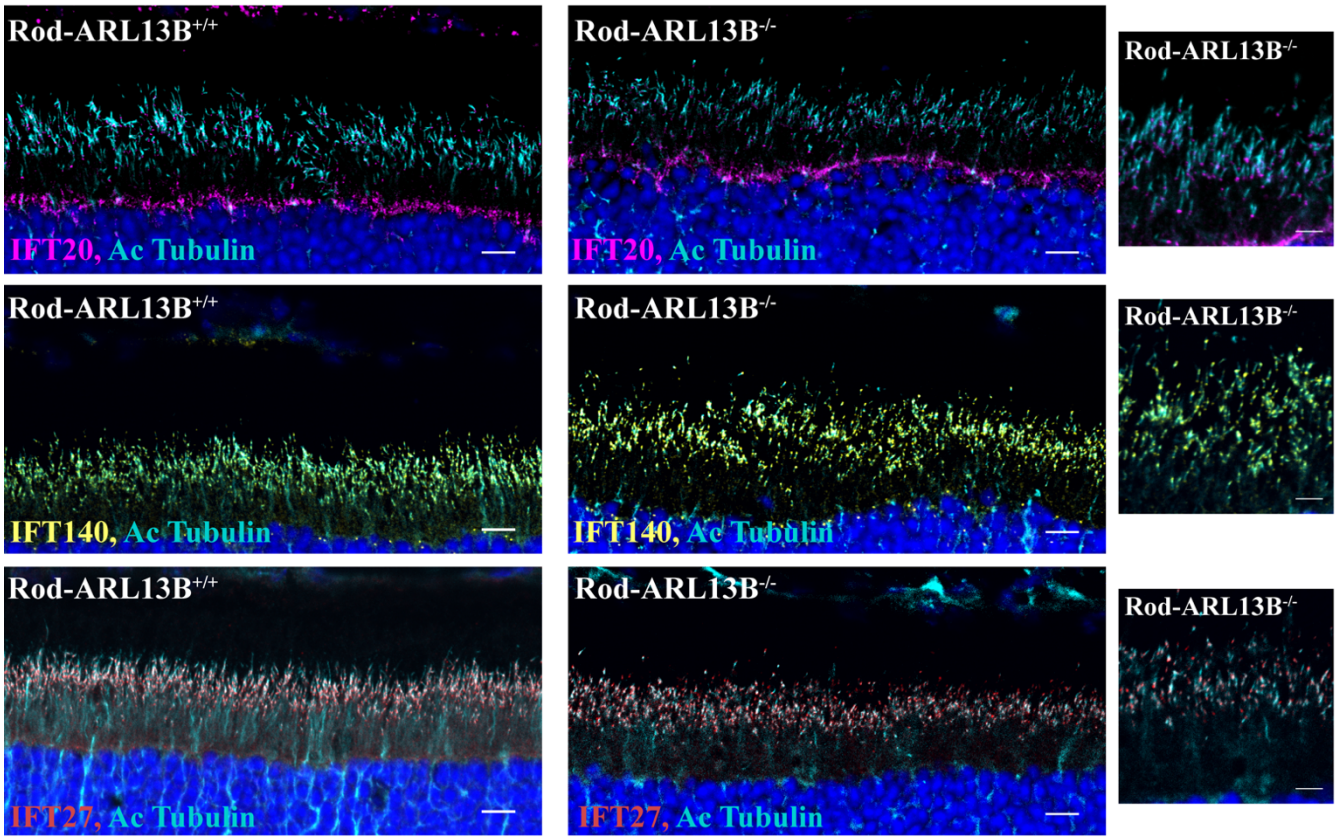

Figure 4.1.3 IFT complex proteins 140,27 and 20 are properly localized in rods lacking ARL13B. Immunofluorescence of retinal cross-sections of tamoxifen-inducible ARL13B mouse models two weeks after ARL13B deletion, showing no observable differences in localization of IFT trains in ARL13B-null rod photoreceptors (*Middle panel* & *right panel* with 2X magnification) and littermate controls (*Left panel*).

4.1.3 Protein transport to the photoreceptor OS: Rhodopsin, Syntaxin 3 and Phosphodiesterase-6 (PDE6)

Protein transport: Rhodopsin

In the primary cilia of cultured cells and olfactory sensory neurons, the BBSome is important for the trafficking of GPCRs (*222, 223*). So, it was initially thought that the BBSome was mainly involved in protein entry into the primary cilia; however, evidence for BBSome-mediated GPCR trafficking in photoreceptors is not definitive due to the studies being performed at later ages when there is severe photoreceptor degeneration and aberrant outer segment (OS) morphology (*69, 70, 224*). In photoreceptors, the main GPCR transported to the OS is the light-sensing protein Rhodopsin (Zhao et al., 2003; Pawlyk et al., 2016). In our BBS8-null retina, Rhodopsin was properly transported to the OS at P10 before the onset of retinal degeneration. We do see the mislocalization of Rhodopsin from the OS at P17, but at this age, there is significant photoreceptor degeneration, and the outer segment is shorter. Importantly, the mislocalization of Rhodopsin has been observed in other murine models that exhibit aberrant outer segment morphology (*225, 226*). Also, Rhodopsin is highly concentrated in photoreceptor OS's, constituting ~90% of total OS membrane protein (*227*). We hypothesize that impaired Rhodopsin localization from the outer segment is not due to a requirement of BBS8 (BBSome) for Rhodopsin transport, but rather due to loss of outer segment structure. Due to the vast amounts of Rhodopsin molecules present in the system and the shorter and dysmorphic OS's in BBS8-null retina, Rhodopsin could be overloading the proteasomal degradation system, leading to the observed protein accumulation in the IS and cell body. In fact, over-expressing the proteasome cap subunit (PA28α) in rod photoreceptors carrying a Rhodopsin point mutation (P23H mutation) resulted in enhanced proteasome enrichment and improved photoreceptor survival (*228*). To test our hypothesis, similar to what Lobanova and colleagues did, we could breed PA28α-overexpressing mice with our BBS8-null

mutants and determine rhodopsin concentration in the IS and outer nuclear layer (ONL). Alternatively, we cross heterozygous ($rho^{+/-}$) mice—which show ~a 50% reduction in rhodopsin levels and exhibit well-formed outer segments similar to those found in wild-type—with our BBS8-null mouse models and determine Rhodopsin localization (*229*). In both cases, reducing the Rhodopsin load in BBS8-null photoreceptors is the equivalent of treating one symptom of the disease, and theoretically should bring about a delay in retinal disease progression.

On the other hand, ARL13B did show significant miss-accumulation of Rhodopsin in the photoreceptor inner segment (IS) and outer nuclear layer (ONL) in our tamoxifen-inducible system (Figure 4.1.2). Of note, the miss-trafficking of Rhodopsin was observed very early –two weeks after ARL13B deletion in adult animals, before the onset of retinal degeneration and when the OS structure of the ARL13B mutant was starting to show vesicle formation (Chapter 3). Due to IFT88 defects at this same time point, and the strong link between IFT88 activity and Rhodopsin transport (*48*), we hypothesize that this Rhodopsin accumulation is a by-product of IFT-B instability.

Protein transport: Syntaxin 3

A recent role for the BBSome in photoreceptors is that of 'ciliary gatekeeper' since a vast number of proteins typically found in the IS, and synapse are found accumulated in the outer segment of BBS17-null animals (one example used was Syntaxin 3)(*230*). BBS17 is not part of the BBSome, but it regulates ciliary localization of the BBSome (*59*). Similar to BBS17 murine models, we also confirmed the miss-accumulation of Syntaxin 3 in our BBS8-null retina, as early as P10 (Chapter 2). In addition, we generated a conditional line where we ablated BBS8 in cone photoreceptors, and also found Syntaxin

3 accumulation in the cone OS (Chapter 2). Interestingly, the removal of ARL13B in mature photoreceptors led to spurious accumulation (albeit not as severe as BBS8) of Syntaxin 3 to the OS (Figure 4.1.4). At present, Syntaxin 3 miss-accumulation could be a more significant symptom of ciliary dysregulation and not a BBSome-specific defect. Alternatively, ARL13B deletion could be indirectly affecting BBSome function, leading to Syntaxin 3 mistargeting. The initial BBS17 mutant study uncovered close to 138 non-OS resident proteins, which 'leak' into the OS in the absence of BBS17. Future work should focus on corroborating this list in both BBS8 and ARL13B mutant models

Figure 4.1.4 Syntaxin 3 localization in ARL13B-null rod photoreceptors. A) Retinal cross-sections of wild-type littermate controls stained against Syntaxin 3. B) Retinal cross-sections of tamoxifen-induced ARL13B-null rod photoreceptors, 2 weeks after tamoxifen, probed for Syntaxin 3. Scale bar: 10µm

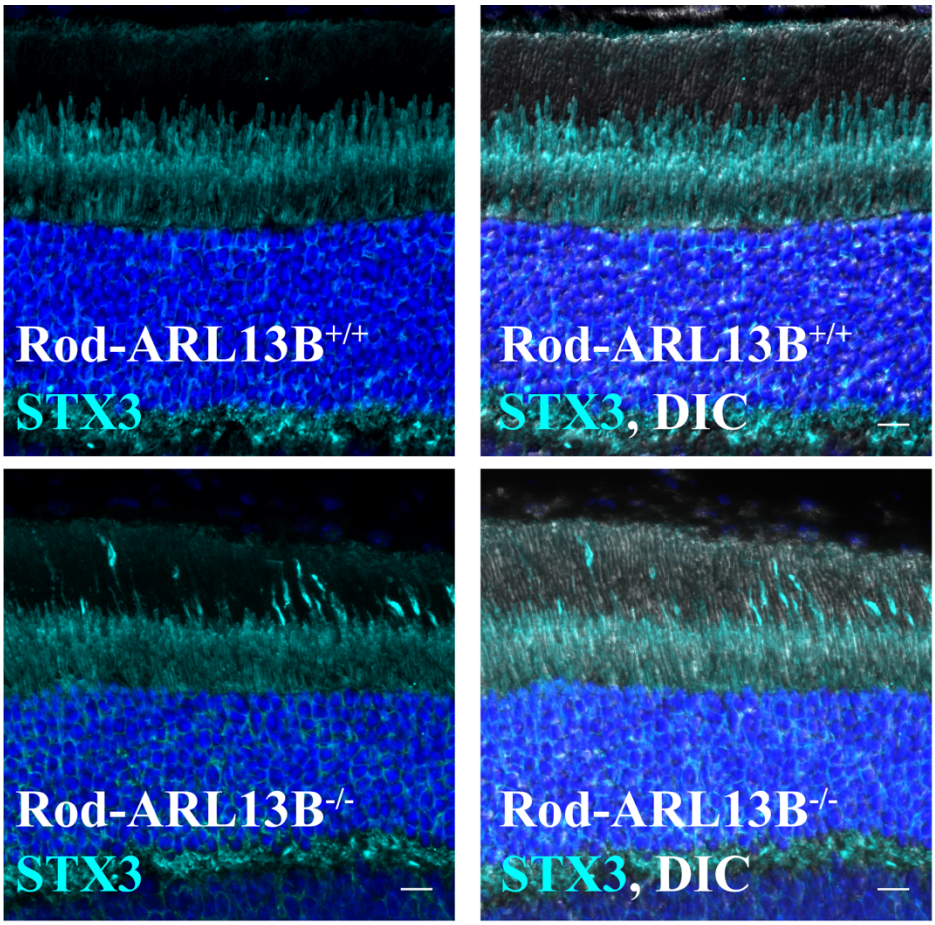

and determining if these proteins are also mislocalized. Additionally, BBSome subunits should be studied in depth in the ARL13B tamoxifen-inducible murine model (slower degeneration model) to determine if, in fact BBSome subunits are dysregulated in the absence of ARL13B.

Protein transport: Phosphodiesterase 6 (PDE6)

As mentioned in chapter 1, active GTP-bound ARL3 is involved in the proper targeting and release of lipidated cargo proteins from their cargo-binding carriers (i.e., PDE6δ and UNC119) within the cilium (*231*). Our lab has previously reported that ARL3-Q71L constitutively active transgenic mice displayed progressive accumulation of prenylated cargo (i.e.PDE6, Rhodopsin Kinase-1 or GRK1) in vesicle-like structures within the photoreceptor inner segment; demonstrating that defective ARL3 turnover leads to inadequate cargo release in photoreceptors (*147*). ARL13B acts as the guanine nucleotide exchange factor (GEF) for ARL3 *in vitro* (*81*). Hence, we hypothesized that in the absence of ARL13B, there would be mistargeting of the protein cargoes associated with ARL3, and we did find miss-accumulation of prenylated PDE6 in the photoreceptor IS. The study was conducted in the tamoxifen-inducible *Cre*-driver line, and PDE6 appeared to stain in a punctate fashion two weeks after ARL13B deletion, before the onset of degeneration. Although the miss-accumulation seen in ARL13B mutant animals is not as severe as that observed in ARL3 dominant active mutants, the result is reminiscent of the initial stages of ARL3 dysregulation (see Figure 4.1.4). Surprisingly, we did not see the defective transport of GRK1 at this time (another ARL3-associated cargo). This result leads us to infer that the mild defects we observe in the transport of prenylated proteins in ARL13B-null photoreceptors are due to GTP-activation of ARL3 not being solely dependent on ARL13B *in vivo*.

ARL13B GEF-activity towards ARL3 has not been studied in depth in an animal model, and at present, we have not identified the nucleotide bound state of ARL3 in ARL13B-null retina. Previous reports have shown PDE6δ as an effector of active-GTP bound ARL3 (*231*). PDE6δ binds farnesylated, and geranylgeranylated cargo and subsequent binding of activated GTP-ARL3 to PDE6δ induces the conformational changes needed for the release of the cargo (*146, 232, 233*). In our system, it may be possible to quantify ARL3 activation in ARL13B-null retina by affinity-precipitating ARL3-GTP with

Figure 4.1.4 Comparing PDE6 accumulation in the photoreceptor IS of ARL3 dominant-active transgenic animals and ARL13B-null photoreceptors. A) Immunofluorescence of retinal cross-sections probing for Rhodopsin and PDE6β, two weeks after ARL13B removal in photoreceptors. B) PDE6β staining with increased contrast showing accumulation within the IS in photoreceptors lacking *ARL13B*. C) Retina from transgenic animals that express constitutively active ARL3 (Tg+) display the initial stages of PDE6 accumulation in the IS at P25 reminiscent of the initial stages of PDE6 accumulation in ARL13B-null retina.

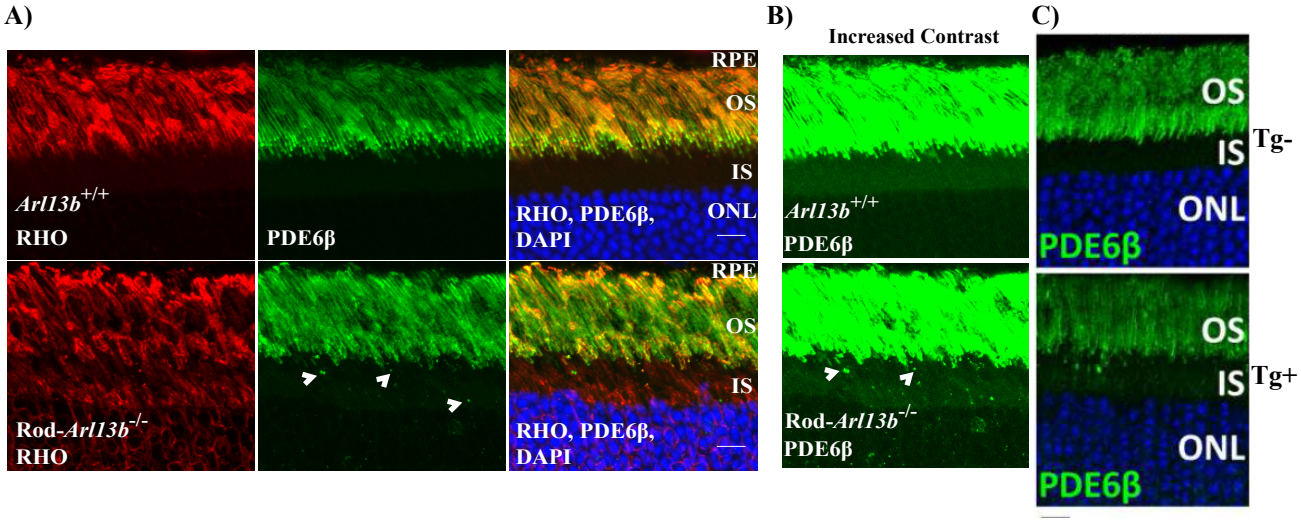

the effector GST-PDE6δ (*81, 234*) and subsequently compare relative protein levels between ARL13B-null retina and littermate controls. Affinity purification using GST-PDE6δ in ARL13B-null retinal lysates can then be further corroborated using a commercially-available antibody, which only recognizes active, GTP-bound ARL3. If our hypothesis is correct, ARL13B-null retina should still have significant

levels of GTP-bound ARL3, accounting for the mild defects we observe in the miss-accumulation of ARL3-associated cargoes in ARL13B mutants.

4.1.4 Photoreceptor Maintenance

The deletion of ARL13B and BBS8 in fully mature photoreceptors leads to opposing outcomes in terms of photoreceptor maintenance and viability. Visual photoresponse at P15 (the age at which animals start opening their eyes) in BBS8-null retina showed a 50% reduction in rod visual response compared to littermate controls. Contrary to the early development phenotype observed in BBS8-null retina (*Six3*-Cre model), ablating BBS8 in mature rod photoreceptors using a tamoxifen-inducible *Cre*-driver line resulted in slow loss of visual response (Figure 4.1.5). It took an average of three months after BBS8 ablation in mature rods to exhibit a significant reduction of rod photoresponse (Figure 4.1.5). This slow progressive loss of visual response is similar to other BBS mutants (*69, 70*). Our results suggest that fully mature photoreceptors are more resistant to the absence of BBS8, which could likely be due to the presence of an altered BBSome "sub-complex" (see 4.2.1 for more details on BBSome subcomplexes), which might be sufficient to maintain photoreceptor homeostasis in mature photoreceptors. Contrary to BBS8, removal of ARL13B in adult rod photoreceptors precipitated significant reduction of rod photoresponse as early as three weeks post-tamoxifen-induced deletion and complete loss of photoreceptor nuclei layers was found five weeks after tamoxifen-induced deletion (Chapter 3). Taken together, the absence of BBS8 in the developing photoreceptor leads to defective photoreceptor function and viability, but the protein is not as crucial in the maintenance stage. ARL13B is not only vital to retinogenesis, photoreceptor outer segment morphogenesis, and viability but also needed for photoreceptor maintenance throughout the animal's lifetime.

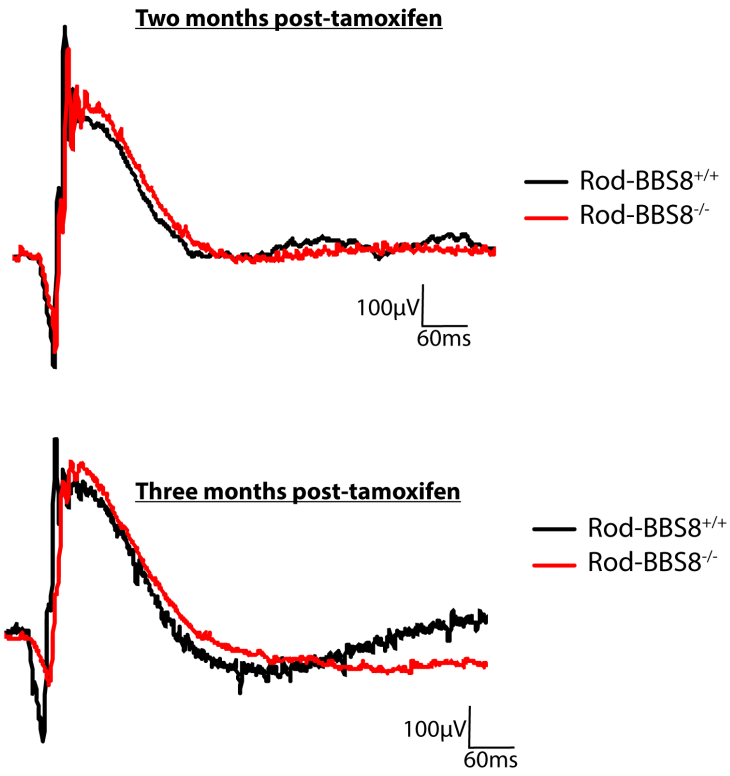

Figure 4.1.5 Rod photoresponse measured by Electroretinography (ERG) in mature rods lacking BBS8. (*Top panel*) ERG traces two months after tamoxifen-induced deletion of BBS8 displaying no significant changes in mutant animals (Rod-BBS8$^{-/-}$) compared to wild-type littermate controls (Rod-BBS8$^{+/+}$). (*Bottom Panel*) ERG traces three months after tamoxifen-induced deletion of BBS8 displaying significant reduction in rod photoresponse.

4.2 Piecing it together: Hypothetical models for ARL13B and BBS8 in photoreceptor neurons

4.2.1 The BBSome, a complex involved in the photoreceptor ciliary gate or ciliary exit? Both?

It is tempting to accept the model of the BBSome as that of a ciliary gatekeeper, especially with new work published this year showing Syntaxin 3 accumulation in the photoreceptor OS of Cep290 truncated mutants (*235*). CEP290 is a connecting cilia/transition zone resident protein that in *Chlamydomonas reinhardtii* and *Caenorhabditis elegans* is required for the formation of Y-shaped linkers that extend from the axonemal microtubules to the ciliary membrane (*236-238*). CEP290 has long been considered a strong candidate involved in the ciliary diffusion barrier, with the absence of the protein leading to altered cilia composition (*239*). When BBSome subunits are missing, we also see profound changes in the protein composition of the outer segment (*230*). There are, however, some inconsistencies with this

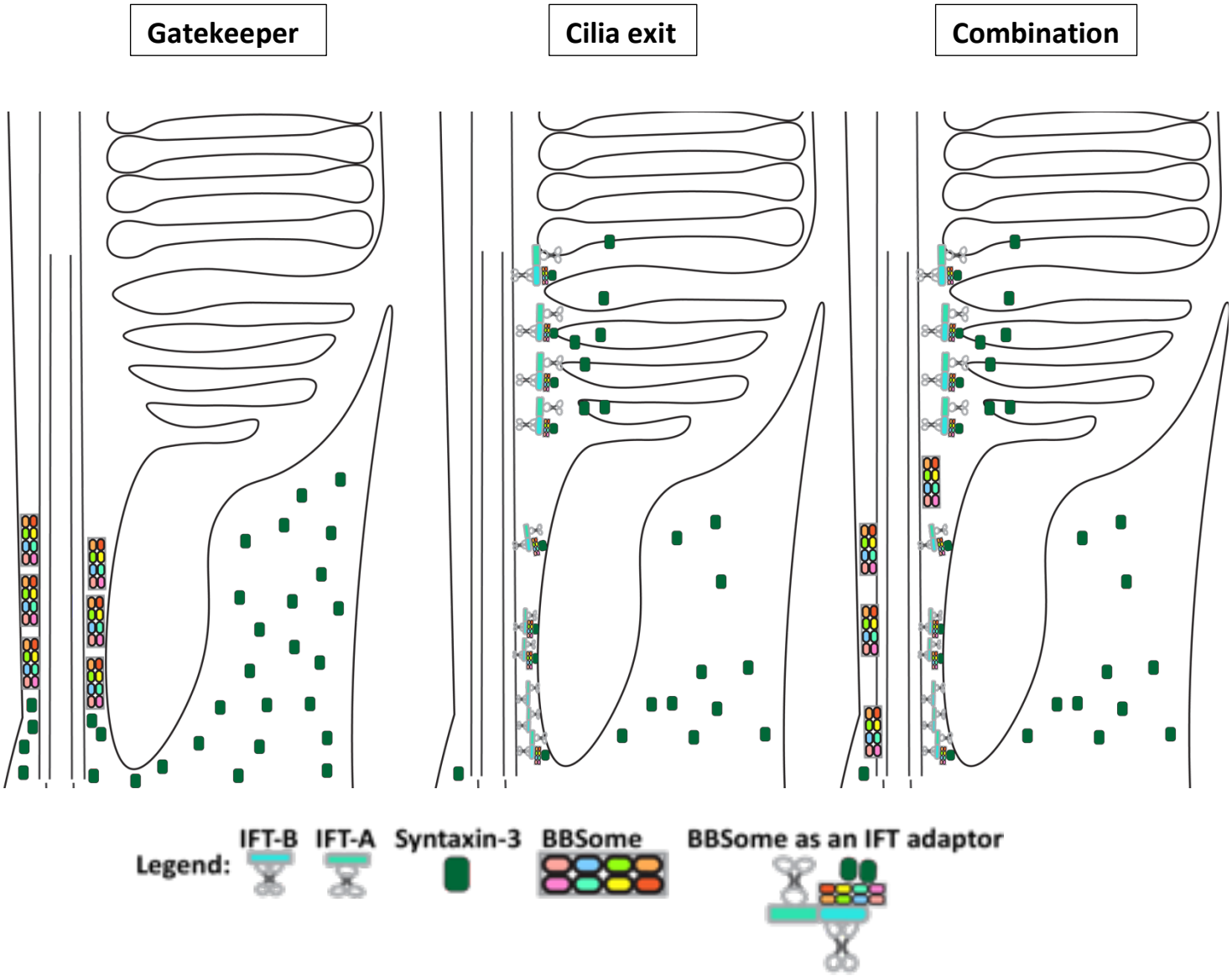

Figure 4.2.1 Reported models for the role of the BBSome. (Left panel) The BBSome acting as a ciliary gatekeep along the connecting cilia/transition zone, aiding in keeping inner segment proteins out of the outer segment (i.e., Syntaxin 3). (Middle Panel) The BBSome in association with the IFT complex aiding in retrograde (exit) transport along the photoreceptors, clearing out proteins that diffuse in (i.e., Syntaxin 3). (Right panel) Due to the assumption (Chou et al., 2019) that the BBSome core complex (lacking BBS2 and BBS7) could also be stable in tissues, different BBSome subcomplexes could be fulfilling multiple roles in photoreceptor cilia (both gatekeeper and ciliary exit).

model (Figure 4.2.1). The ciliary gatekeeper role does not clarify why the BBSome is dynamic and can travel at IFT velocities in olfactory sensory neuronal cilia and traditional primary cilia of cell culture

systems (*64, 66*). A subset of researchers in the field believe that the BBSome is involved in retrograde protein transport (cilia tip to base), aiding as an adaptor for IFT trains (Figure 4.2.1). Very recent studies using Stochastic optical reconstruction microscopy (STORM), show BBS subunits are found in clusters throughout the photoreceptor connecting cilia and axoneme (*240*). This variety of locations of BBS subunits cautiously supports the proposed role for the BBSome in the transport of cargo across the connecting cilia, potentially through cooperation with IFT trains. To indeed confirm the retrograde ciliary exit role of the BBSome, the secret now lies in uncovering the identity of BBSome cargoes and the mechanism involved in BBSome- IFT complex interactions. Thus far, biochemical assays employed to determine BBSome interactors and potential cargoes have been unsatisfactory, the issue is that the BBSome, when purified as a complex, rarely ever brings along any other proteins (except for tubulin and αTAT1) (*57*). Similarly, when subunits were studied independently, they mostly interacted with other BBSome subunits, with notable exceptions (i.e., BBS18 and HDAC6) (*209*). It has long been assumed that BBSome-cargo interaction is a very complex process that requires this large octameric complex to be in specific structural conformations. This year two groups have resolved the atomic structure of the BBSome complex and the core complex using Cryo-electron microscopy (*211, 241*). Chou and colleagues resolved the structure of bovine BBSome by first purifying the complex from bovine retina using GST-ARL6 (BBS3) columns (*57, 211*). As mentioned previously, ARL6 preferentially binds the fully assembled BBSome (Chapter 1). Alternatively, Klink and colleagues purified human BBSome subcomplexes by expressing the subunits in insect cell lines (*241*). The BBSome was found to have two conformations: a closed conformation when in solution, and an open conformation when membrane-bound (*211, 241*).

Future studies on the BBSome complex will undoubtedly have a significant structural component to them. Due to recently resolved structures, the focus will be geared towards understanding how cargo

proteins get recognized in the different open and closed conformations of the complex. Hence, future experiments will likely focus on purifying the complete BBSome complex utilizing the Chou et al. method and adding purified 'potential interactors' (i.e., GPCR's, IFT proteins) to the solution to obtain structures of the BBSome complex bound to different cargo proteins.

4.2.2 The dynamic and complex role of ARL13B in photoreceptor biology

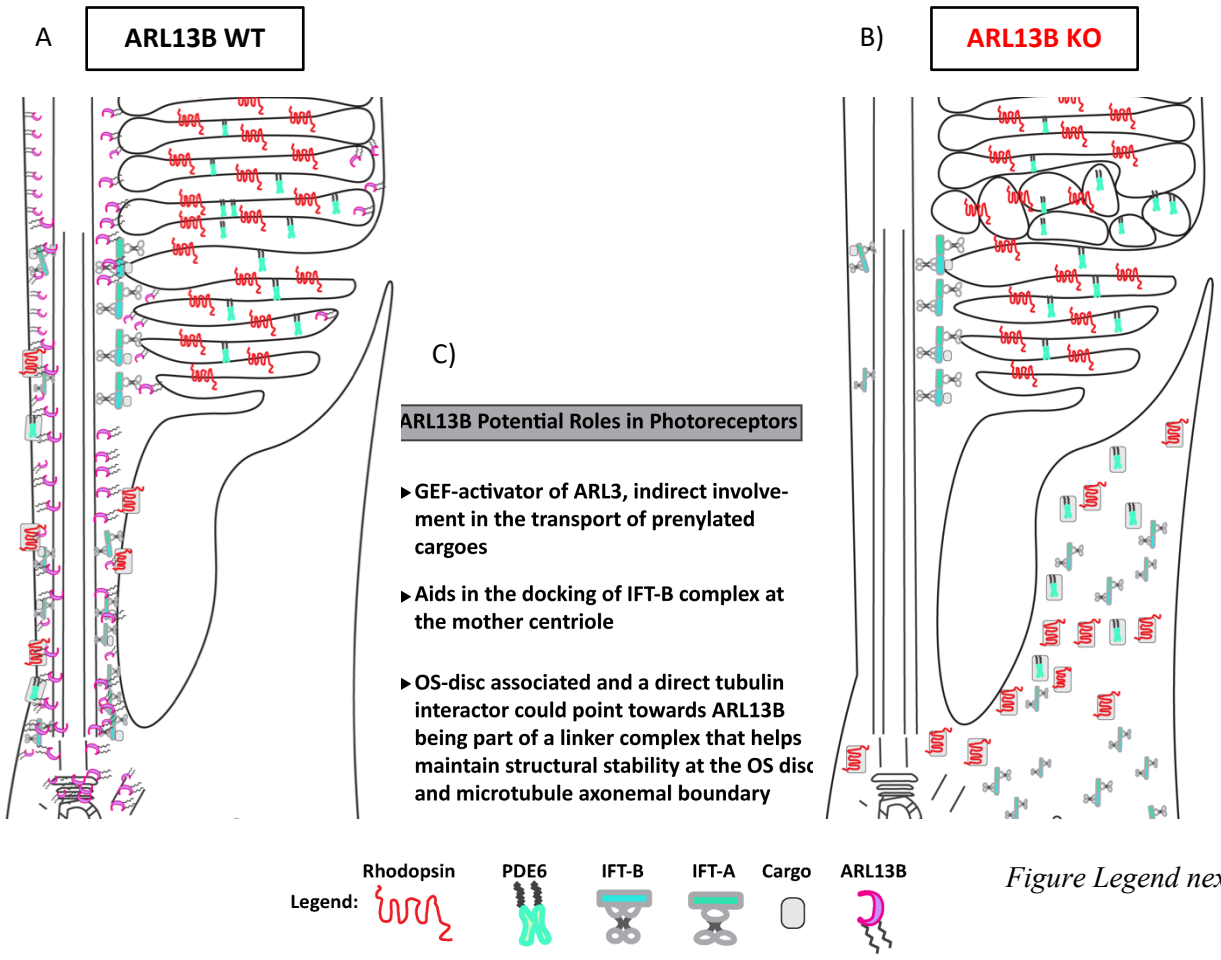

Figure Legend next page

In addition to the problems arising from lack of ARL13B-mediated activation of ARL3 and based on the complex phenotype observed in murine models, we propose ARL13B could be fulfilling multiple roles within photoreceptor neurons (Figure 4.2.2c). Interestingly, ARL13B has been shown to interact, in a

Figure 4.2.2 Potential Roles of ARL13B. A) Schematic model of a wild-type rod photoreceptor showing properly stacked membranous discs with GPCR Rhodopsin and PDE6 bound to the outer segment (OS) disc. IFT88 particles connected to their molecular motors are depicted here in the apical and basal side of the connecting cilium (CC/TZ) as they were observed through immunofluorescence microscopy. B) Schematic diagram illustrating photoreceptor rods 2 weeks after tamoxifen-induced deletion of ARL13B. OS vesicles are starting to accumulate in the OS. Rhodopsin and PDE6 are found mislocalized to the inner segment (IS), and we observe IFT-B (IFT88) proteins lost from the basal side of the CC and apparent in the IS. C) List of potential roles for ARL13B in the context of photoreceptor neurons.

nucleotide-independent manner, directly with tubulin through its G binding domain, with ARL13B mutant (*hennin* mutant) nodal cilia showing disruptions of the outer doublet structure (B-tubule was not completely attached to the A-tubule) (*242, 243*). Moreover, ARL13B immunofluorescence analysis in murine retina follows a diffuse pattern within the photoreceptor OS, with ARL13B displaying high enrichment in the microtubule-rich region of the CC/transition zone and the axoneme (Chapter 3). In addition to immunofluorescence, our preliminary analysis using transmission electron microscopy coupled to immunogold labeling of ARL13B demonstrated high enrichment of ARL13B in the microtubule basal body, connecting cilia and axoneme of photoreceptor cilia (Figure 4.1.2b). As mentioned previously, ARL13B has two palmitoyl anchors at the N-terminal region of the protein, and our results show ARL13B to be found in disc-enriched fractions of our outer segment isolation preps (*79*). We hypothesize that these lipid modifications are essential for the association of ARL13B with the outer segment membranes that are directly adjacent to the axoneme. Taken together, ARL13B could be binding to the photoreceptor axonemal microtubules and maintaining their structural integrity (explaining improper B-tubule closing) as well as providing a direct link between the discs and axoneme and/or as a part of a linker complex. In addition, the high enrichment of ARL13B seen in the mother

centriole (Figure 4.1.2), a region which IFT88 is sequestered to, coupled with the lack of IFT88 staining when ARL13B is ablated, could imply that ARL13B serves in the docking of IFT88 to this cargo loading and assembly zone.

Present studies:

To delineate ARL13B's complex role in photoreceptor biology, it is crucial to determine domain-specific dysfunction in each distinct ARL13B patient phenotype. ARL13B has an atypical extra 20 kDa domain of unknown function, a domain which no other small GTPase possesses (*90*). We can target regions within this domain and study phenotype rescue in both early development (*Six3*-Cre) and maintenance (*PDE6g*-CreERT2) by performing sub-retinal injections of different ARL13B constructs using Adeno-associated viral vector-mediated expression. In addition, identifying the protein interactors of ARL13B within the different sub-ciliary zones in photoreceptor neurons could provide insights into what regulatory roles the small GTPase is exerting in photoreceptors. During the course of our study, we attempted to identify photoreceptor ARL13B interactors in two ways:

1) We performed label-free proteomics using our validated ARL13B antibody in retinal lysates. After going through different parameters (normalized spectral abundance factor (NSAF) scores of at least 3-fold change or higher between control and KO tissue, and elimination of protein hits found in control), we reduced our list of potential candidates to 13 proteins. Using retinal lysates under a variety of different buffers and conditions, as well as protein expression of ARL13B and candidate proteins in cell culture systems, we attempted to corroborate these interactors and, unfortunately, were unsuccessful.

2) To resolve weak or transient interactors of ARL13B, we sought to employ a proximity-ligation based approach (i.e.BioID) (*244*). BioID utilizes a promiscuous biotin ligase (BirA) attached to a bait protein (ARL13B, in this case), which biotinylates proteins based on proximity (*244*). Biotinylated proteins can then be purified (using Streptavidin beads) and further studied via Mass-Spectrometry (*244*). We utilized the newer generations of this enzyme, known for their smaller size and higher efficiency (TurboID and MiniTurboID) (*244, 245*). To confirm that fusing BirA ligase to ARL13B would not affect ARL13B function, we transfected our BioID-ARL13B constructs into mouse embryonic fibroblast lacking ARL13B (MEF *hennin* mutants). Transfecting FLAG-ARL13B to this same cell line rescued the ciliogenesis defects observed in *hennin* mutants. Unfortunately, TurboID-ARL13B and Mini-TurboID-ARL13B did not rescue the ciliogenesis defects found in MEF *hennin* cells. At present, it remains to be determined if the lack of rescue is due to the fusion protein not expressing properly or if the BirA ligase somehow affects (i.e. biotinylates) ARL13B function. Measuring relative protein levels of transfected cells and probing with ARL13B and an antibody against BirA will address the first scenario and performing a Streptavidin bead pulldown assay (recognizes biotinylated proteins) and probing for ARL13B could address the second scenario.

Our lab has recently acquired two ARL13B murine models with different point mutations from our collaborator Dr. Tamara Caspary (Emory). The first model is a V358A variant of ARL13B, which affects ciliary localization by disrupting a known VxPx cilia localization sequence (*86, 246*). The second model is the R79Q variant of ARL13B, a Joubert Syndrome patient mutation which affects the GTP binding domain of the protein (*85*). Recent studies have shown that the R79Q mutation does not affect GTP binding, but it does disrupt ARL13B-ARL3 interactions (*90*). Our most recent

preliminary studies assessing the visual function of the V358A mutant animal show no significant changes between mutant and wild-type littermates at P30 (Moakedi et al., unpublished). Later ages are being tested currently. At present, R79Q animals have not been tested for the visual response due to low mutant yield (and the student writing her thesis). To summarize, we find that ARL13B plays an intricate role in photoreceptor development and maintenance. Future directions should focus on targeting ARL13B domains and comparing the phenotypic profiles observed with ARL13B mutants and the original knockout animal model studies (Chapter 3), in order to find any inconsistencies between the two. The previously mentioned ARL13B mutant mouse models are a step towards that goal.

4.3 Concluding remarks

Dysfunction of ciliary proteins in the context of photoreceptor biology gives rise to very similar phenotypes, and these similarities make it challenging to dissect protein-specific molecular roles during each developmental process. In our study, we sought to perform a careful analysis of the different phenotypic profiles present in both BBS8 and ARL13B models. We were able to show apparent deviations in photoreceptor cellular processes ranging from early retinogenesis, photoreceptor outer segment development, maintenance, and protein transport. With the recent advancements in super-resolution microscopy, additional roles for BBS8 and ARL13B are likely to be uncovered and will greatly contribute to our understanding of developmental mechanisms and ciliopathy diseases.

References:

1. T. Jayasundera *et al.*, RP2 phenotype and pathogenetic correlations in X-linked retinitis pigmentosa. *Archives of ophthalmology (Chicago, Ill. : 1960)* **128**, 915-923 (2010).
2. S. P. Strom *et al.*, De Novo Occurrence of a Variant in ARL3 and Apparent Autosomal Dominant Transmission of Retinitis Pigmentosa. *PloS one* **11**, e0150944 (2016).
3. J.-D. Ding, R. Y. Salinas, V. Y. Arshavsky, Discs of mammalian rod photoreceptors form through the membrane evagination mechanism. *The Journal of cell biology* **211**, 495-502 (2015).
4. C.-H. Sung, J.-Z. Chuang, The cell biology of vision. *The Journal of cell biology* **190**, 953-963 (2010).
5. S. A. Baccus, Timing and Computation in Inner Retinal Circuitry. *Annual Review of Physiology* **69**, 271-290 (2007).
6. J. N. Pearring, R. Y. Salinas, S. A. Baker, V. Y. Arshavsky, Protein sorting, targeting and trafficking in photoreceptor cells. *Prog Retin Eye Res* **36**, 24-51 (2013).
7. C. W. Morgans, Presynaptic proteins of ribbon synapses in the retina. *Microscopy Research and Technique* **50**, 141-150 (2000).
8. F. Schmitz, The Making of Synaptic Ribbons: How They Are Built and What They Do. *The Neuroscientist* **15**, 611-624 (2009).
9. R. W. Young, The renewal of photoreceptor cell outer segments. *The Journal of cell biology* **33**, 61-72 (1967).
10. J. J. Malicki, C. A. Johnson, The Cilium: Cellular Antenna and Central Processing Unit. *Trends Cell Biol* **27**, 126-140 (2017).
11. M. Mirvis, T. Stearns, W. James Nelson, Cilium structure, assembly, and disassembly regulated by the cytoskeleton. *Biochemical Journal* **475**, 2329-2353 (2018).
12. S. Huang, Y. Hirota, K. Sawamoto, Various facets of vertebrate cilia: motility, signaling, and role in adult neurogenesis. *Proc Jpn Acad Ser B Phys Biol Sci* **85**, 324-336 (2009).
13. M. Owa *et al.*, Inner lumen proteins stabilize doublet microtubules in cilia and flagella. *Nat Commun* **10**, 1143 (2019).
14. H. Ishikawa, W. F. Marshall, Ciliogenesis: building the cell's antenna. *Nature Reviews Molecular Cell Biology* **12**, 222-234 (2011).
15. A. I. Cohen, The ultrastructure of the rods of the mouse retina. *Am J Anat* **107**, 23-48 (1960).
16. R. Roepman, U. Wolfrum, Protein networks and complexes in photoreceptor cilia. *Subcell Biochem* **43**, 209-235 (2007).
17. D. Roof, M. Adamian, D. Jacobs, A. Hayes, Cytoskeletal specializations at the rod photoreceptor distal tip. *Journal of Comparative Neurology* **305**, 289-303 (1991).
18. M. W. Kaplan, R. T. Iwata, R. C. Sears, Lengths of immunolabeled ciliary microtubules in frog photoreceptor outer segments. *Experimental eye research* **44**, 623-632 (1987).
19. W. S. Sale, J. C. Besharse, G. Piperno, Distribution of acetylated alpha-tubulin in retina and in vitro-assembled microtubules. *Cell Motil Cytoskeleton* **9**, 243-253 (1988).
20. M. S. Eckmiller, Renewal of the ciliary axoneme in cone outer segments of the retina of Xenopus laevis. *Cell and Tissue Research* **285**, 165-169 (1996).

21. K. Luby-Phelps, J. Fogerty, S. A. Baker, G. J. Pazour, J. C. Besharse, Spatial distribution of intraflagellar transport proteins in vertebrate photoreceptors. *Vision research* **48**, 413-423 (2008).
22. J. C. Gilliam *et al.*, Three-dimensional architecture of the rod sensory cilium and its disruption in retinal neurodegeneration. *Cell* **151**, 1029-1041 (2012).
23. J. C. Besharse, D. M. Forestner, D. M. Defoe, Membrane assembly in retinal photoreceptors. III. Distinct membrane domains of the connecting cilium of developing rods. *The Journal of neuroscience : the official journal of the Society for Neuroscience* **5**, 1035-1048 (1985).
24. H. L. Kee *et al.*, A size-exclusion permeability barrier and nucleoporins characterize a ciliary pore complex that regulates transport into cilia. *Nat Cell Biol* **14**, 431-437 (2012).
25. D. K. Breslow, E. F. Koslover, F. Seydel, A. J. Spakowitz, M. V. Nachury, An in vitro assay for entry into cilia reveals unique properties of the soluble diffusion barrier. *The Journal of cell biology* **203**, 129-147 (2013).
26. Y.-C. Lin *et al.*, Chemically inducible diffusion trap at cilia reveals molecular sieve-like barrier. *Nature chemical biology* **9**, 437-443 (2013).
27. M. Najafi, P. D. Calvert, Transport and localization of signaling proteins in ciliated cells. *Vision research* **75**, 11-18 (2012).
28. D. H. Hong *et al.*, A retinitis pigmentosa GTPase regulator (RPGR)-deficient mouse model for X-linked retinitis pigmentosa (RP3). *Proceedings of the National Academy of Sciences of the United States of America* **97**, 3649-3654 (2000).
29. R. A. Rachel, T. Li, A. Swaroop, Photoreceptor sensory cilia and ciliopathies: focus on CEP290, RPGR and their interacting proteins. *Cilia* **1**, 22 (2012).
30. A. Eblimit *et al.*, Spata7 is a retinal ciliopathy gene critical for correct RPGRIP1 localization and protein trafficking in the retina. *Human molecular genetics* **24**, 1584-1601 (2015).
31. R. Dharmat *et al.*, SPATA7 maintains a novel photoreceptor-specific zone in the distal connecting cilium. *The Journal of Cell Biology* **217**, 2851 (2018).
32. T. Sedmak, U. Wolfrum, Intraflagellar transport molecules in ciliary and nonciliary cells of the retina. *J Cell Biol* **189**, 171-186 (2010).
33. K. A. Johnson, J. L. Rosenbaum, Polarity of flagellar assembly in Chlamydomonas. *The Journal of Cell Biology* **119**, 1605 (1992).
34. K. F. Lechtreck, IFT-Cargo Interactions and Protein Transport in Cilia. *Trends Biochem Sci* **40**, 765-778 (2015).
35. L. B. Pedersen, J. L. Rosenbaum, in *Current Topics in Developmental Biology*. (Academic Press, 2008), vol. 85, pp. 23-61.
36. K. G. Kozminski, K. A. Johnson, P. Forscher, J. L. Rosenbaum, A motility in the eukaryotic flagellum unrelated to flagellar beating. *Proceedings of the National Academy of Sciences of the United States of America* **90**, 5519-5523 (1993).
37. R. D. Sloboda, Intraflagellar transport and the flagellar tip complex. *Journal of Cellular Biochemistry* **94**, 266-272 (2005).
38. J. R. Broekhuis, K. J. Verhey, G. Jansen, Regulation of cilium length and intraflagellar transport by the RCK-kinases ICK and MOK in renal epithelial cells. *PloS one* **9**, e108470-e108470 (2014).
39. M. Taschner, S. Bhogaraju, E. Lorentzen, Architecture and function of IFT complex proteins in ciliogenesis. *Differentiation* **83**, S12-S22 (2012).
40. J. Keeling, L. Tsiokas, D. Maskey, Cellular Mechanisms of Ciliary Length Control. *Cells* **5**, 6 (2016).

41. W. F. Marshall, J. L. Rosenbaum, Intraflagellar transport balances continuous turnover of outer doublet microtubules. *The Journal of Cell Biology* **155**, 405 (2001).
42. S. Bhogaraju *et al.*, Molecular basis of tubulin transport within the cilium by IFT74 and IFT81. *Science (New York, N.Y.)* **341**, 1009-1012 (2013).
43. L. Hao *et al.*, Intraflagellar transport delivers tubulin isotypes to sensory cilium middle and distal segments. *Nat Cell Biol* **13**, 790-798 (2011).
44. J. M. Craft, J. A. Harris, S. Hyman, P. Kner, K. F. Lechtreck, Tubulin transport by IFT is upregulated during ciliary growth by a cilium-autonomous mechanism. *The Journal of cell biology* **208**, 223-237 (2015).
45. A. A. Bizet *et al.*, Mutations in TRAF3IP1/IFT54 reveal a new role for IFT proteins in microtubule stabilization. *Nat Commun* **6**, 8666 (2015).
46. J. M. Gross *et al.*, Identification of zebrafish insertional mutants with defects in visual system development and function. *Genetics* **170**, 245-261 (2005).
47. M. Tsujikawa, J. Malicki, Intraflagellar transport genes are essential for differentiation and survival of vertebrate sensory neurons. *Neuron* **42**, 703-716 (2004).
48. G. J. Pazour *et al.*, The intraflagellar transport protein, IFT88, is essential for vertebrate photoreceptor assembly and maintenance. *The Journal of Cell Biology* **157**, 103-114 (2002).
49. A. F. X. Goldberg, O. L. Moritz, D. S. Williams, Molecular basis for photoreceptor outer segment architecture. *Prog Retin Eye Res* **55**, 52-81 (2016).
50. R. H. Steinberg, S. K. Fisher, D. H. Anderson, Disc morphogenesis in vertebrate photoreceptors. *Journal of Comparative Neurology* **190**, 501-518 (1980).
51. T. G. Wensel *et al.*, Structural and molecular bases of rod photoreceptor morphogenesis and disease. *Prog Retin Eye Res* **55**, 32-51 (2016).
52. K. Boesze-Battaglia, J. Dispoto, M. A. Kahoe, Association of a photoreceptor-specific tetraspanin protein, ROM-1, with triton X-100-resistant membrane rafts from rod outer segment disk membranes. *The Journal of biological chemistry* **277**, 41843-41849 (2002).
53. C. L. Makino *et al.*, Rhodopsin Expression Level Affects Rod Outer Segment Morphology and Photoresponse Kinetics. *PloS one* **7**, e37832 (2012).
54. X.-H. Wen *et al.*, Overexpression of rhodopsin alters the structure and photoresponse of rod photoreceptors. *Biophys J* **96**, 939-950 (2009).
55. J. F. Reiter, M. R. Leroux, Genes and molecular pathways underpinning ciliopathies. *Nat Rev Mol Cell Biol* **18**, 533-547 (2017).
56. E. Manara *et al.*, Mutation profile of BBS genes in patients with Bardet-Biedl syndrome: an Italian study. *Ital J Pediatr* **45**, 72-72 (2019).
57. H. Jin *et al.*, The conserved Bardet-Biedl syndrome proteins assemble a coat that traffics membrane proteins to cilia. *Cell* **141**, 1208-1219 (2010).
58. M. V. Nachury *et al.*, A core complex of BBS proteins cooperates with the GTPase Rab8 to promote ciliary membrane biogenesis. *Cell* **129**, 1201-1213 (2007).
59. S. Seo *et al.*, A Novel Protein LZTFL1 Regulates Ciliary Trafficking of the BBSome and Smoothened. *PLOS Genetics* **7**, e1002358 (2011).
60. S. Sinha, M. Belcastro, P. Datta, S. Seo, M. Sokolov, Essential role of the chaperonin CCT in rod outer segment biogenesis. *Investigative ophthalmology & visual science* **55**, 3775-3785 (2014).
61. A. Mourão, A. R. Nager, M. V. Nachury, E. Lorentzen, Structural basis for membrane targeting of the BBSome by ARL6. *Nat Struct Mol Biol* **21**, 1035-1041 (2014).

62. J. A. Green *et al.*, Recruitment of β-Arrestin into Neuronal Cilia Modulates Somatostatin Receptor Subtype 3 Ciliary Localization. *Molecular and Cellular Biology* **36**, 223 (2016).
63. N. F. Berbari, J. S. Lewis, G. A. Bishop, C. C. Askwith, K. Mykytyn, Bardet–Biedl syndrome proteins are required for the localization of G protein-coupled receptors to primary cilia. *Proceedings of the National Academy of Sciences* **105**, 4242 (2008).
64. F. Ye, A. R. Nager, M. V. Nachury, BBSome trains remove activated GPCRs from cilia by enabling passage through the transition zone. *The Journal of Cell Biology* **217**, 1847 (2018).
65. A. R. Nager *et al.*, An Actin Network Dispatches Ciliary GPCRs into Extracellular Vesicles to Modulate Signaling. *Cell* **168**, 252-263.e214 (2017).
66. C. L. Williams *et al.*, Direct evidence for BBSome-associated intraflagellar transport reveals distinct properties of native mammalian cilia. *Nat Commun* **5**, 5813-5813 (2014).
67. Q. Wei *et al.*, The BBSome controls IFT assembly and turnaround in cilia. *Nat Cell Biol* **14**, 950-957 (2012).
68. J. L. Wingfield, K.-F. Lechtreck, E. Lorentzen, Trafficking of ciliary membrane proteins by the intraflagellar transport/BBSome machinery. *Essays Biochem* **62**, 753-763 (2018).
69. D. Y. Nishimura *et al.*, Bbs2-null mice have neurosensory deficits, a defect in social dominance, and retinopathy associated with mislocalization of rhodopsin. *Proceedings of the National Academy of Sciences of the United States of America* **101**, 16588 (2004).
70. K. Mykytyn *et al.*, Bardet–Biedl syndrome type 4 (BBS4)-null mice implicate Bbs4 in flagella formation but not global cilia assembly. *Proceedings of the National Academy of Sciences of the United States of America* **101**, 8664 (2004).
71. Q. Zhang *et al.*, BBS7 is required for BBSome formation and its absence in mice results in Bardet-Biedl syndrome phenotypes and selective abnormalities in membrane protein trafficking. *Journal of cell science* **126**, 2372-2380 (2013).
72. S. A. Riazuddin *et al.*, A splice-site mutation in a retina-specific exon of BBS8 causes nonsyndromic retinitis pigmentosa. *American journal of human genetics* **86**, 805-812 (2010).
73. S. Goyal, M. Jäger, P. N. Robinson, V. Vanita, Confirmation of TTC8 as a disease gene for nonsyndromic autosomal recessive retinitis pigmentosa (RP51). *Clinical Genetics* **89**, 454-460 (2016).
74. D. Murphy, R. Singh, S. Kolandaivelu, V. Ramamurthy, P. Stoilov, Alternative Splicing Shapes the Phenotype of a Mutation in BBS8 To Cause Nonsyndromic Retinitis Pigmentosa. *Molecular and cellular biology* **35**, 1860-1870 (2015).
75. J. Cherfils, M. Zeghouf, Regulation of small GTPases by GEFs, GAPs, and GDIs. *Physiol Rev* **93**, 269-309 (2013).
76. A. K. Mishra, D. G. Lambright, Invited review: Small GTPases and their GAPs. *Biopolymers* **105**, 431-448 (2016).
77. S. Cevik *et al.*, Joubert syndrome Arl13b functions at ciliary membranes and stabilizes protein transport in Caenorhabditis elegans. *J Cell Biol* **188**, 953-969 (2010).
78. T. Caspary, C. E. Larkins, K. V. Anderson, The graded response to Sonic Hedgehog depends on cilia architecture. *Dev Cell* **12**, 767-778 (2007).
79. K. Roy *et al.*, Palmitoylation of the ciliary GTPase ARL13b is necessary for its stability and its role in cilia formation. *J Biol Chem* **292**, 17703-17717 (2017).
80. N. A. Duldulao, S. Lee, Z. Sun, Cilia localization is essential for in vivo functions of the Joubert syndrome protein Arl13b/Scorpion. *Development* **136**, 4033-4042 (2009).

81. K. Gotthardt *et al.*, A G-protein activation cascade from Arl13B to Arl3 and implications for ciliary targeting of lipidated proteins. *Elife* **4**, (2015).
82. C. Hanke-Gogokhia *et al.*, Arf-like Protein 3 (ARL3) Regulates Protein Trafficking and Ciliogenesis in Mouse Photoreceptors. *J Biol Chem* **291**, 7142-7155 (2016).
83. Z. C. Wright *et al.*, ARL3 regulates trafficking of prenylated phototransduction proteins to the rod outer segment. *Human molecular genetics* **25**, 2031-2044 (2016).
84. Z. Sun *et al.*, A genetic screen in zebrafish identifies cilia genes as a principal cause of cystic kidney. *Development* **131**, 4085-4093 (2004).
85. V. Cantagrel *et al.*, Mutations in the cilia gene ARL13B lead to the classical form of Joubert syndrome. *American journal of human genetics* **83**, 170-179 (2008).
86. L. E. Mariani *et al.*, Arl13b regulates Shh signaling from both inside and outside the cilium. *Molecular biology of the cell* **27**, 3780-3790 (2016).
87. V. L. Horner, T. Caspary, Disrupted dorsal neural tube BMP signaling in the cilia mutant Arl13b hnn stems from abnormal Shh signaling. *Developmental biology* **355**, 43-54 (2011).
88. C. E. Larkins, G. D. Aviles, M. P. East, R. A. Kahn, T. Caspary, Arl13b regulates ciliogenesis and the dynamic localization of Shh signaling proteins. *Mol Biol Cell* **22**, 4694-4703 (2011).
89. C. Hanke-Gogokhia *et al.*, The guanine nucleotide exchange factor Arf-like protein 13b is essential for assembly of the mouse photoreceptor transition zone and outer segment. *J Biol Chem* **292**, 21442-21456 (2017).
90. A. A. Ivanova *et al.*, Biochemical characterization of purified mammalian ARL13B protein indicates that it is an atypical GTPase and ARL3 guanine nucleotide exchange factor (GEF). *J Biol Chem* **292**, 11091-11108 (2017).
91. R. A. Rachel *et al.*, CEP290 alleles in mice disrupt tissue-specific cilia biogenesis and recapitulate features of syndromic ciliopathies. *Human molecular genetics* **24**, 3775-3791 (2015).
92. S. Thomas *et al.*, Identification of a novel ARL13B variant in a Joubert syndrome-affected patient with retinal impairment and obesity. *Eur J Hum Genet* **23**, 621-627 (2015).
93. P. Song, L. Dudinsky, J. Fogerty, R. Gaivin, B. D. Perkins, Arl13b Interacts With Vangl2 to Regulate Cilia and Photoreceptor Outer Segment Length in Zebrafish. *Investigative ophthalmology & visual science* **57**, 4517-4526 (2016).
94. S. J. Ansley *et al.*, Basal body dysfunction is a likely cause of pleiotropic Bardet-Biedl syndrome. *Nature* **425**, 628-633 (2003).
95. E. Forsythe, P. L. Beales, Bardet-Biedl syndrome. *Eur J Hum Genet* **21**, 8-13 (2013).
96. R. Novas, M. Cardenas-Rodriguez, F. Irigoin, J. L. Badano, Bardet-Biedl syndrome: Is it only cilia dysfunction? *FEBS Lett* **589**, 3479-3491 (2015).
97. N. A. Zaghloul, N. Katsanis, Mechanistic insights into Bardet-Biedl syndrome, a model ciliopathy. *J Clin Invest* **119**, 428-437 (2009).
98. E. Heon *et al.*, Mutations in C8ORF37 cause Bardet Biedl syndrome (BBS21). *Hum Mol Genet* **25**, 2283-2294 (2016).
99. A. Lindstrand *et al.*, Copy-Number Variation Contributes to the Mutational Load of Bardet-Biedl Syndrome. *Am J Hum Genet* **99**, 318-336 (2016).
100. Q. Zhang, D. Yu, S. Seo, E. M. Stone, V. C. Sheffield, Intrinsic protein-protein interaction-mediated and chaperonin-assisted sequential assembly of stable bardet-biedl syndrome protein complex, the BBSome. *J Biol Chem* **287**, 20625-20635 (2012).
101. A. V. Loktev *et al.*, A BBSome subunit links ciliogenesis, microtubule stability, and acetylation. *Dev Cell* **15**, 854-865 (2008).

102. N. F. Berbari, J. S. Lewis, G. A. Bishop, C. C. Askwith, K. Mykytyn, Bardet-Biedl syndrome proteins are required for the localization of G protein-coupled receptors to primary cilia. *Proc Natl Acad Sci U S A* **105**, 4242-4246 (2008).
103. A. L. Tadenev *et al.*, Loss of Bardet-Biedl syndrome protein-8 (BBS8) perturbs olfactory function, protein localization, and axon targeting. *Proc Natl Acad Sci U S A* **108**, 10320-10325 (2011).
104. J. N. Pearring, R. Y. Salinas, S. A. Baker, V. Y. Arshavsky, Protein sorting, targeting and trafficking in photoreceptor cells. *Prog Retin Eye Res* **36**, 24-51 (2013).
105. T. G. Wensel *et al.*, Structural and molecular bases of rod photoreceptor morphogenesis and disease. *Prog Retin Eye Res* **55**, 32-51 (2016).
106. R. W. Young, The renewal of photoreceptor cell outer segments. *J Cell Biol* **33**, 61-72 (1967).
107. P. Datta *et al.*, Accumulation of non-outer segment proteins in the outer segment underlies photoreceptor degeneration in Bardet-Biedl syndrome. *Proc Natl Acad Sci U S A* **112**, E4400-4409 (2015).
108. S. Goyal, M. Jager, P. N. Robinson, V. Vanita, Confirmation of TTC8 as a disease gene for nonsyndromic autosomal recessive retinitis pigmentosa (RP51). *Clin Genet*, (2015).
109. S. A. Riazuddin *et al.*, A splice-site mutation in a retina-specific exon of BBS8 causes nonsyndromic retinitis pigmentosa. *Am J Hum Genet* **86**, 805-812 (2010).
110. D. Murphy, R. Singh, S. Kolandaivelu, V. Ramamurthy, P. Stoilov, Alternative Splicing Shapes the Phenotype of a Mutation in BBS8 To Cause Nonsyndromic Retinitis Pigmentosa. *Mol Cell Biol* **35**, 1860-1870 (2015).
111. J. G. Robson, L. J. Frishman, Dissecting the dark-adapted electroretinogram. *Doc Ophthalmol* **95**, 187-215 (1998).
112. H. Jin *et al.*, The conserved Bardet-Biedl syndrome proteins assemble a coat that traffics membrane proteins to cilia. *Cell* **141**, 1208-1219 (2010).
113. J. C. Kim *et al.*, The Bardet-Biedl protein BBS4 targets cargo to the pericentriolar region and is required for microtubule anchoring and cell cycle progression. *Nat Genet* **36**, 462-470 (2004).
114. D. H. Hong *et al.*, RPGR isoforms in photoreceptor connecting cilia and the transitional zone of motile cilia. *Invest Ophthalmol Vis Sci* **44**, 2413-2421 (2003).
115. Y. Zhao *et al.*, The retinitis pigmentosa GTPase regulator (RPGR)- interacting protein: subserving RPGR function and participating in disk morphogenesis. *Proc Natl Acad Sci U S A* **100**, 3965-3970 (2003).
116. Q. Liu, A. Lyubarsky, J. H. Skalet, E. N. Pugh, Jr., E. A. Pierce, RP1 is required for the correct stacking of outer segment discs. *Invest Ophthalmol Vis Sci* **44**, 4171-4183 (2003).
117. Q. Liu, J. Zuo, E. A. Pierce, The retinitis pigmentosa 1 protein is a photoreceptor microtubule-associated protein. *J Neurosci* **24**, 6427-6436 (2004).
118. Y. Omori *et al.*, Negative regulation of ciliary length by ciliary male germ cell-associated kinase (Mak) is required for retinal photoreceptor survival. *Proc Natl Acad Sci U S A* **107**, 22671-22676 (2010).
119. K. Arikawa, D. S. Williams, Acetylated alpha-tubulin in the connecting cilium of developing rat photoreceptors. *Invest Ophthalmol Vis Sci* **34**, 2145-2149 (1993).
120. Y. Z. Le *et al.*, Targeted expression of Cre recombinase to cone photoreceptors in transgenic mice. *Mol Vis* **10**, 1011-1018 (2004).

121. T. S. Smith *et al.*, Light-dependent phosphorylation of Bardet-Biedl syndrome 5 in photoreceptor cells modulates its interaction with arrestin1. *Cell Mol Life Sci* **70**, 4603-4616 (2013).
122. M. M. Abd-El-Barr *et al.*, Impaired photoreceptor protein transport and synaptic transmission in a mouse model of Bardet-Biedl syndrome. *Vision Res* **47**, 3394-3407 (2007).
123. D. Y. Nishimura *et al.*, Bbs2-null mice have neurosensory deficits, a defect in social dominance, and retinopathy associated with mislocalization of rhodopsin. *Proc Natl Acad Sci U S A* **101**, 16588-16593 (2004).
124. S. Scheidecker *et al.*, Predominantly Cone-System Dysfunction as Rare Form of Retinal Degeneration in Patients With Molecularly Confirmed Bardet-Biedl Syndrome. *Am J Ophthalmol* **160**, 364-372 e361 (2015).
125. A. R. Nager *et al.*, An Actin Network Dispatches Ciliary GPCRs into Extracellular Vesicles to Modulate Signaling. *Cell* **168**, 252-263 e214 (2017).
126. G. J. Pazour *et al.*, The intraflagellar transport protein, IFT88, is essential for vertebrate photoreceptor assembly and maintenance. *The Journal of cell biology* **157**, 103-113 (2002).
127. R. Y. Salinas *et al.*, Photoreceptor discs form through peripherin-dependent suppression of ciliary ectosome release. *J Cell Biol* **216**, 1489-1499 (2017).
128. D. Portran, L. Schaedel, Z. Xu, M. Thery, M. V. Nachury, Tubulin acetylation protects long-lived microtubules against mechanical ageing. *Nat Cell Biol* **19**, 391-398 (2017).
129. Z. Xu *et al.*, Microtubules acquire resistance from mechanical breakage through intralumenal acetylation. *Science* **356**, 328-332 (2017).
130. T. Shida, J. G. Cueva, Z. Xu, M. B. Goodman, M. V. Nachury, The major alpha-tubulin K40 acetyltransferase alphaTAT1 promotes rapid ciliogenesis and efficient mechanosensation. *Proc Natl Acad Sci U S A* **107**, 21517-21522 (2010).
131. J. C. Blanks, R. J. Mullen, M. M. LaVail, Retinal degeneration in the pcd cerebellar mutant mouse. II. Electron microscopic analysis. *J Comp Neurol* **212**, 231-246 (1982).
132. M. Bosch Grau *et al.*, Alterations in the balance of tubulin glycylation and glutamylation in photoreceptors leads to retinal degeneration. *J Cell Sci* **130**, 938-949 (2017).
133. M. M. LaVail, J. C. Blanks, R. J. Mullen, Retinal degeneration in the pcd cerebellar mutant mouse. I. Light microscopic and autoradiographic analysis. *J Comp Neurol* **212**, 217-230 (1982).
134. M. J. Mattapallil *et al.*, The Rd8 mutation of the Crb1 gene is present in vendor lines of C57BL/6N mice and embryonic stem cells, and confounds ocular induced mutant phenotypes. *Invest Ophthalmol Vis Sci* **53**, 2921-2927 (2012).
135. Y. Furuta, O. Lagutin, B. L. Hogan, G. C. Oliver, Retina- and ventral forebrain-specific Cre recombinase activity in transgenic mice. *Genesis* **26**, 130-132 (2000).
136. L. T. Kirschman *et al.*, The Leber congenital amaurosis protein, AIPL1, is needed for the viability and functioning of cone photoreceptor cells. *Hum Mol Genet* **19**, 1076-1087 (2010).
137. C. A. Ku *et al.*, Viral-mediated vision rescue of a novel AIPL1 cone-rod dystrophy model. *Hum Mol Genet* **24**, 670-684 (2015).
138. A. L. Bishop, A. Hall, Rho GTPases and their effector proteins. *Biochem J* **348 Pt 2**, 241-255 (2000).

139. Y. Hori, T. Kobayashi, Y. Kikko, K. Kontani, T. Katada, Domain architecture of the atypical Arf-family GTPase Arl13b involved in cilia formation. *Biochemical and Biophysical Research Communications* **373**, 119-124 (2008).
140. M. Miertzschke, C. Koerner, M. Spoerner, A. Wittinghofer, Structural insights into the small G-protein Arl13B and implications for Joubert syndrome. *Biochem J* **457**, 301-311 (2014).
141. S. Cevik *et al.*, Joubert syndrome Arl13b functions at ciliary membranes and stabilizes protein transport in Caenorhabditis elegans. *The Journal of Cell Biology* **188**, 953-969 (2010).
142. V. Cantagrel *et al.*, Mutations in the cilia gene ARL13B lead to the classical form of Joubert syndrome. *Am J Hum Genet* **83**, 170-179 (2008).
143. Y. Li *et al.*, Deletion of ADP Ribosylation Factor-Like GTPase 13B Leads to Kidney Cysts. *J Am Soc Nephrol* **27**, 3628-3638 (2016).
144. H. Lu *et al.*, A function for the Joubert syndrome protein Arl13b in ciliary membrane extension and ciliary length regulation. *Dev Biol* **397**, 225-236 (2015).
145. Q. Zhang *et al.*, GTP-binding of ARL-3 is activated by ARL-13 as a GEF and stabilized by UNC-119. *Scientific Reports* **6**, 24534 (2016).
146. S. A. Ismail *et al.*, Structural basis for Arl3-specific release of myristoylated ciliary cargo from UNC119. *EMBO J* **31**, 4085-4094 (2012).
147. Z. C. Wright *et al.*, ARL3 regulates trafficking of prenylated phototransduction proteins to the rod outer segment. *Human Molecular Genetics* **25**, 2031-2044 (2016).
148. K. Hua, R. J. Ferland, Fixation methods can differentially affect ciliary protein immunolabeling. *Cilia* **6**, 5 (2017).
149. N. P. Skiba *et al.*, Proteomic identification of unique photoreceptor disc components reveals the presence of PRCD, a protein linked to retinal degeneration. *J Proteome Res* **12**, 3010-3018 (2013).
150. T. Rakshit, S. Senapati, S. Sinha, A. M. Whited, P. S. H. Park, Rhodopsin Forms Nanodomains in Rod Outer Segment Disc Membranes of the Cold-Blooded Xenopus laevis. *PLOS ONE* **10**, e0141114 (2015).
151. S. Nickell, P. S.-H. Park, W. Baumeister, K. Palczewski, Three-dimensional architecture of murine rod outer segments determined by cryoelectron tomography. *The Journal of Cell Biology* **177**, 917-925 (2007).
152. V. Noga, Alpha subunit of Go localizes in the dendritic tips of ON bipolar cells. *Journal of Comparative Neurology* **395**, 43-52 (1998).
153. C.-Y. Su, S. N. Bay, L. E. Mariani, M. J. Hillman, T. Caspary, Temporal deletion of Arl13b reveals that a mispatterned neural tube corrects cell fate over time. *Development (Cambridge, England)* **139**, 4062-4071 (2012).
154. Q. Quinteros, M. L. Benedetto, M. M. Maldonado, A. C. V. d. P. E, M. A. Contin, Electroretinography: A biopotential to assess the function/dysfunction of the retina. *Journal of Physics: Conference Series* **705**, 012053 (2016).
155. L. H. Pinto, B. Invergo, K. Shimomura, J. S. Takahashi, J. B. Troy, Interpretation of the mouse electroretinogram. *Documenta ophthalmologica. Advances in ophthalmology* **115**, 127-136 (2007).
156. S. N. Bay, A. B. Long, T. Caspary, Disruption of the ciliary GTPase Arl13b suppresses Sonic hedgehog overactivation and inhibits medulloblastoma formation. *Proc Natl Acad Sci U S A* **115**, 1570-1575 (2018).

157. M. Mongan *et al.*, Loss of MAP3K1 enhances proliferation and apoptosis during retinal development. *Development* **138**, 4001-4012 (2011).
158. A. Suga, K. Sadamoto, M. Fujii, M. Mandai, M. Takahashi, Proliferation Potential of Müller Glia after Retinal Damage Varies between Mouse Strains. *PLOS ONE* **9**, e94556 (2014).
159. M. J. Hendzel *et al.*, Mitosis-specific phosphorylation of histone H3 initiates primarily within pericentromeric heterochromatin during G2 and spreads in an ordered fashion coincident with mitotic chromosome condensation. *Chromosoma* **106**, 348-360 (1997).
160. Y. Omori *et al.*, Negative regulation of ciliary length by ciliary male germ cell-associated kinase (Mak) is required for retinal photoreceptor survival. *Proceedings of the National Academy of Sciences* **107**, 22671-22676 (2010).
161. Q. Liu, J. Zuo, E. A. Pierce, The Retinitis Pigmentosa 1 Protein Is a Photoreceptor Microtubule-Associated Protein. *The Journal of neuroscience : the official journal of the Society for Neuroscience* **24**, 6427-6436 (2004).
162. D. Portran, L. Schaedel, Z. Xu, M. Théry, M. V. Nachury, Tubulin acetylation protects long-lived microtubules against mechanical aging. *Nature cell biology* **19**, 391-398 (2017).
163. K. Arikawa, D. S. Williams, Acetylated alpha-tubulin in the connecting cilium of developing rat photoreceptors. *Investigative Ophthalmology & Visual Science* **34**, 2145-2149 (1993).
164. S. F. Koch *et al.*, Halting progressive neurodegeneration in advanced retinitis pigmentosa. *J Clin Invest* **125**, 3704-3713 (2015).
165. S. Nozaki *et al.*, Regulation of ciliary retrograde protein trafficking by the Joubert syndrome proteins ARL13B and INPP5E. *J Cell Sci* **130**, 563-576 (2017).
166. C. Hanke-Gogokhia *et al.*, The guanine nucleotide exchange factor, Arf-like protein 13b, is essential for assembly of the mouse photoreceptor transition zone and outer segment. *Journal of Biological Chemistry*, (2017).
167. M. Pruski *et al.*, The ciliary GTPase Arl13b regulates cell migration and cell cycle progression. *Cell Adh Migr* **10**, 393-405 (2016).
168. G. D. Dakubo, V. A. Wallace, Hedgehogs and retinal ganglion cells: organizers of the mammalian retina. *Neuroreport* **15**, 479-482 (2004).
169. A. Moshiri, C. R. McGuire, T. A. Reh, Sonic hedgehog regulates proliferation of the retinal ciliary marginal zone in posthatch chicks. *Dev Dyn* **233**, 66-75 (2005).
170. D. S. Wall *et al.*, Progenitor cell proliferation in the retina is dependent on Notch-independent Sonic hedgehog/Hes1 activity. *J Cell Biol* **184**, 101-112 (2009).
171. V. L. Horner, T. Caspary, Disrupted dorsal neural tube BMP signaling in the cilia mutant Arl13b(hnn) stems from abnormal Shh signaling. *Developmental biology* **355**, 43-54 (2011).
172. P. Song, L. Dudinsky, J. Fogerty, R. Gaivin, B. D. Perkins, Arl13b Interacts With Vangl2 to Regulate Cilia and Photoreceptor Outer Segment Length in Zebrafish. *Invest Ophthalmol Vis Sci* **57**, 4517-4526 (2016).
173. D. Deretic, S. Schmerl, P. A. Hargrave, A. Arendt, J. H. McDowell, Regulation of sorting and post-Golgi trafficking of rhodopsin by its C-terminal sequence QVS(A)PA. *Proceedings of the National Academy of Sciences of the United States of America* **95**, 10620-10625 (1998).
174. B. M. Tam, O. L. Moritz, D. S. Papermaster, The C terminus of peripherin/rds participates in rod outer segment targeting and alignment of disk incisures. *Mol Biol Cell* **15**, 2027-2037 (2004).
175. R. Y. Salinas *et al.*, Photoreceptor discs form through peripherin-dependent suppression of ciliary ectosome release. *The Journal of Cell Biology* **216**, 1489-1499 (2017).

176. T. L. Dilan *et al.*, Bardet–Biedl syndrome-8 (BBS8) protein is crucial for the development of outer segments in photoreceptor neurons. *Human Molecular Genetics* **27**, 283-294 (2018).
177. R. S. Molday, A. F. X. Goldberg, Peripherin diverts ciliary ectosome release to photoreceptor disc morphogenesis. *The Journal of Cell Biology*, (2017).
178. K. F. Lechtreck, IFT-Cargo Interactions and Protein Transport in Cilia. *Trends Biochem Sci* **40**, 765-778 (2015).
179. M. Taschner, E. Lorentzen, The Intraflagellar Transport Machinery. *Cold Spring Harb Perspect Biol* **8**, (2016).
180. J. A. Harris, J. M. Van De Weghe, T. Kubo, G. B. Witman, K. Lechtreck, Diffusion rather than IFT provides most of the tubulin required for axonemal assembly. *bioRxiv*, (2018).
181. S. Cevik *et al.*, Active transport and diffusion barriers restrict Joubert Syndrome-associated ARL13B/ARL-13 to an Inv-like ciliary membrane subdomain. *PLoS Genet* **9**, e1003977 (2013).
182. E. Gimenez, L. Montoliu, A simple polymerase chain reaction assay for genotyping the retinal degeneration mutation (Pdeb(rd1)) in FVB/N-derived transgenic mice. *Laboratory animals* **35**, 153-156 (2001).
183. V. Ramamurthy, G. A. Niemi, T. A. Reh, J. B. Hurley, Leber congenital amaurosis linked to AIPL1: A mouse model reveals destabilization of cGMP phosphodiesterase. *Proceedings of the National Academy of Sciences of the United States of America* **101**, 13897-13902 (2004).
184. A. F. Goldberg *et al.*, An intramembrane glutamic acid governs peripherin/rds function for photoreceptor disk morphogenesis. *Invest Ophthalmol Vis Sci* **48**, 2975-2986 (2007).
185. Y. Furuta, O. Lagutin, B. L. M. Hogan, G. C. Oliver, Retina- and ventral forebrain-specific Cre recombinase activity in transgenic mice. *genesis* **26**, 130-132 (2000).
186. E. M. Levine, H. Roelink, J. Turner, T. A. Reh, Sonic Hedgehog Promotes Rod Photoreceptor Differentiation in Mammalian Retinal Cells <em>In Vitro</em&gt. *The Journal of Neuroscience* **17**, 6277 (1997).
187. G. D. Dakubo *et al.*, Retinal ganglion cell-derived sonic hedgehog signaling is required for optic disc and stalk neuroepithelial cell development. *Development* **130**, 2967 (2003).
188. Y. P. Wang *et al.*, Development of normal retinal organization depends on Sonic hedgehog signaling from ganglion cells. *Nature Neuroscience* **5**, 831 (2002).
189. X. M. Zhang, X. J. Yang, Regulation of retinal ganglion cell production by Sonic hedgehog. *Development* **128**, 943 (2001).
190. D. Huangfu *et al.*, Hedgehog signalling in the mouse requires intraflagellar transport proteins. *Nature* **426**, 83-87 (2003).
191. S. C. Goetz, K. V. Anderson, The primary cilium: a signalling centre during vertebrate development. *Nat Rev Genet* **11**, 331-344 (2010).
192. K. C. Corbit *et al.*, Vertebrate Smoothened functions at the primary cilium. *Nature* **437**, 1018-1021 (2005).
193. A. M. Jensen, V. A. Wallace, Expression of Sonic hedgehog and its putative role as a precursor cell mitogen in the developing mouse retina. *Development* **124**, 363 (1997).
194. C. E. Holt, T. W. Bertsch, H. M. Ellis, W. A. Harris, Cellular determination in the Xenopus retina is independent of lineage and birth date. *Neuron* **1**, 15-26 (1988).
195. D. L. Turner, C. L. Cepko, A common progenitor for neurons and glia persists in rat retina late in development. *Nature* **328**, 131-136 (1987).
196. R. Wetts, S. E. Fraser, Multipotent precursors can give rise to all major cell types of the frog retina. *Science* **239**, 1142 (1988).

197. Y. Wang, G. D. Dakubo, S. Thurig, C. J. Mazerolle, V. A. Wallace, Retinal ganglion cell-derived sonic hedgehog locally controls proliferation and the timing of RGC development in the embryonic mouse retina. *Development* **132**, 5103-5113 (2005).
198. H. L. Park *et al.*, Mouse Gli1 mutants are viable but have defects in SHH signaling in combination with a Gli2 mutation. *Development* **127**, 1593 (2000).
199. C. B. Bai, W. Auerbach, J. S. Lee, D. Stephen, A. L. Joyner, Gli2, but not Gli1, is required for initial Shh signaling and ectopic activation of the Shh pathway. *Development* **129**, 4753 (2002).
200. D. S. Wall *et al.*, Progenitor cell proliferation in the retina is dependent on Notch-independent Sonic hedgehog/Hes1 activity. *The Journal of Cell Biology* **184**, 101 (2009).
201. L. E. Drayson, J. W. Triplett, A Chrnb3-Cre BAC transgenic mouse line for manipulation of gene expression in retinal ganglion cells. *genesis* **57**, e23305 (2019).
202. S. Fukuda *et al.*, Functional endothelial progenitor cells selectively recruit neurovascular protective monocyte-derived F4/80+/Ly6c+ macrophages in a mouse model of retinal degeneration. *STEM CELLS* **31**, 2149-2161 (2013).
203. A.-C. Vion *et al.*, Primary cilia sensitize endothelial cells to BMP and prevent excessive vascular regression. *The Journal of Cell Biology* **217**, 1651 (2018).
204. J. G. Goetz *et al.*, Endothelial cilia mediate low flow sensing during zebrafish vascular development. *Cell Rep* **6**, 799-808 (2014).
205. J. Wang, M. M. Barr, Ciliary Extracellular Vesicles: Txt Msg Organelles. *Cell Mol Neurobiol* **36**, 449-457 (2016).
206. M. C. Hogan *et al.*, Characterization of PKD Protein-Positive Exosome-Like Vesicles. *Journal of the American Society of Nephrology* **20**, 278 (2009).
207. R. Y. Salinas *et al.*, Photoreceptor discs form through peripherin-dependent suppression of ciliary ectosome release. *The Journal of Cell Biology*, (2017).
208. D. Wloga, E. Joachimiak, P. Louka, J. Gaertig, Posttranslational Modifications of Tubulin and Cilia. *Cold Spring Harb Perspect Biol* **9**, a028159 (2017).
209. A. Loktev *et al.*, A BBSome Subunit Links Ciliogenesis, Microtubule Stability, and Acetylation. *Developmental cell* **15**, 854-865 (2009).
210. N. F. Berbari *et al.*, Microtubule modifications and stability are altered by cilia perturbation and in cystic kidney disease. *Cytoskeleton* **70**, 24-31 (2013).
211. H. T. Chou *et al.*, The Molecular Architecture of Native BBSome Obtained by an Integrated Structural Approach. *Structure (London, England : 1993)* **27**, 1384-1394.e1384 (2019).
212. C. Hubbert *et al.*, HDAC6 is a microtubule-associated deacetylase. *Nature* **417**, 455-458 (2002).
213. E. N. Pugacheva, S. A. Jablonski, T. R. Hartman, E. P. Henske, E. A. Golemis, HEF1-dependent Aurora A activation induces disassembly of the primary cilium. *Cell* **129**, 1351-1363 (2007).
214. J. Ran, Y. Yang, D. Li, M. Liu, J. Zhou, Deacetylation of α-tubulin and cortactin is required for HDAC6 to trigger ciliary disassembly. *Scientific reports* **5**, 12917-12917 (2015).
215. N. Kalebic *et al.*, αTAT1 is the major α-tubulin acetyltransferase in mice. *Nat Commun* **4**, 1962 (2013).
216. J. S. Akella *et al.*, MEC-17 is an alpha-tubulin acetyltransferase. *Nature* **467**, 218-222 (2010).

217. T. Shida, J. G. Cueva, Z. Xu, M. B. Goodman, M. V. Nachury, The major α-tubulin K40 acetyltransferase αTAT1 promotes rapid ciliogenesis and efficient mechanosensation. *Proceedings of the National Academy of Sciences* **107**, 21517 (2010).
218. A. Sánchez de Diego, A. Alonso Guerrero, C. Martínez-A, K. H. M. van Wely, Dido3-dependent HDAC6 targeting controls cilium size. *Nat Commun* **5**, 3500-3500 (2014).
219. T. Nakakura *et al.*, Intracellular localization of α-tubulin acetyltransferase ATAT1 in rat ciliated cells. *Medical molecular morphology* **49**, (2015).
220. R. Luscan *et al.*, Mutations in TUBB4B Cause a Distinctive Sensorineural Disease. *American journal of human genetics* **101**, 1006-1012 (2017).
221. M. Bosch Grau *et al.*, Alterations in the balance of tubulin glycylation and glutamylation in photoreceptors leads to retinal degeneration. *Journal of Cell Science* **130**, 938-949 (2017).
222. A. L. D. Tadenev *et al.*, Loss of Bardet-Biedl syndrome protein-8 (BBS8) perturbs olfactory function, protein localization, and axon targeting. *Proceedings of the National Academy of Sciences of the United States of America* **108**, 10320-10325 (2011).
223. N. F. Berbari, A. D. Johnson, J. S. Lewis, C. C. Askwith, K. Mykytyn, Identification of ciliary localization sequences within the third intracellular loop of G protein-coupled receptors. *Molecular biology of the cell* **19**, 1540-1547 (2008).
224. J. Jiang *et al.*, Depletion of BBS Protein LZTFL1 Affects Growth and Causes Retinal Degeneration in Mice. *J Genet Genomics* **43**, 381-391 (2016).
225. B. S. Pawlyk *et al.*, Photoreceptor rescue by an abbreviated human RPGR gene in a murine model of X-linked retinitis pigmentosa. *Gene Ther* **23**, 196-204 (2016).
226. Y. Zhao *et al.*, The retinitis pigmentosa GTPase regulator (RPGR)- interacting protein: Subserving RPGR function and participating in disk morphogenesis. *Proceedings of the National Academy of Sciences* **100**, 3965 (2003).
227. D. S. Papermaster, W. J. Dreyer, Rhodopsin content in the outer segment membranes of bovine and frog retinal rods. *Biochemistry* **13**, 2438-2444 (1974).
228. E. S. Lobanova *et al.*, Increased proteasomal activity supports photoreceptor survival in inherited retinal degeneration. *Nat Commun* **9**, 1738-1738 (2018).
229. D. Chakraborty, S. M. Conley, M. R. Al-Ubaidi, M. I. Naash, Initiation of rod outer segment disc formation requires RDS. *PloS one* **9**, e98939-e98939 (2014).
230. P. Datta *et al.*, Accumulation of non-outer segment proteins in the outer segment underlies photoreceptor degeneration in Bardet-Biedl syndrome. *Proceedings of the National Academy of Sciences of the United States of America* **112**, E4400-E4409 (2015).
231. E. K. Fansa, A. Wittinghofer, Sorting of lipidated cargo by the Arl2/Arl3 system. *Small GTPases* **7**, 222-230 (2016).
232. S. A. Ismail *et al.*, Arl2-GTP and Arl3-GTP regulate a GDI-like transport system for farnesylated cargo. *Nature Chemical Biology* **7**, 942-949 (2011).
233. K. J. Wright *et al.*, An ARL3-UNC119-RP2 GTPase cycle targets myristoylated NPHP3 to the primary cilium. *Genes & development* **25**, 2347-2360 (2011).
234. M. Linari *et al.*, The retinitis pigmentosa GTPase regulator, RPGR, interacts with the delta subunit of rod cyclic GMP phosphodiesterase. *Proceedings of the National Academy of Sciences* **96**, 1315 (1999).
235. P. Datta, B. Hendrickson, S. Brendalen, A. Ruffcorn, S. Seo, The myosin-tail homology domain of centrosomal protein 290 is essential for protein confinement between the inner and outer segments in photoreceptors. *J Biol Chem*, (2019).

236. C. L. Williams *et al.*, MKS and NPHP modules cooperate to establish basal body/transition zone membrane associations and ciliary gate function during ciliogenesis. *The Journal of Cell Biology* **192**, 1023 (2011).
237. C. Li *et al.*, MKS5 and CEP290 Dependent Assembly Pathway of the Ciliary Transition Zone. *PLOS Biology* **14**, e1002416 (2016).
238. B. Craige *et al.*, CEP290 tethers flagellar transition zone microtubules to the membrane and regulates flagellar protein content. *The Journal of cell biology* **190**, 927-940 (2010).
239. H. Shimada *et al.*, In Vitro Modeling Using Ciliopathy-Patient-Derived Cells Reveals Distinct Cilia Dysfunctions Caused by CEP290 Mutations. *Cell Rep* **20**, 384-396 (2017).
240. M. A. Robichaux *et al.*, Defining the layers of a sensory cilium with STORM and cryoelectron nanoscopy. *Proceedings of the National Academy of Sciences* **116**, 23562 (2019).
241. B. U. Klink, C. Gatsogiannis, O. Hofnagel, A. Wittinghofer, S. Raunser, Structure of the human BBSome core complex in the open conformation. *bioRxiv*, 845982 (2019).
242. E. Revenkova, Q. Liu, G. L. Gusella, C. Iomini, The Joubert syndrome protein ARL13B binds tubulin to maintain uniform distribution of proteins along the ciliary membrane. *J Cell Sci* **131**, (2018).
243. T. Caspary, C. E. Larkins, K. V. Anderson, The Graded Response to Sonic Hedgehog Depends on Cilia Architecture. *Developmental Cell* **12**, 767-778 (2007).
244. K. J. Roux, D. I. Kim, M. Raida, B. Burke, A promiscuous biotin ligase fusion protein identifies proximal and interacting proteins in mammalian cells. *The Journal of cell biology* **196**, 801-810 (2012).
245. T. C. Branon *et al.*, Efficient proximity labeling in living cells and organisms with TurboID. *Nat Biotechnol* **36**, 880-887 (2018).
246. H. Higginbotham *et al.*, Arl13b in primary cilia regulates the migration and placement of interneurons in the developing cerebral cortex. *Developmental cell* **23**, 925-938 (2012).